Do myosins contribute to metastasis of prostate cancer cells?

Katarzyna Anna Makowska

Submitted in accordance with the requirements for the degree of
Doctor of Philosophy

The University of Leeds
Faculty of Biological Sciences

September, 2015

The candidate confirms that the work submitted is her own, except where work which has formed part of jointly-authored publications has been included. The contribution of the candidate and the other authors to this work has been explicitly indicated below. The candidate confirms that appropriate credit has been given within the thesis where reference has been made to the work of others.

Makowska, K.A., Hughes, R.E., White, K.J., Wells, C.M., Peckham, M., (2015) *Specific Myosins Control Actin Organization, Cell Morphology, and Migration in Prostate Cancer Cells*. Cell Reports 13, 1-8

The part of the experimental work described in Chapter 3 and Chapter 4 of the thesis and included in the publication is directly attributable to the candidate, unless stated otherwise.

Contributions of other members of the group have been as follows: Dr Kathryn White has performed the qPCR analysis presented in Section 3.2.2 and in Figure 3.3, including design of the primers (Table 2.1). Professor Michelle Peckham has done the immunoblotting after Myo9b knockdown experiment described in Figure 4.9.

Acknowledgements

I would like to thank my supervisor, Professor Michelle Peckham, for all the help and support. I really appreciate all the visits to the microscope room, long discussions and all the guidance. Thank you to my co-supervisor Dr Claire Wells, for the helpful discussions, suggestions, and the offered fresh look on the project.

I would also like to express my gratitude to the fantastic Motility Mob! Very big thanks to Kat who taught me so much during the first year, and the whole team: Marcin, Fran, Ada, Marta, Mara, Anna, Matt, Alistair… and especially Ruth, for being such a patient companion, when searching for lost reagents and all other lab adventures.. Guys, it's been a pleasure!

Also thanks to Gareth Howell and Sally Boxall for the useful assistance with the microscopes. Thanks to Drs Darren Tomlinson and Stephan Muller from Sheffield, who helped me with screens that did not make it into this thesis but where nonetheless informative. Thank you to Dr Steven Rosenfeld for the collaboration on glioblastoma.

Thank you to Cancer Research UK for the funding.

Thank you to all my friends in Leeds for a wonderful adventure: Gloria, Merce, Ambra, Rocio, Yoselin (and Jessica) Hijas! Sois lo mejor que me podía pasar! I am also forever thankful for Jurek and Remy and their constant optimism and company at all times. Thanks to Helena's Bellydancers and the LUU Bellydance Society for adding the extra sparkle on top of my scientific life. I feel like I should also thank the Caedmon Clan for feeding me in the crucial final weeks before my submission deadline.

And finally, thank you to my family for their constant belief in me. Jestem bardzo wdzięczna mojej rodzinie za ciągłe wsparcie i nieustanną wiarę we mnie.

Abstract

Prostate cancer is the second most common cause of death from cancer in men in the UK. Localised disease can be treated with surgery or radiotherapy, but metastasis remains a great therapeutic challenge. Cancer cell migration involves rearrangements of the actin cytoskeleton, which is mediated by its interaction with myosins, a large and diverse family of motor proteins involved in many processes crucial for cell migration, such as cell adhesion, cell polarity or endocytosis. It is likely that the activity of myosins contributes to metastatic spread.

I investigated the myosin expression profile in prostate cancer cell lines and found that Myo1b, Myo9b, Myo10 and Myo18a were expressed at higher levels in cells with high metastatic potential. Using an siRNA-based approach, knockdown of each myosin resulted in distinct phenotypes. Myo10 knockdown drastically decreased filopodia of PC3 cells, Myo18a knockdown increased filaments of non-muscle myosin 2A, knockdown of Myo1b and Myo9b increased stress fibre formation. Loss of Myo10 affected cell migration in 2D. In all cases, cell spread area was increased and 3D migration potential was decreased for Myo1b, Myo10 and Myo18a. Myo1b, Myo10 and Myo18a were also expressed in benign prostatic hyperplasia although knockdown of these myosins in benign tissue did not have very clear effects. Glioblastoma cells expressed high levels of Myo10 and showed decreased protrusions after Myo10 knockdown.

Taken together, myosins act as molecular motors but also directly influence actin organisation and cell morphology and migration, which can contribute to the metastatic phenotype of cancer cells.

Table of Contents

List of Tables

List of Figures

List of Abbreviations

ADP   Adenosine 5'-diphosphate
AF   Alexa Fluor
ANOVA   Analysis of Variance
APS   Ammonium Persulfate
Arp2/3   Actin Related Protein 2/3 Complex
ATP   Adenosine 5'-triphosphate
ATPase   Adenosine triphosphatase

BCA   Bicinchoninic Acid
BPH   Benign Prostatic Hyperplasia
BSA   Bovine Serum Albumin

cDNA   Complimentary DNA
C-terminal Carboxy-terminal
CRPC   Castration-resistant prostate cancer

DAPI   4',6'-diamidino-2-phenylindole
DCC   Deleted in Colon Cancer
DMEM   Dulbecco's Modified Eagles Medium
DNA   Deoxyribonucleic Acid

EDTA   Ethylenediaminetetraacetic Acid
EEA1   Early Endosome Antigen-1
eGFP   Enhanced Green Fluorescent Protein
ELC   Essential Light Chain

F-Actin   Filamentous Actin
FBS   Foetal Bovine Serum

GAP   GTPase Activating Protein
GFP   Green Fluorescent Protein

HEPES   4-(2-hydroxyethyl)-1-piperazineethanesulfonic acid
HRP   Horseradish Peroxidase

IF   Immunofluorescence

kDa   Kilodaltons

M   Molar
MLC   Myosin Light Chain

N-terminal Amino-terminal

P (p)	Probability
PAGE	Polyacrylamide Gel Electrophoresis
PBS	Phosphate Buffered Saline
PCR	Polymerase Chain Reaction
PIP	Phosphatidylinositol Phosphate
pMLC	Phosphorylated Myosin Light Chain
RLC	Regulatory Light Chain
RNA	Ribonucleic Acid
RNAi	RNA Interference
ROCK	Rho-associated protein kinase
S.D.	Standard Deviation
S.E.	Standard Error
SDS	Sodium Dodecyl Sulphate
siRNA	Small Interfering RNA
TEMED	N, N, N', N'-Tetramethylethylenediamine
v/v	Volume by Volume
WB	Western Blotting
w/v	Weight by Volume

Chapter 1
Introduction

1.1 Cancer characterisation

Cancer is not just a single disease, but a group of diseases characterised by the uncontrolled growth and spread of abnormal cells. The complexity of this group of diseases can be described through the underlying principles, also known as the hallmarks of cancer (Hanahan and Weinberg, 2000):

- Self-sufficiency in growth signals
- Evading apoptosis
- Insensitivity to anti-growth signals
- Tissue invasion & metastasis
- Limitless replicative potential
- Sustained angiogenesis

These have been complemented by the "next generation" hallmarks (Hanahan and Weinberg, 2011):

- Avoiding immune destruction
- Deregulating cellular energetics
- Genome instability and mutation
- Tumour-promoting inflammation

Even though the field of cancer research has grown extensively, there are still many questions that remain unanswered. In my study, I have focused on the metastasis of prostate cancer, trying to examine the mechanisms underlying this process.

1.1.1 Prostate cancer statistics

Almost 7.5 million men worldwide were diagnosed with cancer in 2012 (Torre et al., 2015). Out of these, prostate cancer accounted for 1.1 million cases, or 15%, making it the second most common cancer in men

worldwide, after lung cancer (Torre et al., 2015). The incidence rates vary up to 100-fold across the world, remaining very low in most of Asia and Africa. The rates are highest in Australia, North America and Western Europe, where almost 70% of all cases occurred (759 000 in 2012) (Figure 1.1) (Torre et al., 2015). In the UK, prostate cancer accounts for 25% of male cases of cancer and is the most common cancer type (Cancer Research UK website) (more than 41 000 out of 167 000 in 2011). Prostate cancer is the fifth leading cause of death from cancer in men worldwide (estimated 307 000 deaths in 2012) (Torre et al., 2015) and second in the UK (around 10 800 deaths in 2012, Cancer Research UK website). Mortality rates worldwide show less variation than incidence, with the number of deaths generally high in predominantly black populations (Caribbean and sub-Saharan Africa, among others), very low in Asia and intermediate in the Americas and Oceania (Jemal et al., 2011).

Much of the variation in incidence reflects differences in cancer detection. The high incidence rates reported especially in developed countries largely result from the widely used prostate specific antigen (PSA) testing that detects clinically important tumours but also slow-growing, benign cancers that might otherwise have escaped diagnosis, which in turn creates the potential for overdiagnosis (Etzioni et al., 2002). Screening for prostate cancer using PSA testing remains a controversial subject, since multiple studies into using the test have had conflicting results and there is currently no clear evidence that PSA testing reduces prostate cancer mortality (Etzioni et al., 2002). By the age of 80, most men will have some cancerous cells in their prostate, but only 1 in 25 of them will die from prostate cancer (Cancer Research UK website). On the other hand, some prostate cancers will grow quickly and spread to other parts of the body within a few years. For screening to be most helpful, it should only pick up prostate cancers that are faster growing and likely to be a threat to health, but there is currently no test that can reliably do this.

Older age, race (black), and family history remain the only well-established risk factors for prostate cancer (Jemal et al., 2011). Currently no preventable

2

risk factors for prostate cancer have been established (Jemal et al., 2011), although some studies suggest that, similarly to other cancer types, lifestyle could be important in prostate cancer prevention (Holly et al., 2013). The reason for the high prostate cancer risk among some populations of African descent is still poorly understood, though it may in part reflect differences in genetic susceptibility (Zeigler-Johnson et al., 2008).

1.1.2 Prostate cancer stages and therapies

The majority of prostate tumours are adenocarcinomas, which means they originate from the glandular epithelium in the prostate, mostly in the peripheral zone (Long et al., 2005). Prostate cancer tends to progress slowly (i.e. 83.8% of men experience a 10-year survival in England and Wales following diagnosis). Many cancers stay benign, but a fraction become metastatic at various stages and an absolute prediction of when a localised cancer will spread is not possible. Nonetheless, several factors are used to decide if cancer is low or high risk and therefore choose the treatment necessary (Cancer Research UK website). These include monitoring the levels of PSA in the blood, generating a Gleason score resulting from histological analysis of biopsies; the score is low if cells resemble normal prostate tissue (low grade cancer) and high if cells appear de-differentiated or invading the surrounding tissue (high grade/high risk cancer), and TNM staging, which assesses the size of the tumour (T), the spread to lymph nodes (N) and secondary cases (Metastases, M).

Currently used standard of care options for prostate cancer depend on the stage at which the disease is detected. Different treatments are optimised for the best results at different stages and can be combined to obtain higher efficiency. The most popular therapy strategies for localised prostate cancer include: surgery (e.g. radical prostatectomy), radiotherapy (external beam radiation therapy or radioactive seed implants in the prostate) and/or active surveillance or watchful waiting.
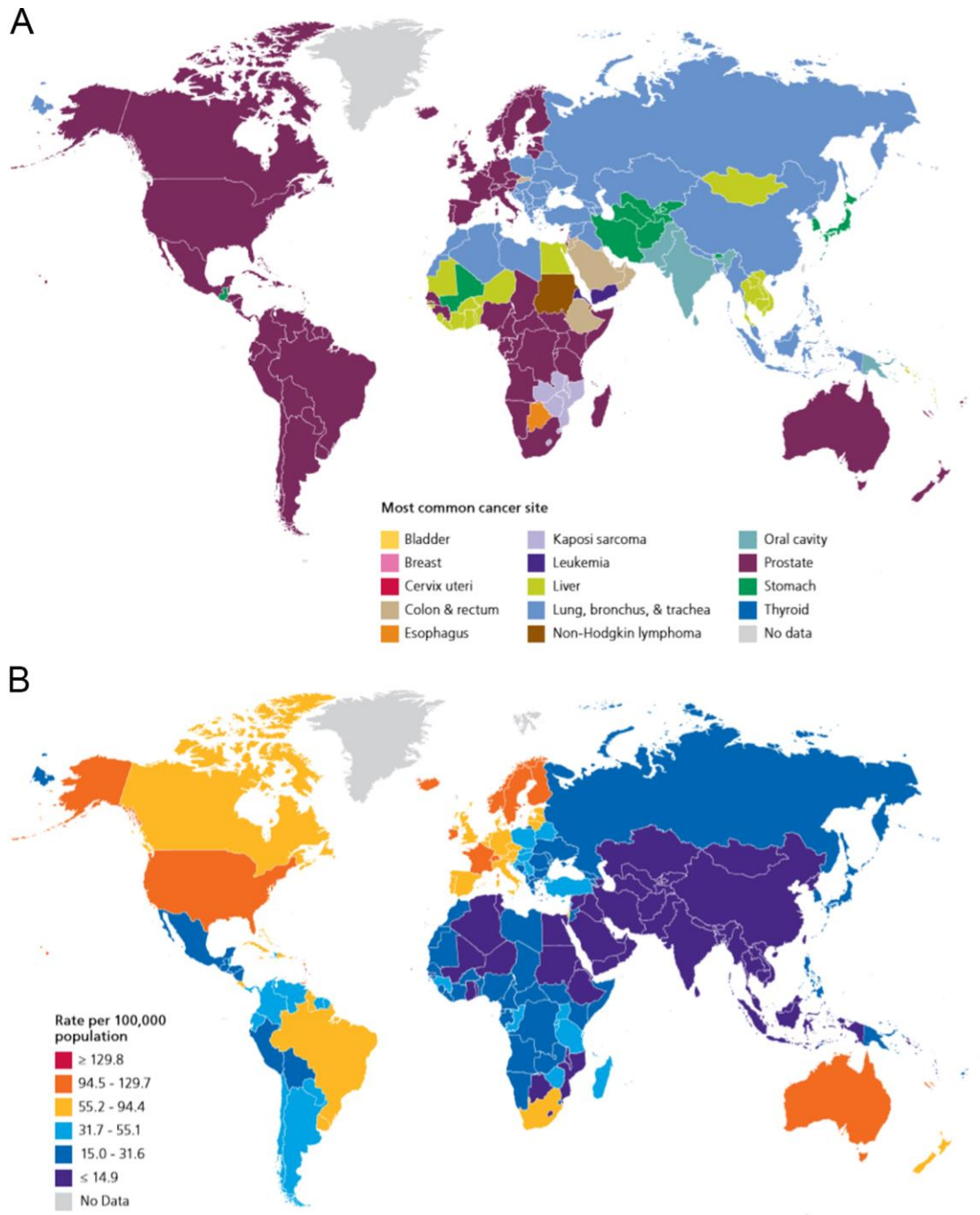
Figure 1.1 Prostate cancer worldwide. A. Most common cancer sites worldwide in males, 2012. Prostate cancer marked by purple colour. B. International variation in prostate cancer incidence rates, 2012 (per 100,000, age standardized to the World Standard Population). (Torre et al., 2015)

The prostate as well as prostate cancer depends on testosterone, the most well-known androgen, for growth. This means that hormone therapy can also be used to lower the levels of testosterone, especially if the tumour has started invading neighbouring tissues or spreading to other organs. Androgen deprivation therapy is one of the most effective forms of treatment for patients with disseminated disease (Augello et al., 2014). However, progression of prostate cancer is also connected with a loss of response to androgen levels (Sharifi et al., 2010). As a consequence, hormone therapy is therefore efficient for some time, but after 2-3 years cancer can progress into castration-resistant prostate cancer (CRPC). At this stage chemotherapy is used, such as treatment with taxane, although current methods only extend patients life by up to several months (D'Amico et al., 1998; Sharifi et al., 2010; Wolff and Mason, 2012). Prostate cancer very often metastasises to the bone, and in addition to chemotherapy, a new radioactive reagent has recently been approved to treat CRPC of the bone (Bishr and Saad, 2013; Parker et al., 2013).

Apart from the risk associated with the tumour itself, the choice of treatment depends on the age of the patient and his health (Hoskin et al., 2013). However, despite all the strategies available, both for early detection and treatment of localised prostate cancer, a number of patients will develop the disseminated metastatic disease, which remains largely untreatable (Albertsen et al., 2005; Wolff and Mason, 2012). This brings the need to study the mechanisms responsible for prostate cancer progression and metastasis. Understanding the biology of prostate tumours may help focus new research and the development of effective therapies to combat metastatic disease, and diagnostic factors to more accurately predict the risk of its potential progression.

1.1.3 Prostate cancer models

Despite considerable scientific effort, relatively little is known about the biological events causing the initiation and progression of prostate cancer.

To better understand the cellular and molecular events underlying the disease, many models of prostate cancer have been developed. These include animal models such as genetically engineered mice, xenografts and rat models, and transformed human prostate epithelial cell lines, such as LNCaP, DU145, PC3 and others.

Different models have inherent advantages and disadvantages, for example animal models can include the important interaction with the tumour microenvironment, stroma, immune cells, blood vessels etc., but prostate disease can be different in animals than in humans (Grabowska et al., 2014). Mice are quite resistant to developing invasive prostate cancer, and once they have invasive disease, it often does not resemble the human disease (reviewed in (Grabowska et al., 2014)). On the other hand, tissue culture models, although simplistic, represent human cells and are useful in understanding basic biology of prostate cancer or can serve as a good means for an initial screen.

Amongst the most popular cell lines developed and described in prostate cancer are the well-characterised "classic" cell lines: LNCaP, DU145 and PC3, which were amongst the first to be established. The three cell lines are derived from metastatic prostate cancer and have quite different properties (Table 1.1). As a model representing benign-like prostate tissue, Benign Prostatic Hyperplasia cell line (BPH-1) is also described in the table and will be used in this study.

Table 1.1 Prostate disorders and prostate cancer cell lines

	BPH-1	LNCaP	DU145	PC3
Origin	Benign prostate hyperplasia	Metastasis from supra-clavicular lymph node	Metastasis from the brain	Metastasis from bone (Gleason grade IV)
Response to androgen	Androgen-dependent	Androgen-dependent	Androgen-independent	Androgen-independent
Invasive-ness	None	Low	Medium	High
Ploidy	Aneuploid (76 chromosomes)	Hypotetraploid	Hypotriploid	Near-triploid
p53 status	wt (dysfunctional)	wt	mutant	null
Reference:	(Hayward et al., 1995)	(Horoszewicz et al., 1983)	(Stone et al., 1978)	(Kaighn et al., 1981)

BPH-1 (Benign Prostatic Hyperplasia) is an epithelial cell line that has been established from hyperplastic human prostate tissue. Benign prostatic hyperplasia is a prostate disorder that is not considered to act as a precursor to prostate cancer (in contrast to prostatic intraepithelial neoplasia, PIN) (Orsted and Bojesen, 2013), partly because it appears in a different region of the prostate to prostate cancer and PIN. In contrast, the likelihood of prostate cancer development in patients exhibiting PIN increases with the detection of elevated serum levels of the PSA (Zlotta and Schulman, 1999). The BPH-1 cell line has been immortalised but not transformed, and it retains some important characteristics of benign prostatic epithelium *in vivo*.

In comparison to DU145 and PC3, the LNCaP cell line represents an 'early' stage of prostate cancer metastasis, because it is still androgen-sensitive and has low invasive potential (Horoszewicz et al., 1983). The invasive or metastatic potential can be measured by the cell line ability to migrate through trans-wells and into matrices, or their ability to form tumours (metastases) when injected into nude mice. PC3 cell line is the most malignant, highly proliferative and invasive cells (prostate cancer grade IV)

(Kaighn et al., 1981). PC3 represent a more advanced/ aggressive phase of cancer cell development and possess characteristics of highly malignant neoplasm, 100% cells are aneuploid, and this cell line lacks the wild-type p53 protein, a tumour suppressor. The PI 3-Kinase/Akt pathway, which is one of the major intracellular pathways responsible for promoting cell survival, is constantly active in PC3 cells (Goc et al., 2011).

1.2 Cell migration

1.2.1 Cytoskeleton

The cytoskeleton is a highly dynamic, interconnected network that provides support, structure and organisation to cells. The main components of cytoskeleton include actin filaments and microtubules, which serve as tracks for intercellular transport, and intermediate filaments (Hartman and Spudich, 2012). Both actin filaments and microtubules have a polarity, which means that they each have two structurally and functionally distinct ends. In actin filaments, one end is known as the plus (or barbed) end as it is the faster growing end. The other is known as the minus (or pointed) end (reviewed in (Akhmanova and Hammer, 2010)). The cytoskeleton is vital in many aspects of cell migration. Both through actin polymerisation and actomyosin contractility, the cytoskeleton provides the main driving force for cell motility and is involved in establishment and maintenance of cell adhesion (Ridley, 2011). Cytoplasmic domains of transmembrane cell adhesion receptors (integrins in the case of cell-extracellular matrix contacts and cadherins in the case of cell-cell contacts) interact with actin binding proteins that link them to actin filaments (Krendel and Mooseker, 2005). Although highly organized, the cytoskeleton changes upon cues from a wide variety of sources, such as entry into mitosis or in response to external signals. The cytoskeleton interacts with dozens of associated motor proteins and other accessory proteins, which can mediate many such changes (Goode et al., 2000).

1.2.2 Cell motility in metastasis

The ability to invade other tissues and create metastases is considered one of the hallmarks of cancer (Hanahan and Weinberg, 2000). Cancer cells become able to change position within the tissues and to enter the lymphatic and blood vessels for dissemination into the circulation, and then undergo metastatic growth in distant organs (Friedl and Wolf, 2003). To spread within the tissues, tumour cells use migration mechanisms that are similar, if not identical, to those that occur in normal, non-neoplastic cells during physiological processes such as embryonic morphogenesis, wound healing and immune-cell trafficking (Friedl and Wolf, 2003). Invasiveness and metastasis are very complex processes, and an important field of study, since metastasis is the cause of 90% of deaths from solid tumours (Gupta and Massague, 2006).

For the cells to become metastatic, they must overcome numerous obstacles barring metastasis, multiple intrinsic mechanisms in the cell, as well as extrinsic barriers (Fidler, 2003). Factors in the tumour microenvironment that limit its progression include extracellular matrix components, basement membranes, reactive oxygen species, the limited availability of nutrients and oxygen and attack by the immune system, and can be classified as chemical, physical and biological in nature (Gupta and Massague, 2006). This means that the cell must meet certain requirements, which are reflected in several steps that create the biological cascade of metastasis (Gupta and Massague, 2006), summarised in Figure 2. These include the growth of the primary tumour (proliferation and angiogenesis), followed by a loss of cellular adhesion (detachment from the primary tumour), an increased motility and invasiveness, and then entry and survival in the circulation (in blood or lymphatic vessels). The cells can then exit into new tissue and start to colonise a distant site (survival in a new microenvironment). However, growth of the primary tumour is not a necessary step before metastasis, as micrometastases can be found even in seemingly small cancers (Mitas et al., 2001).
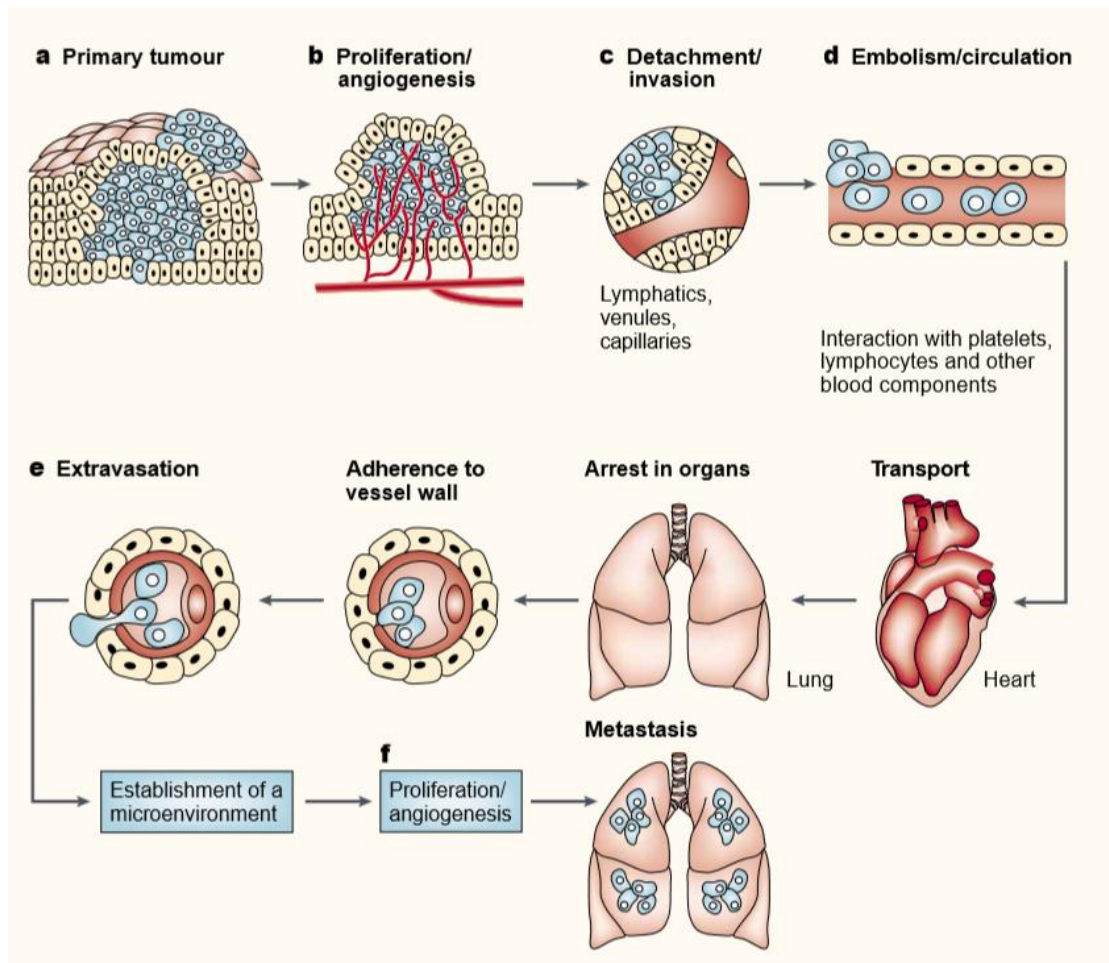
Figure 1.2 Main steps in the formation of metastasis. a) Cellular transformation and tumour growth. b) Vascularisation. c) Local invasion of the stroma by some cells. d) Detachment of some cells and entering the blood or lymphatic vessels. The cells can be trapped in the capillary beds of distant organs. e) Extravasation or leaving the bloodstream/lymphatic vessels. f) Proliferation within the new organ completes the metastatic process. To continue growing, the micrometastasis must develop a vascular network and evade destruction by host defences. Adapted by permission from Macmillan Publishers Ltd: Nature Reviews. Cancer (Fidler, 2003), copyright (2003)

The described process is broadly regulated by a developmental regulatory programme referred to as the 'epithelial-mesenchymal transition' (EMT), which has become implicated as a means by which transformed epithelial cells can acquire the abilities to invade, to resist apoptosis, and to disseminate. It is a multistep process where epithelial cells lose their cell-cell and cell-substratum adhesions and acquire properties required for independent cell migration (Polyak and Weinberg, 2009).

A molecular depiction of cell migration in *in vitro* models involves a continuous cycle of interdependent events: dynamic cytoskeletal changes, cell-matrix interactions, localised proteolysis, actin-myosin contractions and focal contact disassembly (reviewed in (Fidler, 2003; Friedl and Wolf, 2003; Gupta and Massague, 2006)). First, the moving cell becomes polarised and elongated. It can form filopodia, thin actin-rich protrusions which can probe the environment for cues (Heckman and Plummer, 2013). A pseudopod is formed via extension of the cell's leading edge. Then the lamellipodium elongates, a process that is driven by actin assembly into filaments, which connect to adaptor proteins and push the cell membrane in an outward direction. The pseudopod/lamellipodium attaches to the ECM (extracellular matrix) substrate and interacts with it via receptors from the integrin family, which create so called focal contacts. Surface proteases, such as matrix metalloproteinases (MMPs) are employed to cleave elements of the ECM, including collagen, laminins or fibronectins, and make space for the cell to move. Subsequently, regions of the entire cell body contract, generating force that leads to the gradual forward movement of the cell body and its trailing edge. This happens as a result of the contractile interaction between non-muscle myosin 2 and actin (actomyosin). Finally, at the rear edge of the cell, the tail detaches, disassembling the focal contacts, and then recycles all the molecules. Unlike physiological processes of cell invasion, the migration of tumour cells seems to be activated by a dominance of promigratory events in the absence of counteracting stop signals. This imbalance of signals allows cancer cells to become continuously migratory and invasive, leading to tumour expansion across tissue boundaries, followed by metastasis.

Cancer cells exhibit various types of cell migration, as individual cells or in solid cell groups, strands or clusters in 'collective cell migration' (Friedl and Wolf, 2003). Individual cells or leading cells in collective migration can use mesenchymal cell migration which depends on the cell's adhesion to extracellular matrix (ECM) (Kawauchi, 2012). Individual cells migrating *in vivo* can also have an amoeboid form of cell migration that involves low affinity substrate binding and is driven by acto-myosin protrusive forces (Friedl and Wolf, 2003; Kawauchi, 2012).

1.2.3 Filopodia and other protrusions

Migrating cells can exhibit different types of protrusions, including invadopodia, which contain proteases, podosomes, and filopodia (Heckman and Plummer, 2013). Filopodia are thin, finger-like protrusions that contain tightly packed parallel actin filaments and sense the microenvironment around the cell (reviewed in (Jacquemet et al., 2015)). The actin filaments are tightly packed into bundles by proteins such as fascin, and one of the myosins, Myo10, is known to transport various proteins, including transmembrane receptors, along actin filaments to the tips of filopodia (Figure 1.3). Tips of filopodia contain cell-cell and cell-ECM adhesion receptors, as well as cytokine receptors. By transporting integrins, a key family of adhesion receptors, filopodia play a central role in modulating cell adhesion (Albuschies and Vogel, 2013). Finally, filopodia and filopodial proteins make a critical contribution to cancer metastasis and therefore constitute attractive therapeutic targets to block cancer dissemination. Thus, an important focus for the future will be to identify compounds that inhibit filopodia formation and to assess their efficiency to block metastases both *in vitro* and *in vivo*.
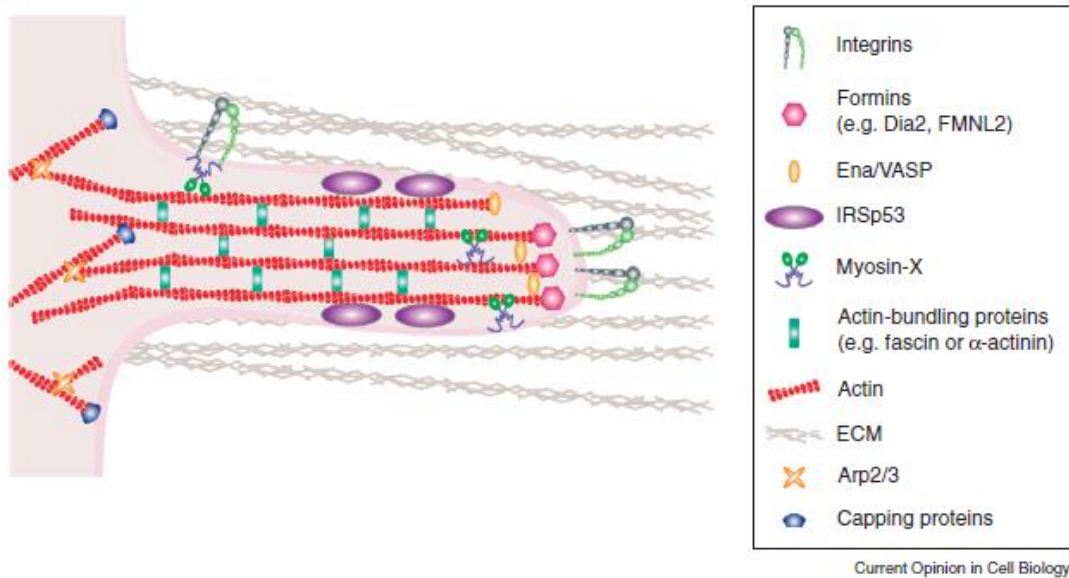
Figure 1.3 Schematic representation of a filopodium during cell migration on a planar substrate. Filopodia are in contact with the ECM. Filopodia extension is driven by actin polymerisation, mediated by proteins such as formins and regulated by actin capping proteins, actin regulators such as Ena/VASP (enabled/vasodilator-stimulated phosphoprotein), which promote actin filament elongation, and I-Bar proteins like insulin-receptor substrate p53 (IRSp53), which deform the plasma membrane (revised in (Arjonen et al., 2011)). Source: (Jacquemet et al., 2015).

1.3 Myosin superfamily

1.3.1 Myosins: structure and function

Myosins are a large family of motor proteins that are able to move along actin tracks, powered by adenosine triphosphate (ATP) hydrolysis (reviewed in (Berg et al., 2001; Coluccio, 2008). Next to microtubule-based kinesins and dyneins, myosins are the only motor proteins linked to actin, and they predominantly move to the barbed end of the actin filament. The only exception to date is the pointed end-directed motor myosin 6 (Myo6) (Buss and Kendrick-Jones, 2011). The myosin superfamily contains more than 20 distinct classes. In humans, as many as 40 genes for various myosins are expressed, which can be divided into 12 classes (Figure 1.4) (Foth et al., 2006; Peckham and Knight, 2009). Muscle myosins that build the thick filaments are the most well-known, but myosins are quite abundant: with each cell expressing up to ~20 different non-muscle myosin isoforms, depending on the cellular function (Berg et al., 2001).

The myosin protein family is diverse but all myosins share a similar body plan, which consists of 3 domains (e.g. non-muscle myosin 2 in Figure 1.5) (Berg et al., 2001; Coluccio, 2008):

a)   Motor domain ('head') at the N-terminus, which is conserved among isoforms and contains actin- and nucleotide-binding sites

b)   Lever domain ('neck'), which transmits the force and can be stabilised by binding of calmodulin or calmodulin-like regulatory proteins / light chains

c)   C-terminal domain ('tail'), which is highly diverse among different myosin classes and is responsible for cargo binding, thus dictating the function of each myosin (Foth et al., 2006)

Myosins from class 2, class 5 and class 18 can form dimers (reviewed in (Allsop and Peckham, 2011)). The remaining myosins are monomeric, which does not rule out the possibility that they could become dimerised in cells via adaptors. But at least as isolated molecules, these myosins should be

considered monomeric, which will have implications for their function and regulation (Peckham and Knight, 2009).
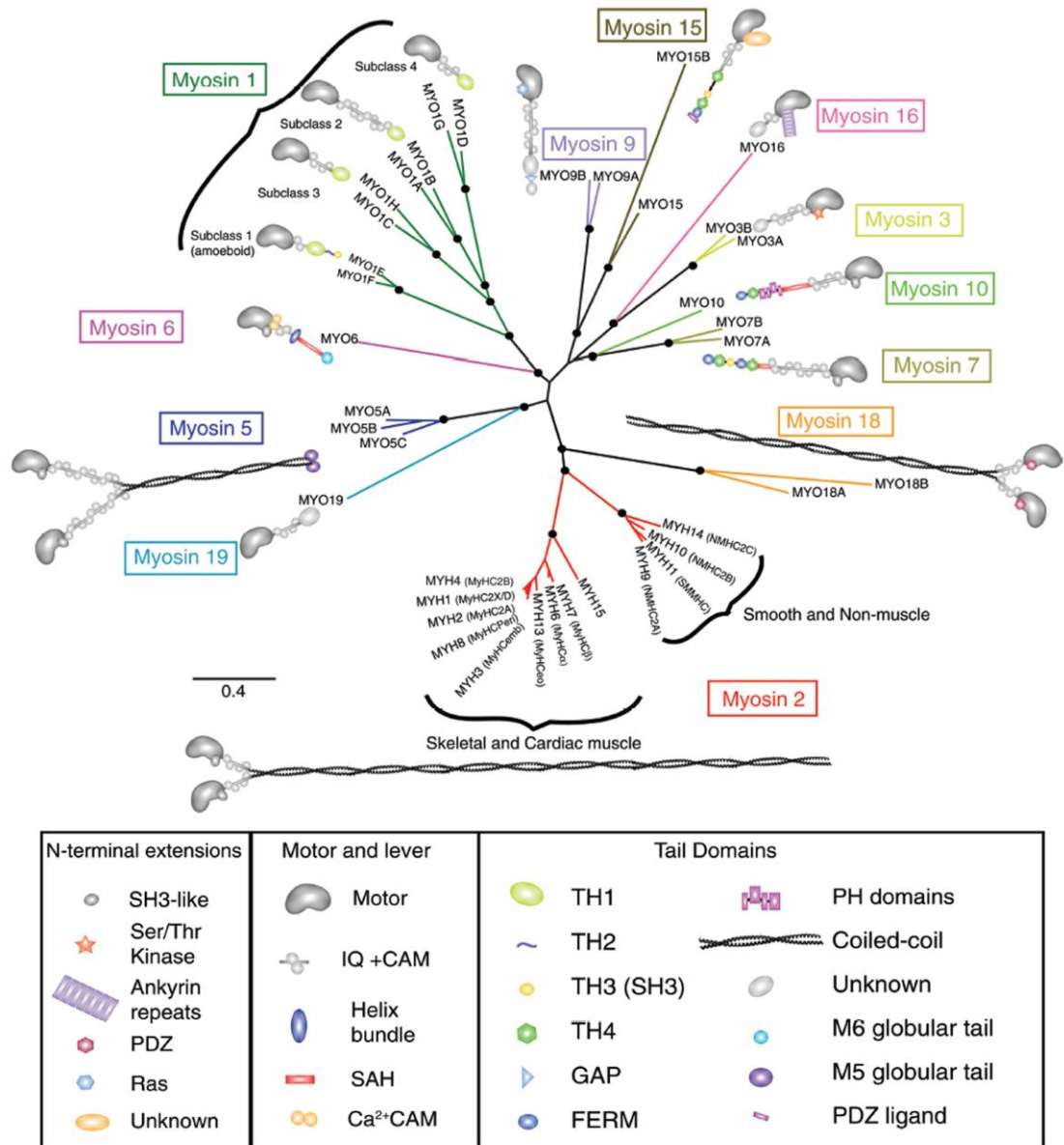
Figure 1.4 The myosin family tree in humans, generated using multiple sequence alignment of the motor domain sequences. The 39 genes encoding myosins are organised into 12 classes. Myosins have a variety of N-terminal extensions to their motor domains and diverse domains in their tail, depending on their function (Source: Peckham and Knight, 2009).

1.3.2 Conventional myosin: class 2

Class 2 skeletal muscle myosin, which plays a role in muscle contraction, was the first one to be studied biochemically (Coluccio, 2008). A myosin 2 molecule is a hexamer composed of two heavy chains and four light chains (Figure 1.5) (Bresnick, 1999). Muscle myosin dimers can be further assembled into thick filaments that promote the contraction of muscle fibres. In skeletal and cardiac muscle, the myosins assemble into bipolar filaments that contain 294 myosin molecules (reviewed in (Craig and Woodhead, 2006)). In smooth muscle, the myosins form side polar filaments that do not have a fixed number of myosin molecules (Murphy et al., 1997). Class 2 also includes non-muscle myosins, which form short bipolar filaments that contain 14-20 molecules (Billington et al., 2013). Class 2 myosins are also abundant in non-muscle cells, including non-muscle myosins 2a, 2b and 2c in humans (NM2A, NM2B and NM2C). Non-muscle myosin 2s are involved in important cellular functions, such as cytokinesis, karyokinesis, cell migration, cell polarity during migration and morphological changes (Saha et al., 2011). Class 2 myosins are known as conventional myosins, while the remaining myosins are referred to as unconventional.

Current Opinion in Cell Biology
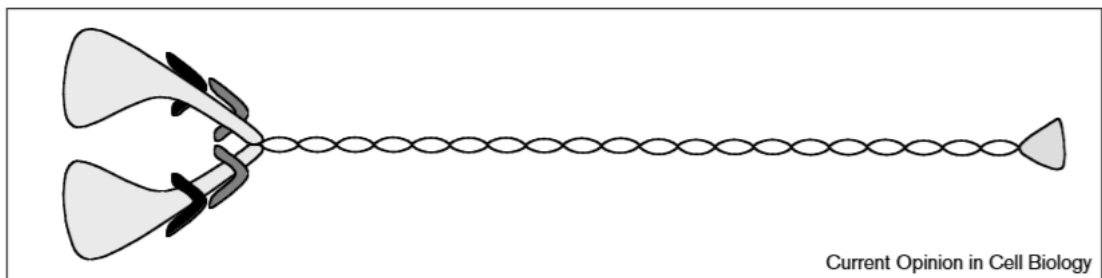
Figure 1.5 Schematic diagram of non-muscle myosin 2 (NM2). Dimer of heavy chains includes: motor and lever domain to the left (light grey) and tail domain (two tail domains forming a coiled coil and a C-terminal non-helical part of the tail at the end (light grey)). Two essential light chains (black) and two regulatory light chains (dark grey) bound to the neck region. Source: (Bresnick, 1999) Copyright © 2013 Landes Bioscience

1.3.3 ATPase activity

Binding of myosin to filamentous actin (F-actin) and its conformational changes are regulated by hydrolysis of ATP by the actin-activated Mg^{2+} ATPase in the motor domain (ATPase cycle), and subsequent release of products (ADP, Pi) (De La Cruz and Ostap, 2004). Briefly, in resting muscle, the myosin crossbridges contain ADP.Pi in their nucleotide binding pockets (the products of ATP hydrolysis). When the muscle is activated, myosin is then able to bind to actin in the thin filaments. Actin catalyses the release of phosphate (Pi) from the nucleotide binding pocket (active site), eliciting a conformational change in the motor domain which results in the 'power stroke' and as a result the motor also binds to actin more tightly. ADP is then released from the active site and ATP binds, and releases the motor domain from actin. ATP is then hydrolysed in the detached heads, and the cycle can continue. The small change in conformation in the motor domain resulting from the release of phosphate is amplified by the lever, to generate the 'power stroke'.

This cycle is common for all myosins, but the binding affinities and rate constants can be different, properties of each myosin being adapted for their cellular function (Allsop and Peckham, 2011; Berg et al., 2001; Hartman and Spudich, 2012). The proportion of time that myosin molecule spends strongly attached to actin over the entire ATPase cycle is called the duty ratio. The duty ratio varies among myosins, with skeletal myosins having a low duty ratio, and myosin 5 (Myo5) having one of the highest (De La Cruz and Ostap, 2004). The length of the lever arm is different among the classes of myosin motors, which results in different 'step' sizes (Hartman and Spudich, 2012). With each cycle of ATP hydrolysis, myosins take one step. Directed motion also depends on the lever arm, the long lever arm of Myo5 enables a large step of ~20nm, while the shorter lever arm of myosin 2 results in a shorter step of ~5-10nm.

1.3.4 Myosin regulation

Smooth muscle and non-muscle myosin 2 dimers bind essential light chains (ELC) that stabilise the neck domain and regulatory light chains (RLC) that stabilise the neck and regulate motor activity (Figure 1.5) (Trybus, 1994). Myosin 2 is regulated by phosphorylation of RLC, and in a fully dephosphorylated state it adopts a compact, folded structure, where the tail interacts with the motor domain (Ankrett et al., 1991). RLC is phosphorylated on different residues by several kinases, such as myosin light chain kinase (MLCK) or protein kinase C (PKC), suggesting that myosin 2 is subject of regulation by various signal transduction pathways (Beach et al., 2011; Ikebe and Hartshorne, 1985). Phosphorylation at Serine 19 by MLCK causes the myosin to change conformation, increases the actin-activated ATPase activity of the motor and promotes myosin 2 filament assembly (Craig et al., 1983; Dulyaninova and Bresnick, 2013). Several other proteins have been reported to regulate NM2 filament assembly, promoting the depolymerisation of myosin filaments. These include lethal giant larvae (Lvl) (Vasioukhin, 2006), MTS1 (S100A4) (Kriajevska et al., 1994) and S100P (Du et al., 2012) (reviewed in (Dulyaninova and Bresnick, 2013)).

Multiple regulatory mechanisms are known for unconventional myosins, including cargo binding, binding of calmodulin and calmodulin-like proteins (Akhmanova and Hammer, 2010). Similarly to myosin 2, myosins class 5 and 7 can also form compact molecules that have a very low ATPase activity (Umeki et al., 2011; Wang et al., 2008). Myo6 can be regulated by calcium binding via calmodulin, which affects its motor activity, or phosphorylation which correlates with its translocation in the cell (reviewed in (Buss and Kendrick-Jones, 2008)). The function of Myo10 is promoted by DCC (Deleted in Colon Cancer) and suppressed by neogenin, showing a differential balance through the function of different regulators (Liu et al., 2012). Two myosin-specific chaperones are also known in mammals, a "general cell" Unc45a and muscle-specific isoform, Unc45b (Price et al., 2002).

1.3.5 Myosins in a migrating cell

Myosins are abundant, with most cells expressing at least 20 different types of myosin which include representatives of at least six different classes of the myosin superfamily, including several myosin 1 isoforms, non-muscle myosin 2 (NM2) isoforms, and myosins 5, 6, 9 and 10 (reviewed in (Allsop and Peckham, 2011). Myosin isoforms have different mechanochemical properties, such as the duty ratio or processivity (reviewed in (Ouderkirk and Krendel, 2014)). For example, myosins with low duty ratio may function in rapid contractile events or serve as dynamic, short-lived tethers between actin filaments and the cargo, while isoforms with high duty ratio are suited to generating sustained tension. This diversity allows myosins to contribute to many processes important for cell motility, including cell migration and invasion through the extracellular matrix, regulation of protein and organelle localization, cell shape changes, and cell signalling.

Many myosins have multiple or partly overlapping functions which include roles in cell adhesion and intracellular motility, including cytoskeleton dynamics, endocytosis, exocytosis and secretory pathways (Allsop and Peckham, 2011). Myosins localise to a number of intracellular compartments and participate in many trafficking and anchoring events (Hartman Spudich 2012). These functions are often class-dependent and some of them are summarised in Figure 1.6. Class 1 myosins contain in their C-terminal tail membrane-binding and protein interaction domains. This allows them a simultaneous binding to phosphatidyl inositol phospholipids (PIPs) and vesicles and/or in the plasma membrane and other proteins necessary for active membrane deformation or intracellular vesicle trafficking, as well as cytoplasmic domains of transmembrane receptors (McConnell and Tyska, 2010; Wenzel et al., 2015). Class 5 myosins are well known to be involved in trafficking a variety of cargo in cells (Wang et al., 2008). Some myosins have a more specialised role, such as myosin 19 (Myo19), shown to traffic mitochondria in cells (Quintero et al., 2009) or a role in actin-based projections, such as myosin 10 (Myo10) present in filopodia (Liu et al.,

2012). Myo6 is associated with endocytic vesicles and endosomes (Buss and Kendrick-Jones, 2011). During cell migration, non-muscle myosin 2a (NM2A) is dynamic and responsible for the movement forward; by contrast, NM2B incorporates into preformed F-actin bundles and has a role in defining the rear of the migrating cell and tail retraction (Dahan et al., 2012; Swailes et al., 2006). The different location and expression levels of different non-muscle myosins are likely to play a major role in cell shape and cell-cell adhesion (Swailes et al., 2006). Myosin 2-dependent contractility may play an important role in coordination of cell migration and directional motility by preventing formation of lateral pseudopods and limiting pseudopodial/lamellipodial protrusion to the leading edge of the cell (Krendel and Mooseker, 2005).
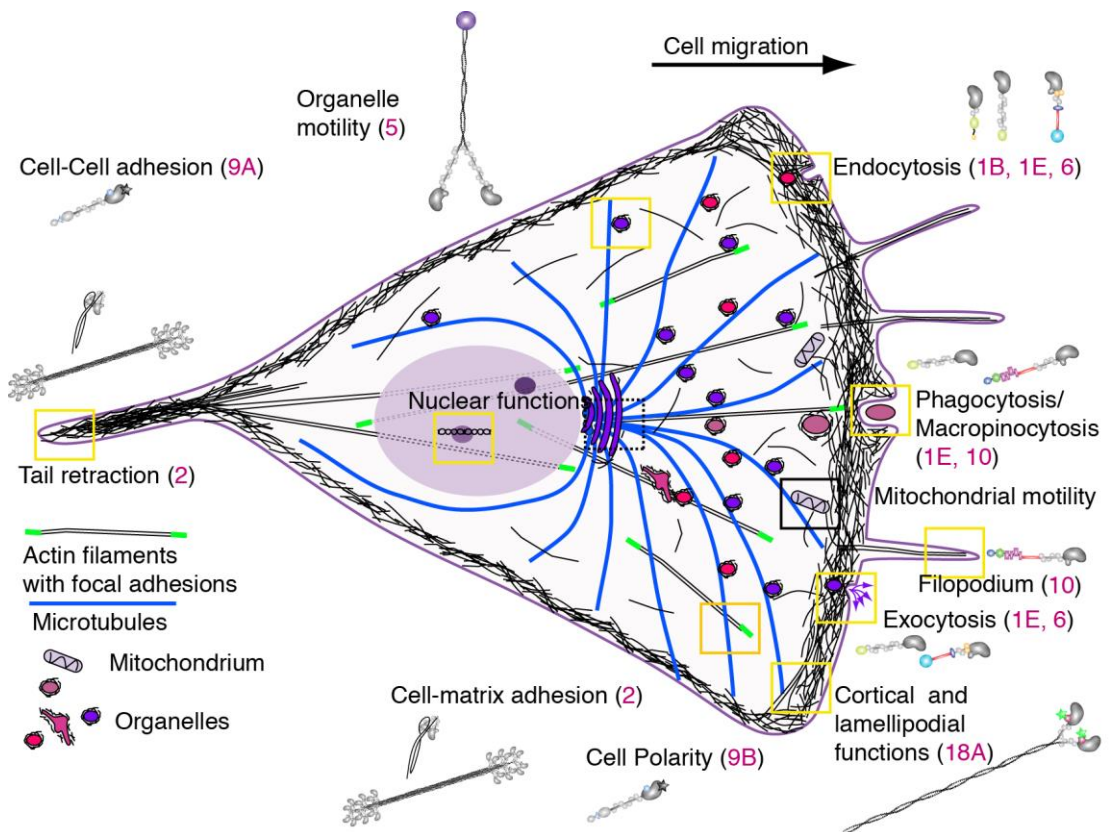
Figure 1.6 Myosins in a migrating cell. Various myosins have different functions (detailed description and references in the main text body). Class 1 myosins seen at the membrane; Myosin 2 responsible for contractility and tail retraction, among others; according to their functions, Myo6 involved in endocytosis, Myo10 at the filopodia; Myo18a in the lamellipodium. (From M. Peckham, with permission). Yellow boxes represent respective labelled processes (from left to right: tail retraction, nuclear function, organelle motility, cell-matrix adhesion, endocytosis, cortical and lamellipodial functions, exocytosis, phagocytosis/micropinocytosis, filopodium).

1.4 Objectives of this study

Despite multiple approaches available and considerate research effort, prostate cancer at metastatic stage remains largely untreatable, bringing the need to study the mechanisms responsible for prostate cancer progression and metastasis. The main aim of this project is thus to establish if myosins contribute to metastasis of prostate cancer. An initial screen identified the myosins present in prostate cancer cell lines and tissue, including isoforms upregulated in metastatic prostate cancer. This was followed by an analysis of chosen myosins on functional level using siRNA technique, to investigate their effect on morphology and migration of prostate cancer. Finally, I also looked at myosins in other types of tissue, including benign prostate cells and another type of cancer (glioblastoma).

Chapter 2
Materials and methods

2.1 Cell lines and cell culture

2.1.1 Prostate cancer and prostatic hyperplasia cell lines

LNCaP, DU145 and PC3 cells were obtained from ATCC. The BPH-1 cell line was a gift from Dr Sivaprasadarao, University of Leeds. Characteristics of the cell lines are described in more detail in Section 1.1.3. The cells were grown in RPMI-1640 with GlutaMAX™ (Gibco® Life Technologies™) supplemented with 10% heat inactivated FBS (foetal bovine serum) and antibiotics (penicillin (100 units/ml) and streptomycin (100 μg/ml), Gibco® Life Technologies™).

2.1.2 Matched pair of patient cells

1535 NP (Normal Prostate) and 1535 CT (Cancerous Tissue) cells, originally derived from primary adenocarcinomas from the prostate (Bright et al., 1997), were a gift from Suzanne Topalian, John Hopkins University School of Medicine, USA. They were grown in Keratinocyte medium (Gibco® Life Technologies™) supplemented with 10% heat inactivated FBS, 1% L-glutamate, antibiotics (penicillin (100 units/ml) and streptomycin (100 μg/ml), Gibco® Life Technologies™), bovine pituitary extract (50 μg/ml) and epidermal growth factor (5 ng/ml).

2.1.3 Glioblastoma cell culture

p53$^{lox/lox}$ /PTEN$^{lox/lox}$ or PTEN$^{lox/lox}$ glioma cell line (referred to also as glioma p53$^{-/-}$PTEN$^{-/-}$ and PTEN$^{-/-}$ in the text) derived from a mouse model was provided to us as a kind gift from Dr Stephen Rosenfeld, Department of

Cancer Biology, Cleveland Clinic Foundation (unpublished). The cells were grown in BBFP medium (2 units <u>B</u>asal medium, 1 unit <u>B</u>104-conditioned medium (see Section 5.2.2 below), supplemented with 10 ng/ml <u>F</u>GF and 10 ng/ml <u>P</u>DGF). Basal medium comprises: DMEM w/ 4.5 g Glucose, w/glutamine, w/Pyruvate (Gibco® Life Technologies™) with 0.1% (v/v) T3 (3,3′,5-Triiodo-L-thyronine, 20 µg/ml stock solution in DMEM), 1% (v/v) N-2 Supplement (Gibco® Life Technologies™), 1% (v/v) PSA (Penicillin, Streptomycin, Ampicillin; Invitrogen) and 0.5% (v/v) FBS. Cells were grown at 37°C with 5% CO_2 and passaged when reached about 75% confluence. Passaging, harvesting and fixing of the cells was performed as previously described for other cell types (see Sections 2.1 and 2.4). The glioblastoma cells required to grow on surfaces coated with Poly-L-Lysine (as described below in Section 2.1.3.2).

2.1.3.1 Preparation of B104-conditioned medium for glioma cell culture

B104 neuroblastoma cell line (Schechter et al 1984), a gift from Dr Stephen Rosenfeld, was recovered into warm D10 medium (DMEM w/ 4.5 g Glucose, w/ glutamine, w/ NaPyruvate (Gibco® Life Technologies™), 10% heat-inactivated FBS, 1% PSA) and grown at 37°C with 5% CO_2. After reaching confluence (2-3 days), the cells were passaged 1:10 (1 flask into 10, to provide high volume for harvesting the conditioned medium) and grown to confluence again. D10 medium was then replaced with Basal medium (see above Section 5.2.1), in which the confluent B104 cells were incubated for 48 h. B104-enriched medium was then collected, filter sterilised (0.2 µm pore size) and frozen for future use. B104 cells were incubated with fresh Basal media for another 48 h, collection was repeated and the B104 cells were discarded.

2.1.3.2 Coating flasks and coverslips with Poly-L-Lysine

Poly-L-Lysine stock (Sigma Aldrich) was diluted to 20 µg/ml with sterile, distilled H_2O and added to flasks in according volumes: 7 ml for T75, 2.5 ml

for T25, 1 ml for 6-well plates and 0.5 ml or less for 4-well plates. Flasks/plates were then incubated for > 15 min at 37 °C, the liquid was removed and the dishes were left to dry overnight in the incubator at 37 °C without tightly closing the lid if necessary. The plates and flasks were then stored at 4 °C degrees for further use, up to 3 months.

2.1.4 Cell culture

All cells were grown at 37°C with 5% CO_2 and passaged when they reached about 75% confluence. To passage the cells, the medium was removed and the adherent cells were washed once with phosphate buffered saline (PBS, Gibco® Life Technologies™). Cells were then incubated with the trypsin substitute, TrypLE (Gibco® Life Technologies™) for 1 minute, resuspended in fresh medium, centrifuged at 1000 g and resuspended in fresh medium again, in a ratio of 1:3 to 1:5. To harvest cells for downstream analysis (i.e. RNA or protein extraction), cells were detached from the flask with TrypLE, resuspended in fresh medium, centrifuged at 1000 g and washed with PBS. EZ-PCR MycoplasmaTest Kit (Geneflow Ltd) was routinely used to check the cell lines for the presence of any mycoplasma contamination. To seed cells for experiments, the cell density of resuspended cells was estimated using a haemocytometer.

2.2 GEO expression analysis

Gene Expression Omnibus (GEO) Database is a public functional genomics data repository (http://www.ncbi.nlm.nih.gov/geo/). Data deposited there is compliant with MIAME (Minimum Information About a Microarray Experiment) guidelines. In the Database, array- and sequence-based data are accepted and tools are provided to help users query and download experiments and curated gene expression profiles.

Gene expression profile GEO GSE 6919 (Chandran et al., 2007; Yu et al., 2004), comprising 171 patient samples, was one of the largest data sets with

prostate cancer samples. It was also most comprehensive with regards to the number of myosin genes looked at, with data on 15 out of 28 non-muscle myosin genes that were of interest. The set included 81 samples of normal, benign tissue, 65 localised tumour samples and 25 samples from metastatic prostate cancer. The 81 "normal" samples comprised 18 normal prostate tissue samples free of any pathological alteration from organ donor and 63 normal prostate tissue samples adjacent to tumour from patients. These were pooled together for clarity after no significant differences in myosin expression were noted between the two groups. Similarly to what has been previously described (Arjonen et al., 2014), the raw data from a microarray was downloaded, transformed into a log2 format and the subsets for different myosin isoforms were compared using statistical analysis.

2.3 Reverse transcription – PCR

2.3.1 RNA extraction

RNA was extracted using RNeasy Mini Kit (QIAGEN) according to the manufacturer's instructions. Briefly, cell pellets were collected as described in Section 2.1.3, washed once with PBS and centrifuged (1000 g, 5 min.). Pellets were lysed and homogenised in the presence of denaturing guanidine-thiocyanate–containing buffer (with the addition of β-mercaptoethanol (Sigma-Aldrich)), which inactivates RNases. 70% ethanol was added to precipitate RNA and the lysate was applied onto a silica-based membrane, which was then centrifuged (10000 g, 15 sec.). In this process, RNA binds to the membrane while contaminants, such as the remnants of proteins, salts or organic compounds, are washed away. RNA was eluted in 30 µl of nuclease-free water and a spectrophotometer (NanoDrop™, Thermo Scientific) was used to quantify the amount of RNA obtained by measuring the absorbance of the samples at 260 nm.

2.3.2 cDNA synthesis

cDNA was synthesised from 2 µg of RNA. The reaction mix contained: AMV (Avian Myeloblastosis Virus) Reverse Transcriptase (final concentration 1 unit/µl, Promega), AMV Reverse Transcriptase Reaction Buffer (Promega), dNTP mix (final conc. 1 mM) (Invitrogen Life Technologies™), 0.5 µg Oligo(dT)15 Primers (Promega), 0.5 µg Random Primers (Promega) and nuclease-free water (Sigma-Aldrich). 2 µg of RNA suspended in 11 µl of nuclease-free water was first incubated at 65 °C for 3 minutes to remove any secondary structures that could impede cDNA synthesis. The reaction mix was then added and the mixture (total volume of 20 µl) was incubated at 42 °C for 60 minutes, which is the optimum temperature for reverse transcriptase activity. The reaction was then stopped by incubating at 95 °C for 5 minutes to denature the enzyme.

2.3.3 PCR Reaction

Out of 39 myosin genes expressed in humans, 28 were tested. Skeletal, cardiac and smooth muscle myosin genes (11) were not included as we did not expect these genes to be expressed in non-muscle cells. Gene-specific primers were designed by Dr Kathryn White (Table 2.1) and used to determine the presence of mRNA for each of the myosin genes in the cell lines.

The reaction mix contained: Taq DNA Polymerase (50 units/ml, New England Biolabs), ThermoPol Reaction Buffer (New England Biolabs), forward and reverse primers (0.4 µM each, see Table 2.1 for sequences), template DNA (2 µl of 2 µg/ml solution). The reaction conditions were:

- Initial denaturation: 96 °C, 2 minutes
- 30 cycles:
    - denaturation: 96 °C, 20 seconds
    - annealing: 54 °C, 20 seconds
    - extension: 72 °C, 20 seconds
- Final extension: 72 °C, 7 minutes

Table 2.1 Sequences of primers used for PCR reactions.

MYOSIN	FORWARD (5' → 3')	REVERSE (5' → 3')
MYO1A	GGCAGATTTCATCTACAAGAGCA	GTTTGTGGATGGCAAATTGTT
MYO1B	GGGCTTACTGGCTTGGATCT	ACAGCAACTGCATGCTTACG
MYO1C	CTCATCACCAAGGCCAAGA	CCTTTATCACCGAGAATTCAGC
MYO1D	CCCTGCAGACGATTTTCAATA	TGCAACCTTTGCCCTGAC
MYO1E	CAAGACCGTCCGGAACAA	CCACCTGGACTGAACTGGAT
MYO1F	AGACTGTGCGCAACAACAA	CGGCTGAACTGGATCTCAA
MYO1G	CTTCCACGCCTTCTACCAAT	TCTCCAAGTGCAGTTCATGC
MYO1H	ATAGCCCGTGACAGACTGCT	GGAGCGTTCTGGCATTTC
NM2A	TGGAGGACCAGAACTGCAA	GGTTGGTGGTGAACTCAGCTA
NM2B	ATGAACCAGAAACGGGAGGT	AAGGACTCCAAGAGGGGTGT
MYO3A	GAAAAATTAATCAACCTGGCAAA	TGGTTGTCTCTCTGGCATGA
MYO3B	TGTCTTCTCGGATATGCCATC	TGCAAGACCATTTTCTGAACC
MYO5A	GCGTCGGAGCTCTACACAA	TTGAGCAGCTCTGCTGACTT
MYO5B	CCTACCAAGGCCTAAAGCAAG	CCTCCTCCTCATGCTCCA
MYO5C	AAAGACCTTCACGCTTCTGG	GCGGTGATCTGCACATTG
MYO6	CTCCAGCTTCACCCGTACA	CGATCTCCTGTTTCCACTATCC
MYO7A	GCTGGCAGGTCACTGAGAGT	AATCACCATGGTCCCAAGTC
MYO7B	CAAGCACGCAGGGAAGTC	TTTGGCTCCGTAGTTTGCTC
MYO9A	CAGATAACAAAGAAACCCCTCAG	TCCACCGTGAAGCAATCC
MYO9B	CAACCAGCACATCTTCAAGC	TGTTGTGCCACGTGATCC
MYO10	AGGACTTTCCACCTGATTGC	CGTGGACCTGACTCAGCA
MYO15A	ATGAACCAGAAACGGGAGGT	AAGGACTCCAAGAGGGGTGT
MYO15B	GATGCCTACGGCTTTGAGG	GGCTGGAGAAGAGCTGTAGG
MYO16	CCTGCGTGAGAAGAAGGAAC	CACTTTTCGGACTCCCATCT
MYO18A	GGACATGGTGACAAAGTATCAGAA	TTTGACAACCAGGACTTGACC
MYO18B	AGCATGGCCATCTCATCAC	TCTTGTCCTCTTCCCGAATC
MYO19	CGCAGACCTTTCTCCAAGAG	GATATGGATGGTCTCCACGAG
HOUSEKEEPING GENES:		
GAPDH	GAAGGTGAAGGTCGGAGTC	GAAGATGGTGATGGGATTTC
18S rRNA	GTAACCCGTTGAACCCCATT	CCATCCAATCGGTAGTAGCG

2.3.4 Analysis of the PCR results: agarose gel electrophoresis

Agarose gel was prepared by dissolving agarose in TAE buffer (40 mM Tris-Acetate, 1 mM EDTA) at 1% or 2% (w/v) concentration, depending on the size of the DNA fragments being compared. 0.01% ethidium bromide (Fischer Scientific) was added to the gel to enable the detection of DNA using UV light in the GelDoc Image System. The samples were loaded along with molecular markers of appropriate size (New England Biolabs).

2.4 Real-time or quantitative PCR (qPCR)

cDNA was synthesised as described above (Section 2.3.2). Relative myosin expression was monitored by Real-time PCR using SYBR® Green to detect the reaction product (see Table 2.1 for sequences of primers). Analysis was performed using BIO-RAD system and software.

The reaction mix contained: 12.5 µl of iQ™ SYBR® Green Supermix (2x mix containing: dNTPs, iTaq™ DNA polymerase, $MgCl_2$, SYBR® Green I, enhancers, stabilizers, fluorescein) (BIO-RAD), 1 µl of forward and reverse primers (to final concentration of 0.4 µM), template cDNA (5 µl of 40 ng/ml solution (2 µg/ml stock solution diluted 1:50) for the samples; 5 µl of respective serial dilutions for the standard curves, as explained below) and 6.5 µl nuclease-free H_2O. qPCR is a method of relative quantification, and so standard curves were always run for reference, next to the unknown samples. Standard curves were prepared as follows: cDNA (2 µg/ml solution) from the tested specimen was mixed in equal amounts. The mix was then diluted 1:20 (considered 100%) and diluted into 2x serial dilutions of 50%, 25%, down to 3.125%. No template control (NTC) with nuclease-free H_2O instead of cDNA was included in each run.

The optimised reaction conditions were as follows:

- Initial denaturation: 95 °C, 3 minutes
- 40 cycles:
    - denaturation: 95 °C, 10 seconds
    - annealing: 65 °C, 10 seconds
    - extension: 72 °C, 30 seconds
- Denaturation: 95 °C, 10 seconds
- Melt curve: 65 °C to 95 °C, increment 0.5 °C per 5 seconds

SYBR$^{®}$ Green is a general intercalating dye, so melting curves were included in each run to ensure reaction specificity.

2.5 Antibodies

Primary antibodies used in this study can be found in Table 2.2.

Other used antibody and reagents include: HRP-conjugated secondary antibodies for western blotting (Sigma, UK), fluorescent secondary antibodies for immunostaining (Molecular Probes), DAPI and fluorescently-labelled phalloidin for nuclei and F-actin staining, respectively (Sigma, UK).

Table 2.2 Primary antibodies used in this project.

Specificity	Size of the target [kDa]	Organism	Concentration used	Supplier / catalogue number
Myo1b	127	Rbt	WB 1:2000, IF 1:100	Sigma, HPA013607
NM2A	220	Rbt	WB 1:10000, IF 1:500	Biolegend, PRB-440P
Myo6	150	Rbt	WB 1:200, IF 1:50	Santa Cruz, sc-50461
Myo9b	244	Rbt	WB 1:200 IF 1:100	Protein Tech, 12432-1-AP
Myo10	237	Rbt	WB 1:5000, IF 1:100	Sigma, HPA024223
Myo18a	233	Rbt	WB 1:500, IF 1:50	Custom made by Genscript (specific to C-term)
ERK	44	Rbt	WB 1:1000	Cell Signalling, 9102S
GAPDH	36	Rbt	WB 1:2000	Sigma, G9545
Paxillin	65	Mo	IF 1:100	BD Biosciences, #610569
pMLC	18	Mo	WB 1:500	Cell Signaling, #3671
EEA1	162	Rbt	IF 1:100	Cell Signaling, Antibody #2411
DCC	158	Mo	WB 1:1000	Thermo Scientific, #3675S

2.6 Western blotting

2.6.1 Protein extraction

Cells were harvested as described above, cell pellets were then washed once with PBS and centrifuged at 1000 g for 5 min. The pellet was resuspended in 50 µl of lysis buffer (150 mM NaCl, 0.05 M Tris (pH 8), 1% Triton X-100, 1 mM EDTA (pH 8) in double distilled water), which additionally contained protease inhibitors (Halt Protease Inhibitors Cocktail, Thermo Scientific Pierce), added at the time of experiment. The inhibitors included in this cocktail are: AEBSF, aprotinin, bestatin, E-64, leupeptin and pepstatin A.

Cells were incubated 30 minutes at 4 °C, with vortexing every 4-5 minutes to facilitate lysis. The lysates were clarified by centrifugation at 16 000 g for 20 min (at 4 °C).

2.6.2 Protein quantification

Protein samples were quantified using the BCA assay (Micro BCA™ Protein Assay Kit, Thermo Scientific) according to the manufacturer's instructions. Samples for the calibration curve were prepared from a stock solution of bovine serum albumin (BSA, 2 mg/ml), with serial solutions from 2.5 to 100 µg/ml in distilled water. Protein extracts (diluted 1:100) and standard curve solutions were placed in a 96-well plate (in triplicates). An equal amount of working reagent was added to each well, mixed gently by shaking and incubated for 2 hours at 37°C. After cooling the plate to room temperature, the absorbance was measured at the wavelength of 540 nm using a colorimetric plate reader (POLARstar Optima, BMG Labtech). The protein concentration in the experimental samples was calculated from the calibration curve created with BSA standard samples.

2.6.3 Separation of proteins by SDS-PAGE

SDS-PAGE (SDS – polyacrylamide gel electrophoresis) separates proteins on the basis of their molecular size. To prepare the electrophoresis samples, 40 µg of each protein sample was mixed with 2x concentrated gel loading (Laemmli) buffer (4% (w/v) SDS, 20% glycerol, 120 mM Tris-Cl (pH 6.8) and 0.02% (w/v) bromophenol blue (BFB)). Samples were then denatured for 10 min in 100 °C to use on 7.5% or 15% polyacrylamide gels.

The stacking gel contained: 4% acrylamide/bisacrylamide (37.5:1 ratio), 125 mM Tris-HCl (pH8), 0.1% (w/v) SDS, 0.05% (w/v) ammonium persulfate (APS), 0.1% Tetramethylethylenediamine (TEMED). The separating gel mix contained: 7.5% or 15% acrylamide/bisacrylamide (37.5:1 ratio), 375 mM Tris-HCl (pH6.8), 0.1% (w/v) SDS, 0.05% (w/v) APS, 0.1% TEMED. APS and TEMED were added immediately before pouring the gels to catalyse

acrylamide polymerisation. The lower % acrylamide gels were used when subsequently blotting for myosin heavy chain, which has a molecular weight of ~200-250kDa. The higher percentage acrylamide gels were used when subsequently blotting for low molecular weight proteins (e.g. myosin light chain).

The protein samples were loaded along with the molecular markers (PageRuler™ Plus Prestained Protein Ladder, Thermo Scientific) and electrophoresis was run at 100 V for about 2 hours. Gels were routinely run in duplicates, and one of each pair was stained using Coomassie Blue or Instant Blue (Expedeon) and imaged using the Biorad GelDoc® Image System.

2.6.4 Immunoblotting

A fully submerged system was used to transfer the proteins from the gel to a nitrocellulose membrane with 0.45 or 0.2 μm pore size, depending on the size of proteins analysed (Amersham™ Hybond™-ECL, GE Healthcare). (The lower pore size was used for low molecular weight proteins). The transfer sandwiches were immersed in 1 x transfer buffer (Thermo Scientific, #35050) and transfer for carried out at 250 mA for 1-2.5 hours, depending on the size of the proteins under investigation. After the transfer, membranes were blocked in 5% non-fat milk in PBS (w/v) for 1 hour at room temperature and incubated with respective primary antibody solution in 2% non-fat milk in PBS (w/v) (Table 2.2) at 4 ºC with rolling overnight. The membranes were washed in PBS with 0.05% Tween (3 times for 5 minutes, once for 15 minutes), once with PBS for 5 minutes. Membranes were then incubated with HRP-labelled secondary antibody in 2% non-fat milk in PBS (w/v) for 1.5 h at room temperature with rolling and washed as previously.

Chemiluminescence detection was performed according to manufacturers' instructions (West Pico Chemiluminescent, Thermo Scientific). The membranes were exposed to light sensitive (X-ray) film, with multiple exposure times to ensure the signal was within linear range and over-

saturation was avoided. The films were then scanned and analysed using ImageJ.

The stripping solution, Restore Western Blot Stripping Buffer (Thermo Scientific) was used to re-use and re-probe the membranes if required. After stripping, the membrane was again blocked as described above, before use in Western blotting.

2.7 Immunostaining and imaging of fixed cells

Cells were seeded on glass coverslips and grown according to the respective experiment. Cells were fixed using 2% paraformaldehyde (PFA) for 20 min at 37 °C, washed 3 times with PBS, permeabilised with 0.1% Triton X-100 in PBS for 5 min and blocked with 3% BSA in PBS (w/v) for 30 min at room temperature. Cells were incubated with primary antibody in 3% BSA in PBS for 1 h at room temperature, washed 3 times in PBS with 0.05% Tween, 2 times with PBS and incubated with fluorescently-labelled secondary antibody in 3% BSA in PBS for 1 h at room temperature in the dark. Cells were then washed again as above and incubated for a further 20 min in the dark with phalloidin (labelled with either Alexa Fluor 488 or 546 (A12379 and A22283, Thermo Scientific) and DAPI in PBS, for actin and nuclei staining. This was followed by a final wash (as above) and mounting with Prolong Gold mounting medium (Invitrogen). Images of cells were obtained either using a Zeiss LSM700 confocal laser scanning microscope, using the accompanying LSM software, or using DeltaVision Deconvolution inverted system. Images were subsequently processed to generate figures using Photoshop. The images presented are representative of at least 3 separate experiments.

2.7.1 Measurements within images

Filopodia per cell were counted manually for 20 cells in at least 3 separate experiments. Cell area was quantified using ImageJ, using images of cells

stained for actin and the ROI (Region of Interest) Manager tool. Actin bundles were also quantified in ImageJ using images of cells stained for actin. A line scan was drawn across the lamella from edge to middle of the cell, followed by an intensity profile and counting the peaks.

2.8 Transfections

2.8.1 Transfections using small interfering RNA (siRNA)

siGENOME siRNA SMARTpool Human or Mouse and a non-targeting control (GE Healthcare Dharmacon Inc., UK) were used in this study. siGENOME individual siRNA reagents were also used in case of Myo10 where specified. Following the manufacturer's instructions, siRNA reagents were re-suspended to a final concentration of 10 μM in siRNA buffer (60 mM KCl, 6 mM HEPES-pH 7.5, 200 μM MgCl$_2$). Cells were seeded at a density of 20 000 cells/ml in growth media, allowed to adhere to the coverslips/plates and grown overnight. Before transfection, growth medium was replaced with antibiotic-free growth medium. Lipofectamine® RNAiMAX Reagent (Invitrogen™, Life Technologies™, UK) was used for transfections, following the manufacturer's instructions. siRNA and the transfection reagent were first incubated separately in serum-free media for 5 min (1 pmol for 96-well plates, 5 pmol for 4-well plates and 25 pmol for 6-well plates) and then mixed at a 1:1 ratio and incubated together for 20 min at room temperature. The mix was then added to the cells which were grown for further 72 hours before analysis (i.e. staining, immunoblotting, migration assays). A time-course experiment was first performed and it was established that optimum knockdown was achieved after 72 hours.

2.8.2 Overexpression of GFP-labelled Myo10

PC3 and LNCaP cells were transfected with a peGFPC2 plasmid for GFP-Myo10 expression (Berg and Cheney, 2002). Cells were seeded at a density of 75000 cell/ml in growth media on glass coverslips and allowed to grow

overnight. FuGENE® 6 Transfection Reagent (Promega) was used for the transfections. Cells were then allowed to grow for 24 or 48 hours, fixed and immunostained as previously described (see Section 2.7).

2.9 Random cell migration assay in 2D

Cells were plated into glass-bottomed 96-well plates at 5 000 cells/well and transfected as described above. Cells were grown at 37°C for 48 hours, serum starved for 24 hours prior to stimulation with HGF (hepatocyte growth factor, Sigma), and then treated with HGF (25 ng/ml). The cells (a minimum of 3 fields for each replicate or experimental condition) were then filmed overnight, capturing images at 5 minutes intervals using a 20x lens (512 x 512 total pixel size, 2 x 2 binning), and differential interference optics, on a DeltaVision Deconvolusion system (inverted) with motorised stage and incubator. Cell migration was analysed using ImageJ software (MTrackJ plugin).

2.10 Circular invasion assay (3D-like migration)

3D-like migration was examined using a modified circular invasion assay (Yu et al., 2012). Self-adhesive cell-stoppers (Ibidi, #80209) were used to create a cell-free space. Cells were seeded and transfected as described above (Section 2.5) and after 72 h, the stoppers were removed. The cells were then washed gently and covered with a thin layer of Matrigel (4 mg/ml). Pre-cooled tips and tubes were used when handling Matrigel. Cells with a thin layer of Matrigel were left to gelify in the incubator for 20 min in 37 °C and then covered with normal media and allowed to grow and migrate into the matrix for another 24-48 hours. Cells were then fixed in 2% PFA and stained using standard procedures described above.

2.11 Statistics

Data analysis All the data were analysed with the help of GraphPad Prism 5.0 programme (GraphPad Software, La Jolla, California, USA) and is presented as mean with SD or SEM, for at least three separate experiments (n ≥ 3). Two-way ANOVA was used to compare differences between groups and statistical significance was accepted for $P \leq 0.05$.

Chapter 3
Myosin expression and localisation in prostate cancer

3.1 Introduction

Cancer metastasis is a complex process that requires dramatic spatial and temporal reorganisation of the cell cytoskeleton (Fife et al., 2014). While the cytoskeleton components are well regulated in normal cells, mutations or aberrant expression of cytoskeletal and cytoskeleton-associated proteins are often observed in cancer cells (Fife et al., 2014). Myosins are an example of actin-associated protein family with various, isoform-specific roles in the cell (See Section 1.3). Among other functions, myosins play a role in cell polarity and motility, cell adhesion, through their functions in endocytosis and exocytosis they are involved in recycling of cell-adhesion molecules (Allsop and Peckham, 2011).

It is therefore not surprising that some myosin isoforms have already been implicated in cancer. Myosin 1a (Myo1a) has been shown to be frequently inactivated in colorectal cancer, which results in higher tumour growth and accelerated progression (Mazzolini et al., 2013). Myosin 1b (Myo1b) can promote migration of head and neck squamous cell carcinoma (HNSCC) (Ohmura et al., 2015). Myosin 1e (Myo1e) is part of gene signature for basal-like breast cancer with poor prognosis (Hallett et al., 2012). Mutations in Myo1f were found in infant acute leukaemia (Duhoux et al., 2011). NM2A is important for breast cancer invasiveness (Derycke et al., 2011) and NM2B is down-regulated in non-invasive variant of melanoma cells where it is supposed to play a role in melanoma migration by retracting the tail during the migratory cycle (Jacobs et al., 2010). Both NM2A and NM2B have been connected with invasiveness of ovarian cancer (Iwanicki et al., 2011), migration of glioma (Beadle et al., 2008) and development of carcinogen-induced tumours (Saha et al., 2011). Myosin 5a (Myo5a) is required for

cancer cell metastasis by affecting cell motility, and its expression levels positively correlate with metastatic capabilities of several human cancer cell lines (Lan et al., 2010). Myosin 5b (Myo5b) is down-regulated in gastric cancer, which has to do with enhanced MET signalling (Dong et al., 2013). Genetic polymorphisms in myosin 9b (Myo9b) can play a role in aetiology of oesophageal cancer, by increasing the permeability of the epithelial barrier (Menke et al., 2012). Myosin 10 (Myo10) was recently shown to be upregulated in breast cancer with a role in invasiveness and metastasis (Arjonen et al., 2014; Cao et al., 2014) and to have a role in metastasis of lung cancer (Sun et al., 2015). Changes in expression and mutations of myosin 18b (Myo18b) have been correlated to lung, colorectal and ovarian cancer (Nakano et al., 2005; Tani et al., 2004; Yanaihara et al., 2004). When it comes to prostate cancer, so far a strong link has been found between the disease and myosin 6 (Myo6) (Dunn et al., 2006). Myo6 is upregulated in medium-grade tumours and in the LNCaP cell line, where it is involved in protein secretion (Puri et al., 2010). Myo6 is also overexpressed in ovarian cancer (Yoshida et al., 2004).

It is worth noting that many of the described studies focus on a correlation between the disease and expression levels or mutations in myosins, whereas the detailed function of myosins in cancer progression remains unexplored in many cases. As pointed out in a recent review (Ouderkirk and Krendel, 2014), to examine the connections between myosins and cancer, it is important to distinguish between data from findings *in vitro* and genetic, epigenetic or transcriptomic studies of samples *in vivo*. A combination of both of these aspects can offer a strong support for a role of myosin isoform in tumour suppression or progression, which makes looking at the role of myosins in cancer an exciting area of study. At the same time, the complexity of processes and cytoskeleton dynamics during metastasis poses a great challenge. We decided to tackle this question and look at myosins in prostate cancer, to see by a comprehensive study if they are involved in tumour cell migration, invasion and metastasis. In the first part of the study, I looked at the expression of myosins in prostate cancer.

Subsequently, I sought to find out if expression levels of myosin isoforms change in prostate cancer models with different metastatic potential. I also looked at localisation of several of the upregulated isoforms.

3.2 Results

3.2.1 Analysis of myosin expression in patient tissue using the GEO Database shows significant changes in expression for some myosin isoforms

To examine expression of myosins in prostate cancer patients, I first performed an *in silico* analysis of gene expression profile of a large prostate cancer data set (GEO GSE6919) (Chandran et al., 2007; Yu et al., 2004). The high-throughput screen initially analysed almost 40,000 genes, about half of which were consequently discarded (genes whose expression was very similar throughout all the samples and genes consistently displaying low levels of expression that yielded high error rate).

Among almost 20,000 genes, data on 15 myosin isoforms were available for analysis: MYO1A, MYO1B, MYO1C, MYO1D, MYO1E, MYO1F, MYH9 (referred to as NM2A), MYH10 (referred to as NM2B), MYO5A, MYO6, MYO7A, MYO9B, MYO10, MYO16 and MYO18A. I compared the expression levels between normal prostate tissue, localised tumour and metastatic tumours, and I found significant differences in expression levels of 7 of the isoforms analysed (Figure 3.1).

MYO1B and MYO10 expression increased significantly from benign tissue to localised tumour to metastases. Expression levels of MYO1D and MYO1F showed significant increase in metastatic samples in comparison to normal tissue. Expression of MYO5A and MYO9B increased significantly in localised tumours when compared to benign tissue and seemed to slightly decrease in metastatic tumours, although these differences were not significant. MYO6 levels were higher in localised and metastatic tumours than in normal tissue. Again, the expression levels seemed to be lower in metastases than in localised tumours but these differences were not significant. The remaining myosins (MYO1A, MYO1C, MYO1E, MYH9 (NM2A), MYH10 (NM2B), MYO7A, MYO16 and MYO18A) have not shown significant differences in their expression levels.
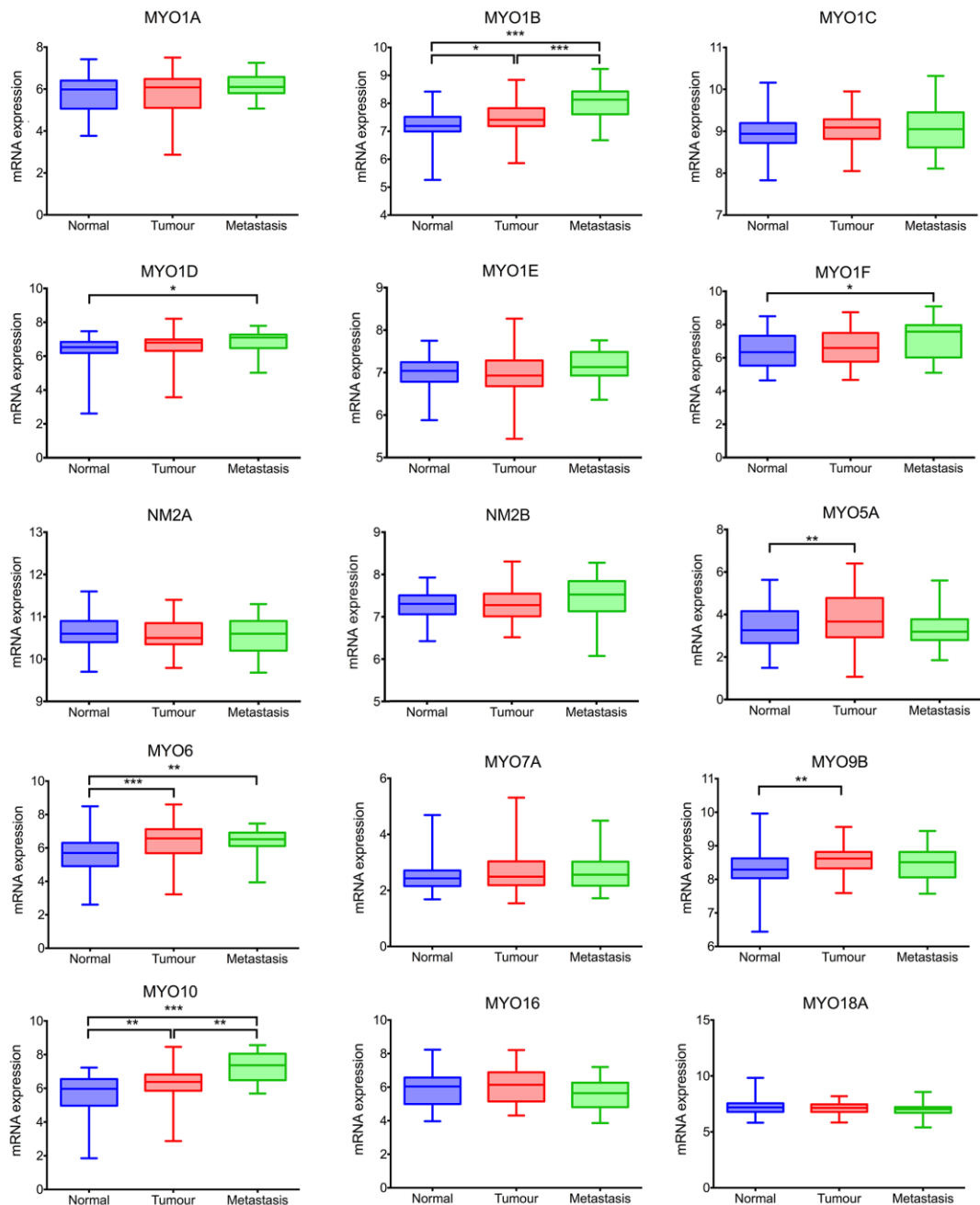
Figure 3.1 Analysis of myosin isoform expression in prostate cancer tissue from patients, based on GEO Microarray expression profile (Accession number: GSE6919). Data for normal prostate tissue (n=81, blue), localised tumours (n=65, red) and metastatic tumours (n=25, green) presented on a log2 scale using box and whisker plots. Statistical analysis was performed using one-way ANOVA. Levels of significance are indicated by: $p < 0.05$ statistically significant (*), $p < 0.01$ very significant (**), $p < 0.001$ extremely significant (***).
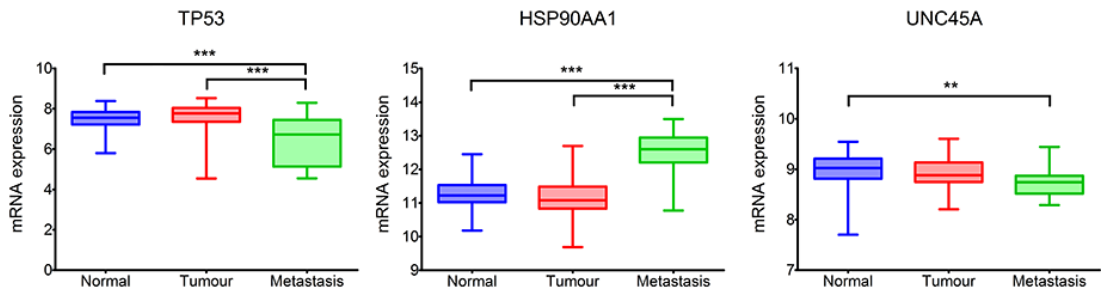
Figure 3.2 Expression of TP53 and chaperones in prostate cancer tissue from patients, based on GEO Microarray expression profile (see Figure 3.1 for detailed Legend).

While analysing the cohort I also checked the levels of factors commonly correlated with cancer: a well-known tumour suppressor TP53, a chaperone HSP90AA1 and, more specifically with myosins in mind, a myosin chaperone UNC45A (Figure 3.2). TP53 was significantly decreased in metastases in comparison to normal tissue and localised tumours. HSP90AA1 showed the contrary trend, being upregulated in metastatic sites, and UNC45A was significantly lower in metastases than in benign prostate tissue.

3.2.2 Reverse-transcription PCR (rt-PCR) confirms which myosin isoforms are expressed in prostate cancer cell models

Before analysing changes in myosin isoform expression in prostate cancer cell models, I performed reverse-transcription PCR (rt-PCR) to determine which myosin isoforms were expressed in these cell lines. 3 metastatic prostate cancer cell lines were used: LNCaP, DU145, PC3 (see Section 1.1.3 for detailed description). These cell lines represent prostate cancer metastasis to lymph node (LNCaP), brain (DU145) and bone (PC3), and are reported to have different metastatic potential (Horoszewicz et al 1983, Wilson and Sinha 1997, Pulukuri et al 2005). PC3 cells have the highest metastatic potential in comparison to DU145 (moderate) and LNCaP cells (low). In addition, I tested a matched pair of cells obtained from the same patient, one of which was from normal prostate tissue and the other from

cancerous tissue from a localised prostate tumour (1535 NP and 1535 CT, respectively) (Bright et al., 1997).

Rt-PCR showed that 12 myosin genes were expressed in all 5 cell lines tested (Table 3.1): MYO1B, MYO1C, MYO1D, MYO1E, MYH9 (NM2A), MYO5C, MYO6, MYO9A, MYO9B, MYO10, MYO18A and MYO19. MYO5B was only detected in 1535 NP and 1535 CT. MYO16 was only detected in PC3, 1535 NP and 1535 CT. MYO1G, MYO3A, MYO5A and MYO7A were only expressed in the DU145 cell line. The expression of the remaining myosin genes was not detected using rt-PCR in any of the cell lines.

It is worth noting that the expression of two of the genes only expressed in DU145 cells is normally highly restricted to certain tissues. MYO3A expression is normally confined to the retina, brain, testis and sacculus (Dose and Burnside, 2002), and MYO7A expression is confined to the retina, inner ear, kidney, lung and testis (Kelley et al., 1997) with no expression in the brain.

3.2.3 Quantitative real-time PCR (qPCR) shows some myosin genes are expressed at higher levels in the more metastatic PC3 cell lines

As part of this project, the results for a quantitative real-time PCR (qPCR) analysis for LNCaP, DU145 and PC3 cell lines (performed by Dr Kathryn White) are presented here for completeness. The 12 myosin genes that were detected in all cell lines (Section 3.2.2.) were analysed using this approach (Figure 3.3A). This showed that the expression levels for 4 myosin genes MYO1B, MYO1D, MYO9B and MYO10 were highest in the more highly metastatic PC3 cell line compared with DU145 and LNCaP. Other 5 myosin isoforms were highest in the DU145 cells: MYO1C, MYO1E, MYO9A, MYO18A, as well as NM2A, although that trend was not statistically significant. In contrast, expression of one myosin isoform, MYO6, was significantly increased in the LNCaP cell line compared with the other two cell lines.

Table 3.1 Expression of myosins in prostate cancer cell lines: LNCaP, DU145, PC3, 1535 NP and 1535 CT. Myosin isoforms were detected (+) or not detected (-) by reverse-transcription PCR.

Myosin	LNCaP	DU145	PC3	1535 NP	1535 CT
MYO1A	-	-	-	-	-
MYO1B	+	+	+	+	+
MYO1C	+	+	+	+	+
MYO1D	+	+	+	+	+
MYO1E	+	+	+	+	+
MYO1F	-	-	-	-	-
MYO1G	-	+	-	-	-
MYO1H	-	-	-	-	-
NM2A (MYH9)	+	+	+	+	+
NM2B (MYH10)	-	-	-	-	-
MYO3A	-	+	-	-	-
MYO3B	-	-	-	-	-
MYO5A	-	+	-	-	-
MYO5B	-	-	-	+	+
MYO5C	+	+	+	+	+
MYO6	+	+	+	+	+
MYO7A	-	+	-	-	-
MYO9A	+	+	+	+	+
MYO9B	+	+	+	+	+
MYO10	+	+	+	+	+
MYO15A	-	-	-	-	-
MYO15B	-	-	-	-	-
MYO16	-	-	+	+	+
MYO18A	+	+	+	+	+
MYO18B	-	-	-	-	-
MYO19	+	+	+	+	+

We then carried out a further analysis of the matched pair of cell lines (1535), looking at genes with particularly high levels in the metastatic PC3 cell line: MYO1B, MYO1E, MYO6, MYO9B, MYO10 and MYO18A. I determined that two of the genes, MYO1B and MYO10, again showed significantly higher expression levels by qPCR in the cancerous cell line 1535 CT compared to the normal prostate cells (1535 NP) (Figure 3.3B). Expression of MYO1E, MYO9B and MYO18A was higher in 1535 CT but the differences were not statistically significant. Somewhat surprisingly, levels of MYO6 expression were higher in 1535 NP, but this difference was not statistically significant.

The unusual expression profile of the DU145 cell (Section 3.2.2) suggested to us that it may not be as reliable a model for prostate cancer as the other cell lines tested, even though it is used quite commonly. What is more, DU145 has been established from a metastatic tumour in the brain, which almost never occurs in prostate cancer (Stone et al., 1978). We therefore decided to abandon routinely using DU145 cell line as a model, focusing on the other cell lines which represent different stages of cancer: LNCaP and PC3 represent metastatic cells with different metastatic potential, whereas 1535 NP and CT model benign prostate tissue and localised cancerous tissue, respectively.
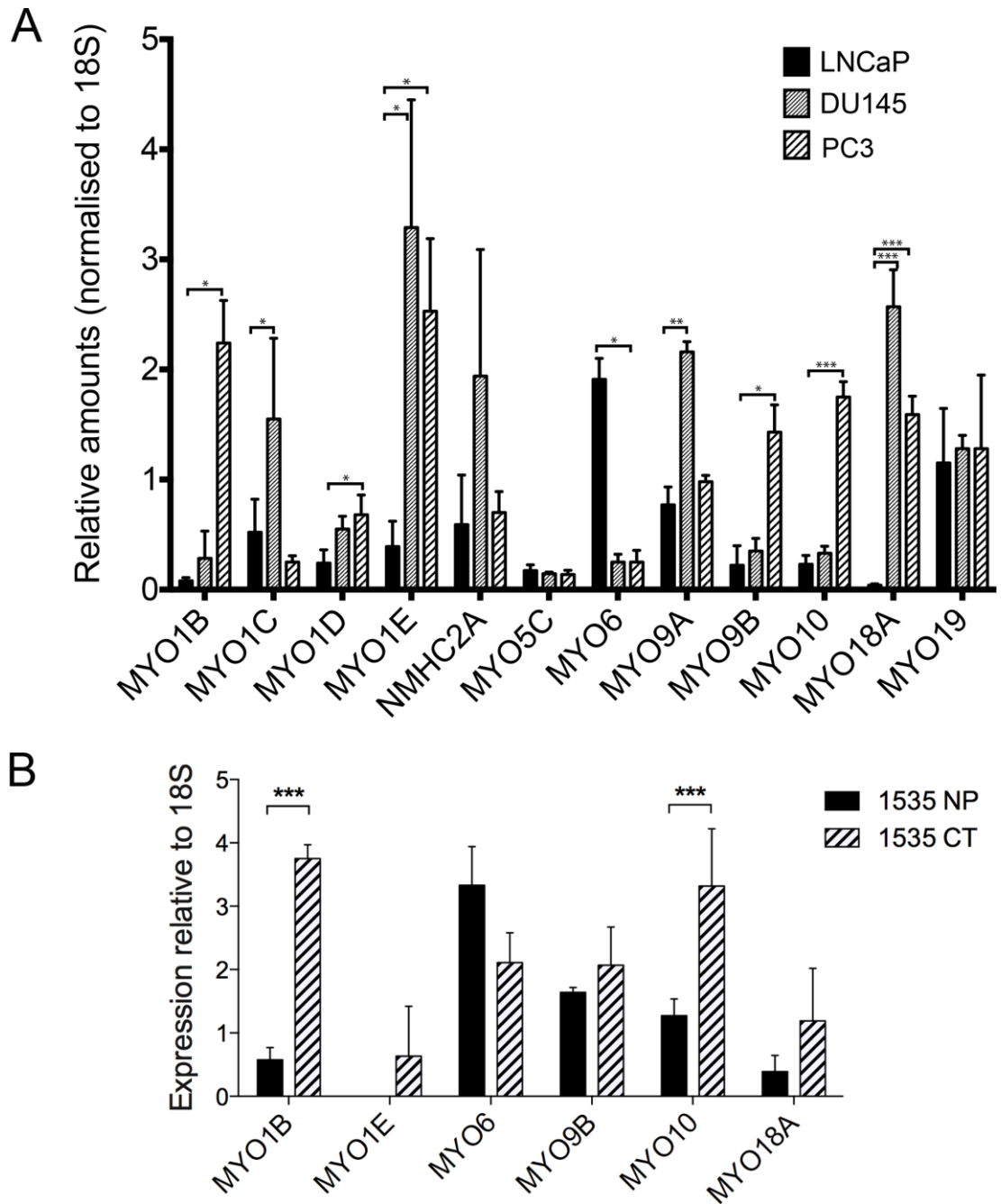
Figure 3.3 Analysis of myosin expression in prostate cancer cell lines.
(A) qPCR shows myosin expression levels for LNCaP, DU145 and PC3 cells, relative to 18S rRNA as internal control. Bars represent mean + standard error, n = 3 (B) qPCR shows myosin expression levels in 1535 NP and 1535 CT, relative to 18S rRNA as internal control. Bars represent mean + S.E., n = 3. Statistical analysis was performed using two-way ANOVA. Levels of significance are indicated by: $p<0.05$ statistically significant (*), $p<0.01$ very significant (**), $p<0.001$ extremely significant (***).

3.2.4 Western blotting (immunoblotting) confirmed changes in expression levels for mRNA at the protein level

I next investigated if the increase in expression levels of the different myosin genes shown by qPCR (MYO1B, MYO6, MYO9B, MYO10 and MYO18A) was reflected by changes at the protein level by western blotting. MYO1E, although significantly upregulated in PC3 cells, was not included in these experiments as good, reliable antibodies were not available at the moment of the study. I also examined the expression levels of non-muscle myosin 2a (NMMHC-2a, referred to as NM2A), a ubiquitous, highly expressed myosin, which did not show changes in expression when analysed by qPCR. It should be noted that Myo18a has two isoforms, alpha and beta (Mori et al., 2005), and in this study I refer to Myo18aα as Myo18a.

I found that higher levels of Myo1b, Myo9b, Myo10 and Myo18a were expressed in PC3 cells compared to LNCaP cells (Figure 3.4A, B). In contrast, levels of Myo6 were significantly higher in LNCaP than in PC3 cells. Levels of NM2A did not change. The trends in myosin expression between LNCaP and PC3 cells shown by western blotting were thus similar to those observed by qPCR. In the matched pair of patient cells 1535 NP and 1535 CT, western blotting also showed a similar trend in myosin expression compared to that observed by qPCR, however, none of the differences were statistically significant (Figure 3.4C, D). Levels of Myo1b and Myo10 were higher in 1535 CT than in 1535 NP. Expression of Myo18a was slightly higher in 1535 CT, and levels of NM2A and Myo6 did not change. Because of time restrictions, expression of Myo9b was not looked at in 1535 cell lines.
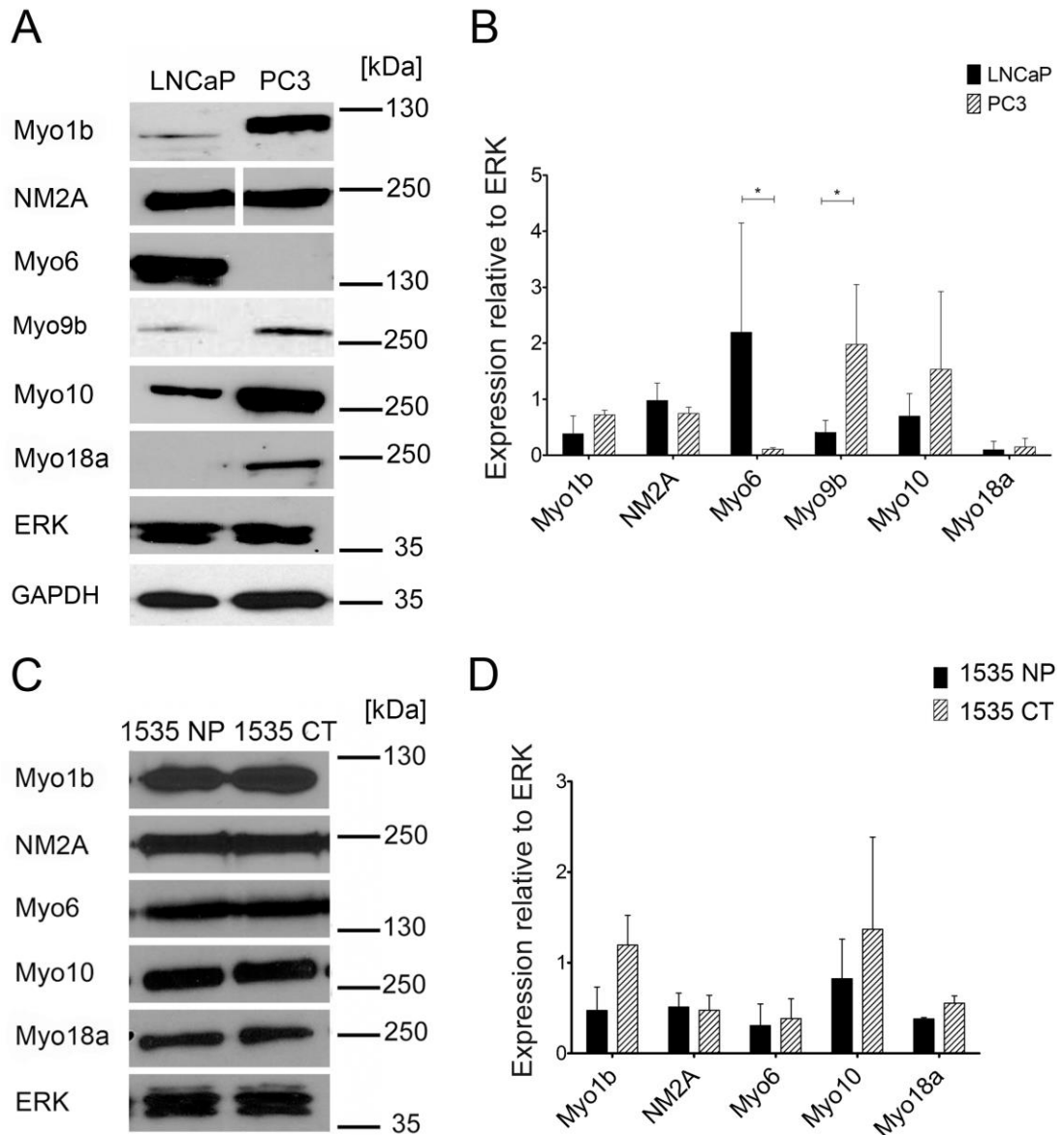
Figure 3.4 Immunoblotting shows expression changes at the protein level in (A, B) LNCaP and PC3 cell lines and (C, D) matched pair of 1535 cell lines. Examples of blots with molecular markers in kDa marked to the right. Total ERK was used as loading control. Quantification of expression relative to ERK, bars represent mean + SD for at least 3 experiments. Statistical analysis was performed using two-way ANOVA. Levels of significance are indicated by: $p < 0.05$ statistically significant (*), $p < 0.01$ very significant (**), $p < 0.001$ extremely significant (***)

3.2.5 Morphology of the cell lines: prevalence of filopodia

I stained the LNCaP and PC3 cells for actin to compare actin organisation and overall cell morphology. Both cell lines are of epithelial origin and are adherent, but their morphology shows interesting differences. The LNCaP cells grow in clumps or colonies and their shape is usually elongated (Figure 3.5A). PC3 cells also have an elongated shape but they grow independently in a monolayer, without forming colonies (Figure 3.5B).

There was a clear difference in the numbers of filopodia between LNCaP and PC3 cells. Filopodia are thin, actin-rich protrusions with a well-established connection to cell motility (described in Section 1.2.3). PC3 cells exhibited numerous filopodia and some cells seemed to be connected through these thin protrusions, which appear to have the features of tunnelling nanotubes (Abounit and Zurzolo, 2012). LNCaP cells had few filopodia. Quantification of the number of filopodia per cell (Figure 3.5C) confirmed that LNCaP cells have a much lower average number of filopodia (0.75 ± 1.45 filopodia per cell, mean ± SD, n = 20) compared to PC3 cells which have a high number (15.35 ± 7.7 filopodia per cell, mean ± SD, n = 20). Interestingly, the increased number of filopodia in PC3 cells correlates directly with the increased levels of Myo10 (Figure 3.4A, B). This is particularly worth noting because Myo10 is a known filopodia-promoting factor (Bohil et al., 2006).
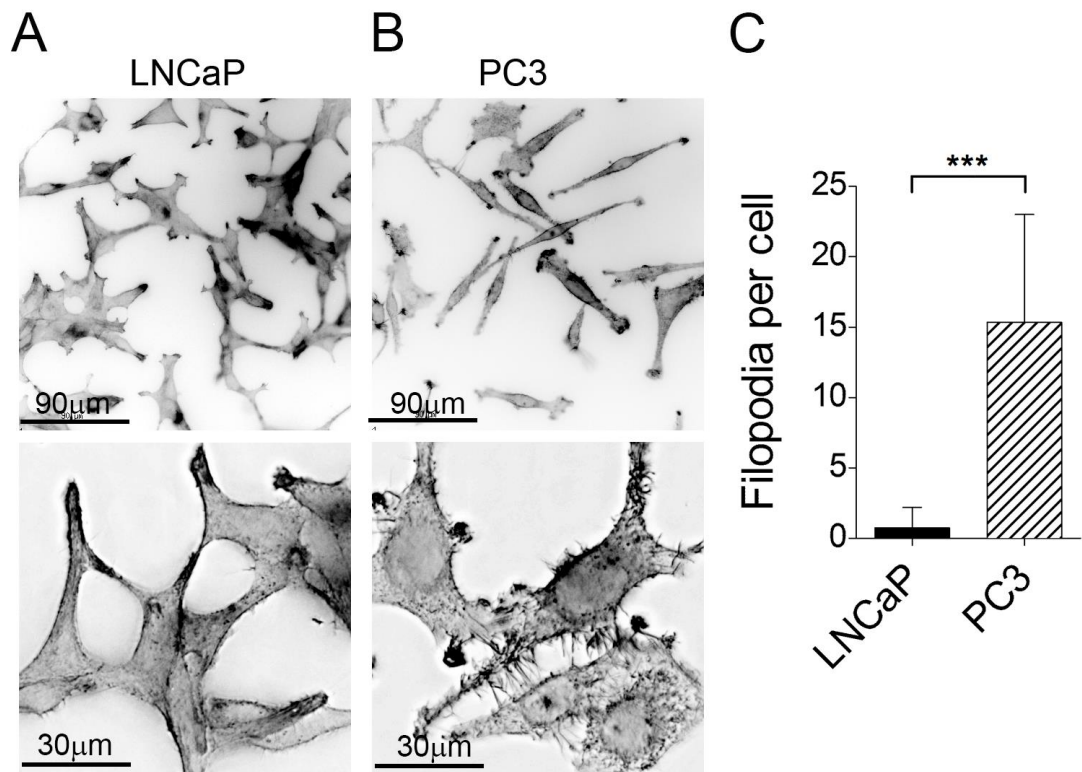
Figure 3.5 Differences in morphology of 2 prostate cancer cell lines: LNCaP and PC3. Low power images (upper panels) and high power images (lower panels) of LNCaP (A) and PC3 (B) cells stained for F-actin using fluorescent phalloidin. The images are shown in grey scale, reverse contrast for increased clarity. Scale bars as shown. (C) Quantification of filopodia per cell, n= 20 cells (from 3 separate experiments), bars represent mean + SD. Statistical analysis was performed using unpaired t-test, (***) is for p<0.001.

3.2.6 Immunostaining shows specific and characteristic localisation of each myosin isoform in each cell line

Immunostaining was used to gain further insight into the potential differences in the localisation of myosins in LNCaP and PC3 cells that might correlate with differences in expression levels. Myo10 localises to the tips of the numerous filopodia in PC3 cells (arrows in Figure 3.6B and Figure 3.7C), in agreement with previous reports for this myosin (Bohil et al., 2006). In the LNCaP cells, which express low levels of this myosin, staining for Myo10 was mostly diffuse and cytoplasmic (Figure 3.6A). Myo10 seems to localise to the scarce filopodia formed by LNCaP, although the staining is very weak and Myo10 is absent from the filopodia tips (Figure 3.7A).

While carrying out this work, it was reported that upregulation of Myo10 is linked to expression of mutant p53 in breast cancer (Arjonen et al., 2014). Protein p53 is a well-known tumour suppressor which can gain tumour-promoting functions when mutated (Lane and Levine, 2010). However, the LNCaP cells express wild-type p53 and PC3 cells are p53-null (Carroll et al., 1993), and thus we did not find a link between Myo10 overexpression and expression of mutant p53. To check whether a prostate cancer cell line expressing mutant p53 would show any correlation, I included the DU145 cell line into this analysis, since they express p53 protein mutated in two codons (Carroll et al., 1993). As shown by qPCR, Myo10 expression in DU145 is only slightly higher than in the LNCaP cells. DU145 cell line has around 8 filopodia per cell (8.75 ± 5.2 filopodia per cell, mean ± SD, n = 20), a number increased compared to LNCaP cells, and Myo10 localises to the filopodia tips (Figure 3.7B). Both Myo10 levels and filopodia numbers are still lower LNCaP and DU145 cells compared to the p53-null PC3 cell line.

Figure 3.6 Localisation of Myo10 in prostate cancer cell lines. LNCaP (A) and PC3 (B) cells stained for nuclei (DAPI - blue), F-actin (AF546-phalloidin - red) and Myo10 (green). Arrows in (B) show Myo10 at the tips of filopodia in PC3 cells. Scale bar = 30 μm. The images are representative of at least 3 separate experiments.
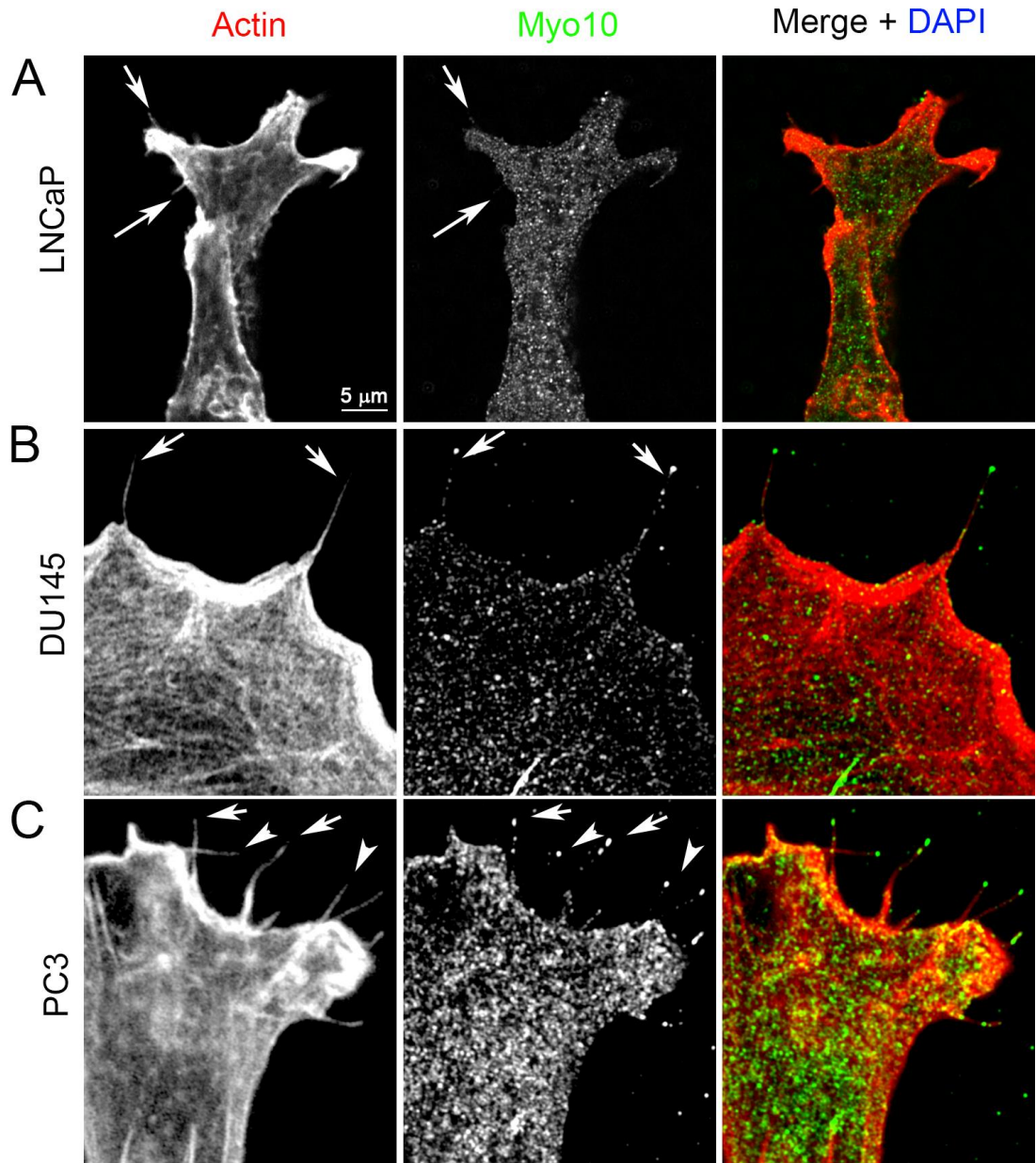
Figure 3.7 Localisation of Myo10 in prostate cancer cell lines (higher magnification). LNCaP (A), DU145 (B) and PC3 (C) cells stained for nuclei (DAPI - blue), F-actin (AF546-phalloidin - red) and Myo10 (green). Arrows in (A) show lack of Myo10 at the tips of rare, short filopodia in LNCaP cells; arrows in (B) show Myo10 at the tips of filopodia in DU145, and in numerous filopodia in PC3 cells (C). Scale bar = 5 μm. The images are representative of at least 3 separate experiments.

Myo1b localised to intracellular vesicles in LNCaP cells (Figure 3.8A, arrows), and there was additionally some localisation to the plasma membrane, where it co-localised with actin (Figure 3.8A, arrowheads). In PC3 cells, Myo1b co-localised with actin and actin-rich areas at the plasma membrane, in membrane ruffles and to intracellular vesicles (Figure 3.8B, arrows). A similar localisation for Myo1b has been previously reported for other cell types (Salas-Cortes et al., 2005; Tang and Ostap, 2001), where Myo1b was found to be concentrated in dynamic membrane areas enriched with actin and associated with punctate structures in the cytoplasm. The intracellular vesicles were previously identified to be endosomes (Raposo et al., 1999; Salas-Cortes et al., 2005). In PC3 cells, there was also some localisation of Myo1b within the filopodia, as found in other studies (Figure 3.8C, arrows) (Kim and Flavell, 2008; Komaba and Coluccio, 2010). The filopodia-like protrusions, however, were often seen between two cells, suggesting it could be tunnelling nanotubes (Abounit and Zurzolo, 2012), which can also be present in cancer cells (Ware et al., 2015).

Neither LNCaP nor PC3 cells showed abundant actomyosin bundles close to the plasma membrane (Figure 3.9A, B), they also lack central stress-fibre bundles that are found in more adherent, non-colony forming cells such as fibroblasts (Vicente-Manzanares et al., 2009). NM2A in the LNCaP cell line had a diffuse, cytoplasmic localisation, with some co-localisation with actin close to the plasma membrane (Figure 3.9A, arrows). PC3 cells also showed some NM2A staining close to the plasma membrane, where it co-localised with actin (Figure 3.9B, arrows).

I found that Myo18a localised to the cytoplasm and in membrane ruffles and/or close to the plasma membrane in both PC3 and LNCaP cells (Figure 3.9C and D, arrows). This localisation is similar to that previously reported for Myo18a and is consistent with its role in modifying actin organisation in the lamellipodium (Hsu et al., 2010; Tan et al., 2008).

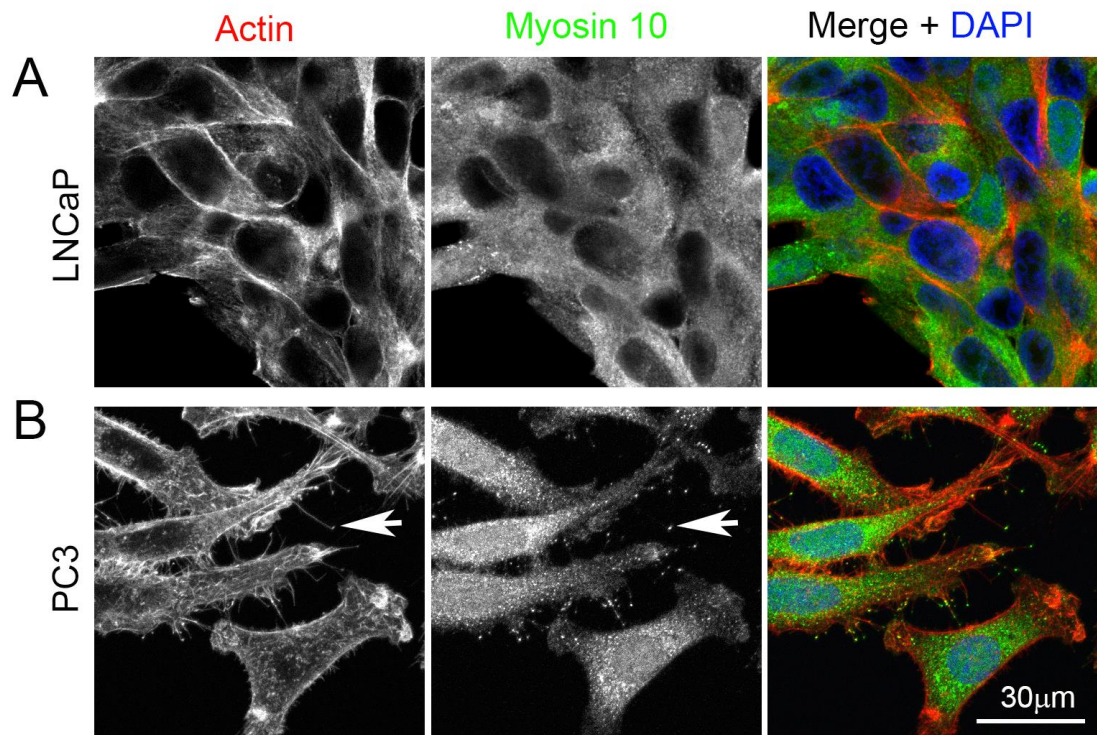**Figure 3.8 Localisation of Myo1b in prostate cancer cell lines.** LNCaP and PC3 cells stained for F-actin (AF546-phalloidin - red), nuclei (DAPI - blue) and Myo1b (green). Arrows in (A) and (B) show that Myo1b localises to vesicles; arrowhead in (A) shows Myo1b at actin-rich regions close to cell border in LNCaP cells; Arrows in (C) point to Myo1b localised in the protrusions (filopodia or tunnelling nanotubes between two cells). Scale bar = 30 μm. The images are representative of at least 3 separate experiments.

Figure 3.9 Localisation of NM2A and Myo18a in prostate cancer cell lines. LNCaP and PC3 cells stained for nuclei (DAPI), F-actin (AF546-phalloidin) and NM2A (A, B) or Myo18a (C, D). Arrows in A, B indicate NM2A co-localising with dynamic actin close to cell membrane; arrows in C, D show Myo18a localising close to actin-rich membrane ruffles. The images are representative of at least 3 separate experiments.

Myo6 showed a diffuse, cytoplasmic staining both in PC3 and LNCaP cells (Figure 3.10A and B). Myo6 has been shown to have a punctate localisation in LNCaP cells (Puri et al., 2010) where it co-localises with early endosomes and the Golgi. Using the commercial antibody (Santa Cruz), I was unable to observe localisation of Myo6 to vesicles. Myo9b was enriched in membrane ruffles/lamellipodia in PC3 cells (Figure 3.9D), consistent with its role in cell polarity and recruitment of RhoGAP to the lamellipodium (Hanley et al., 2010), while the staining in LNCaP cells was diffuse and Myo9b was missing from actin-rich areas (Figure 3.10C).
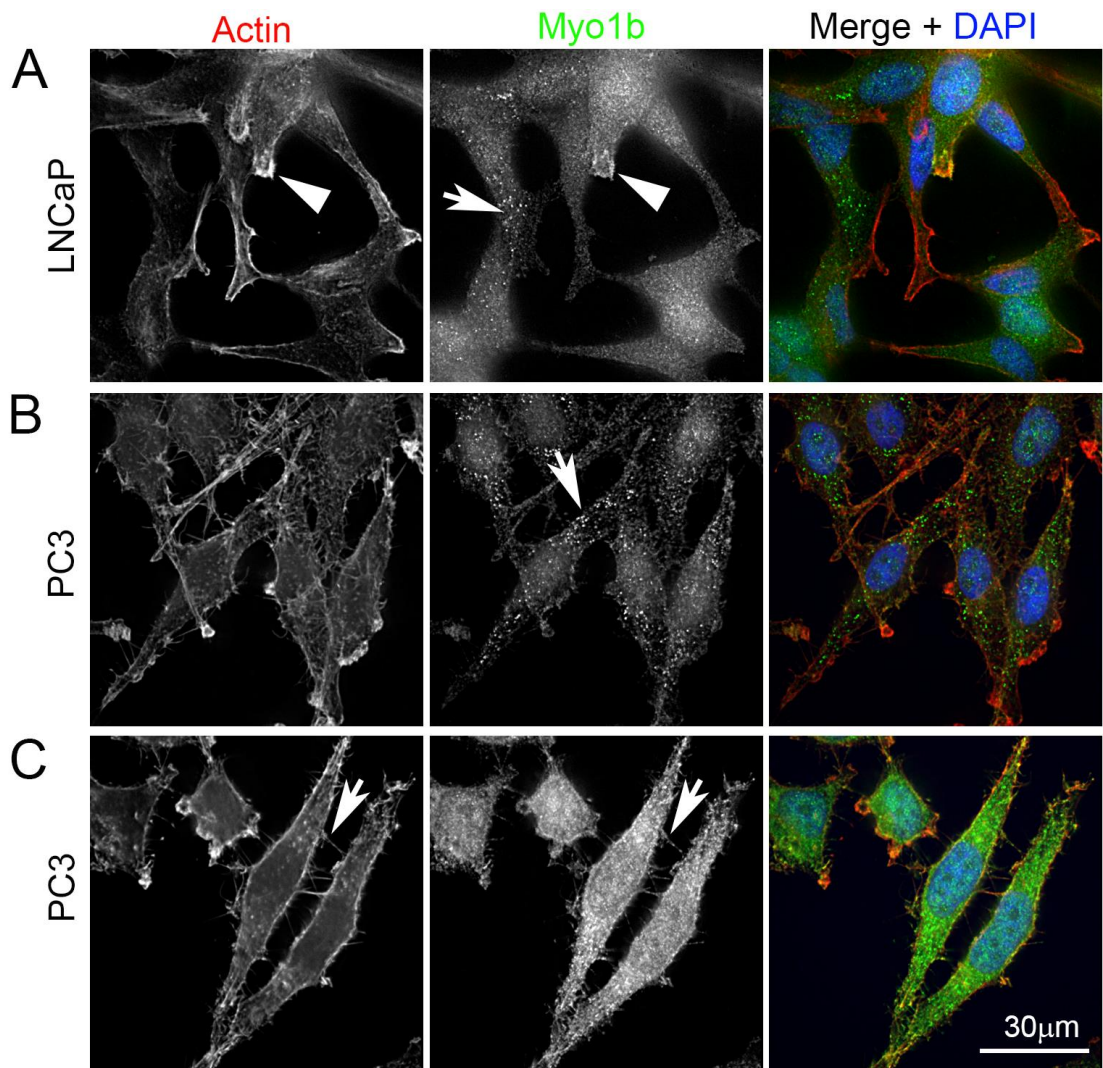
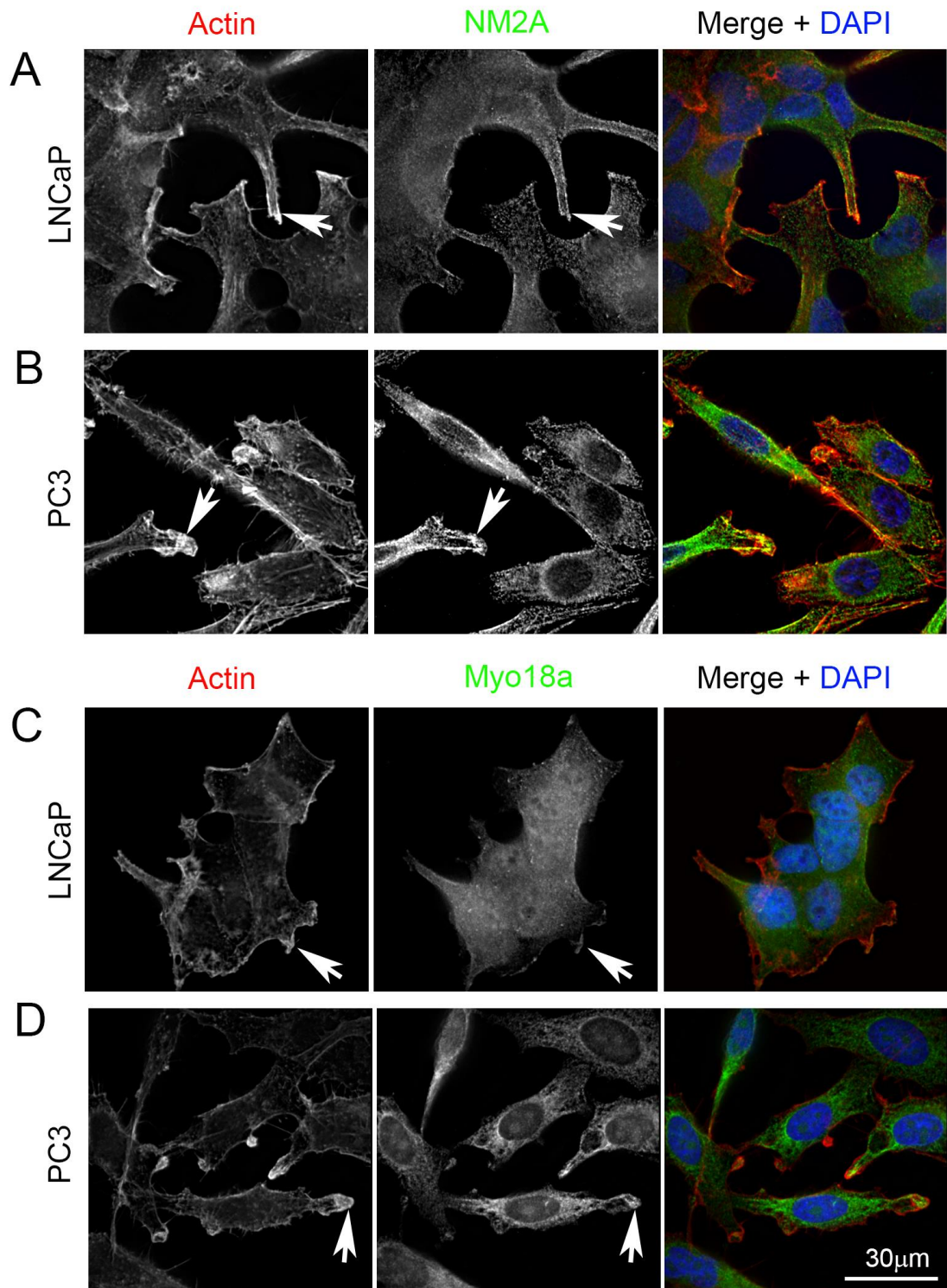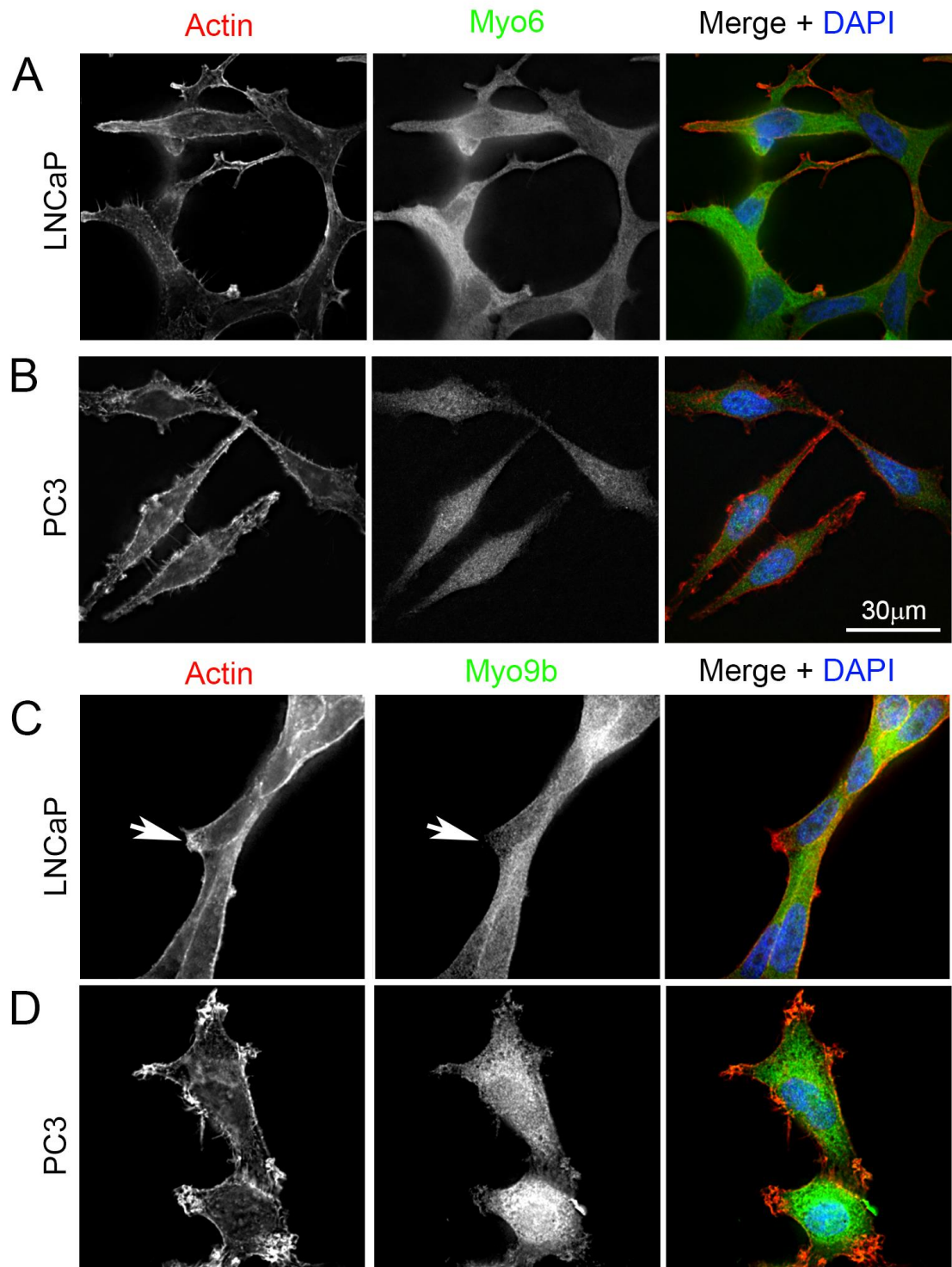**Figure 3.10 Localisation of and Myo6 and Myo9b in prostate cancer cell lines.** LNCaP and PC3 cells stained for F-actin (AF546-phalloidin - red), nuclei (DAPI - blue) and Myo6 (green) (A, B) or Myo9b (green) (C, D). Arrows in (C) indicate lack of Myo9b in actin-rich protrusions. Scale bar = 30 μm. The images are representative of at least 3 separate experiments.

3.3 Discussion

The GEO analysis presented here for patient samples of prostate cancer suggests that the expression level of some types of myosin increases as cells become more metastatic. The expression levels of some myosin isoforms (MYO5A, MYO6, MYO9B) increased in localised tumours, while other increased in metastases (MYO1B, MYO1D, MYO1F, MYO10). Expression levels of other myosins such as MYH9 (NM2A) or MYO18A did not seem to change. Analysing myosin expression levels in commonly used prostate cancer cell lines showed a less clear cut change in myosin expression. However, an increased level of Myo10 expression in the more highly metastatic PC3 cell line was linked to a high level of filopodia, with Myo10 localised to the filopodial tips and Myo1b only found in filopodia in the PC3 cells. These results raise the possibility that myosin expression level and organisation in prostate cancer cell lines are able to influence their phenotype.

Two myosin isoforms, Myo1b and Myo10, showed a clear, significant increase in expression in metastases, in tissue arrays and from the analysis of prostate cell lines by qPCR. Of particular interest was the increased expression of Myo10 in PC3 cell line, which mirrors the increase of Myo10 in metastatic tumours, observed in the GEO analysis. Myo10 has a well-established role in formation of filopodia, which are directly associated with cell migration (Sousa et al., 2006). We observed a 2.9-fold increase in levels of Myo10 in highly malignant PC3 cells in comparison to LNCaP cell line. Interestingly, even though Myo10 is widely expressed in a variety of vertebrate tissues, it is quite sparse as it comprises of only about 0.0005% of total protein in cells (Berg et al., 2000). It is therefore not surprising that a 3-fold difference has an appreciable effect on the phenotype. The connection of Myo10 to filopodia can also be seen in our study, where protein levels of Myo10 (Figure 3.4) correlate neatly with numbers of filopodia in each cell line (Figure 3.5).

Upregulation of Myo10 has recently been linked to mutant p53 expression and invasiveness, where Myo10 was found to be a necessary downstream component for mutant p53-driven invasion in breast cancer and pancreatic carcinoma (PDAC) cells (Arjonen et al., 2014). Mutant p53 is a stable variant of p53 protein, a well-known tumour suppressor and high levels of mutant p53 are often associated with cancer (Lane and Levine, 2010). In metastatic prostate cancer p53 is often either mutated or lost (Chen et al., 2005). An *in silico* analysis of the GEO data showed a significant decrease of TP53 gene in metastatic sites (Figure 3.2). Although highly malignant PC3 cells do not express p53 (Carroll et al., 1993), I have found that they still express high levels of Myo10 and have numerous filopodia. At the same time, LNCaP cells, which show almost no filopodia and low levels of Myo10, express normal p53 (Horoszewicz et al., 1983). DU145 cells, which express low levels of Myo10 and show medium numbers of filopodia per cell, express mutant p53 (Carroll et al., 1993). Taken together, these results confirm that there is no link between expression of Myo10 and mutant p53 in prostate cancer cells, and that the connection between Myo10 and p53 observed in other studies seems therefore to be cancer type-specific.

Levels of Myo1b were clearly increased in metastatic prostate cancer – both in patient tissue and when measured in the cell lines by qPCR and western blotting. Out of the matched pair of patient cell lines, 1535 CT had visibly higher levels of Myo1b in comparison to normal prostate tissue. Myo1b has a role in formation of post-Golgi carriers and in transport of endocytic organelles (Raposo et al., 1999; Salas-Cortes et al., 2005). The role of Myo1b in cancer has not been well investigated, although it was recently found to be upregulated in head and neck squamous cell carcinoma (HNSCC) (Ohmura et al., 2015). The same group observed slight upregulation of Myo1b in prostate cancer and other types of cancer, suggesting that the role of Myo1b in different cancers required further investigation (Ohmura et al., 2015). Here, immunostaining has shown that Myo1b localises to the actin-rich areas at the plasma membrane, vesicles (endosomes) and, somewhat surprisingly, to the filopodia of PC3 cells. Other

groups have previously observed similar Myo1b localisation in other cell types: Myo1b-eGFP and endogenous Myo1b were found to co-localise with actin at the cell periphery, in cytoplasmic punctae and endosomes in normal rat kidney epithelial cells and in human melanoma cell line (Salas-Cortes et al., 2005; Tang and Ostap, 2001). Interestingly, Myo1b has also been found at dynamic actin structures, such as membrane ruffles and large protrusions and filopodia / invadopodia in HeLa cells (Kim and Flavell, 2008; Komaba and Coluccio, 2010). One of the groups found that motor function and binding to phosphatidylinositol 4,5-bisphosphate (PIP_2) was necessary for Myo1b to localise to filopodia (Komaba and Coluccio, 2010), suggesting that binding of Myo1b to phosphoinositides played a role in regulating Myo1b localisation to actin-enriched membrane projections.

Expression of Myo18a observed in the GEO Database was similar across different samples, not showing any changes. We did, however, notice intriguing changes in the qPCR analysis, the difference between LNCaP and PC3 being one of the most obvious, more than 40-fold, as well as a noticeable change in the western blotting. The possible role of Myo18a in cell migration has been described through its interaction with kinases (Hsu et al., 2010). MYO18A was also found in a three-way translocation of Histone-lysine N-methyltransferase 2A gene (MLL or KMT2A) MLL in child acute myeloid leukaemia (Ussowicz et al., 2012). An interesting interaction between Myo18a and NM2A, which has many roles in the cell, has recently been described (Billington et al., 2015), and will be discussed further in Chapter 4. As mentioned previously, Myo18a has two isoforms, alpha and beta (Mori et al., 2005). The isoforms show several differences: Myo18aα is expressed in most tissues, while expression of Myo18aβ is restricted to hematopoietic cells; Myo18aβ lacks a PDZ (PSD-95/Discs-Large/ZO-1) domain towards the N-terminus, and therefore has a molecular weight of around 190 kDa, in comparison to 230 kDa for Myo18aα (Mori et al., 2005). Antibodies used in this study to recognize Myo18a were raised against C-terminus of the protein, but they identified a protein of about 230 kDa,

present in prostate tissue (not hematopoietic). This means that the recognised isoform expressed in examined cells was Myo18aα.

Looking at patient tissue, levels of Myo9b were significantly higher in primary tumours than in normal prostate, as shown by the *in silico* analysis. Myo9b was also significantly upregulated in the malignant PC3 cells, as shown by qPCR and immunoblotting. The observed staining, with Myo9b localising to lamellipodia and membrane ruffles was consistent with its role in cell polarity (Hanley et al., 2010). Myo9b contains in its tail a RhoGAP (GTPase Activating Protein) domain (Reinhard et al., 1995), which regulates the Rho GTPases, which in turn play a major role in actin reorganisation (Ridley et al 2003). Myo9b has been connected to progression of oesophageal cancer (Menke et al., 2012), and another class 9 isoform, Myo9a, has been implicated in migration of epithelial cells (Omelchenko and Hall, 2012). This together suggested that Myo9b could be an interesting isoform to explore further in context of metastasis.

Aggressive, metastatic prostate cancer samples showed increased expression of several myosin isoforms, but an interesting exception to this trend is Myo6, which is highly expressed in localised tumours (Figure 3.1, GEO Microarrays). Myo6 is also the only isoform with expression levels significantly higher in the LNCaP cells with low metastatic potential in comparison to the highly metastatic PC3 cells. This is in agreement with earlier findings that Myo6 is frequently overexpressed in prostate and breast cancer tissues (Su et al., 2001), with higher levels detected in medium-grade androgen-dependent prostate cancers than in more advanced and aggressive cancers (Dunn et al., 2006). Loss of Myo6 has been shown to reduce the motility of ovarian and prostate cancer cells (Dunn et al., 2006; Yoshida et al., 2004), but it is unclear why it is present in very low levels in the malignant PC3 cell line. Our immunostaining showed a diffuse, cytoplasmic localisation of Myo6 in both LNCaP and PC3 cell lines. Myo6 has been previously reported to localise to protrusions and membrane ruffles (Yoshida et al., 2004), as well as in the perinuclear region around the Golgi complex and on endocytic structures (Aschenbrenner et al., 2003; Buss et

63

al., 1998; Maddugoda et al., 2007; Puri et al., 2010). The different staining patterns observed depend on the set of antibodies used (commercial or in-house), and may explain the observed differences between the staining pattern we observed and those from other groups. Additionally, one group used pre-treatment with saponin, a gentle detergent, to remove the unbound, overexpressed Myo6 from LNCaP cells, but the approach was not successful in our study (results not shown).

The connection between Myo6 and human cancer, including prostate cancer, has been relatively well explored. It has been suggested that because of its role in endocytosis, Myo6 could contribute to cancer cell motility by promoting internalisation and recycling of key mediators such as integrins and other receptors (Yoshida et al., 2004). Another group showed overexpression of Myo6 as an example of molecular alterations of the Golgi apparatus in human prostate cancer, with the functional significance to be fully characterised (Wei et al., 2008). Since Myo6 levels are highest in medium-grade prostate cancers, Dunn and colleagues noted that advanced cancers may gain other properties and become less dependent on Myo6 (Dunn et al., 2006). For example, Myo6 stabilizes E-cadherin, which is crucial in border cell migration (Geisbrecht and Montell, 2002), a mode employed by well-differentiated prostate cancers. On the other hand, advanced prostate cancers show perturbed E-cadherin-mediated cell adhesion and express lower levels of E-cadherin (De Marzo et al., 1999). As a result, as (Dunn et al., 2006) speculate, Myo6 can be necessary for regulating migration of medium grade, E-cadherin-positive prostate cancers, but may not be as critical in more advanced cancers (Dunn et al., 2006).

Finally, one study looked specifically at Myo6 in androgen-dependent LNCaP cells (Puri et al., 2010). Importantly, the authors found no connection between androgen receptor translocation into the nucleus and Myo6 expression. They observed that Myo6 is involved in secretion of the prostate-specific marker, PSA, and the vascular endothelial growth factor, VEGF. PSA can increase cellular migration (by either promoting EMC or by cleaving ECM proteins), and VEGF is a key angiogenic factor that mediates

64

the recruitment and cell proliferation of endothelial precursor cells. Therefore, an increase in PSA and VEGF secretion caused by Myo6 overexpression could be a significant factor promoting tumour growth or enhancing cell motility. At present, however, it is unclear why Myo6 is specifically overexpressed in these secretory adenocarcinomas and how exactly upregulation of secretion generates a malignant tissue (Puri et al., 2010).

Using the GEO Database to analyse expression of myosins has the disadvantage that many genes in the GEO Database were discarded before the final analysis (see Section 2.2). Thus some of the myosin isoforms detected by rt-PCR in the cell lines are missing in the GEO analysis (MYO5B, MYO9A and MYO19). In addition, we did not detect additional myosin isoforms identified in patient samples in the GEO database by PCR (MYO1A, MYO1F, NM2B, MYO5A, MYO7A). This could be due to a different detection threshold of the methods used. Moreover, cancers are very diverse and cell lines do not represent all the possible scenarios found in the clinic.

Choosing an appropriate model is crucial for designing relevant experiments, which is why I considered all of the cell lines tested here. Even though the DU145 cell line is a popular prostate cancer model, it originates from a metastatic tumour in the brain, which very rarely occurs in a typical course of prostate cancer (Kaighn et al., 1981). rt-PCR analysis of this cell line showed that it had an unusual expression profile, with expression of MYO7A and MYO3A, myosins that normally only have a restricted tissue expression (Coluccio, 2008; Dose and Burnside, 2002; Richardson et al., 1997; Weil et al., 1995). Thus, we decided to discontinue using this cell line as a model. The LNCaP cells, originally obtained from a tumour in the lymph node, are still androgen-sensitive and maintain their malignant properties (Horoszewicz et al., 1983). They represent an 'early' stage of prostate cancer metastasis. The commonly used PC3 cell line is derived from an osteolytic metastatic site, which is the most common metastatic site for prostate cancer – up to 90% of reported metastases (Bubendorf et al., 2000;

Doctor et al., 2014). PC3 cells are already androgen-independent and therefore represent a more aggressive phase of cancer cell development (Kaighn et al., 1981). PC3 cells do form tumours when injected into nude mice (Ma and Waxman, 2009; Pulukuri et al., 2005). In contrast, LNCaP cells, do not normally form tumours or metastasise (Wu et al., 1994), although there is evidence showing that subpopulations of LNCaP cells form tumours in mice (Hurt et al., 2008). Cell lines, even though they have obvious limitations, are a useful first step in elucidating molecular mechanisms of processes and in identifying potential subjects of interest for further research. Because of its insensitivity to androgens and high level of malignancy, PC3 cell line is a good model for the study and evaluation of metastases of human prostate carcinomas. This is why I chose to focus the consequent study of myosins in prostate cancer on this cell line.

Taken together, the findings from the GEO Database analysis, as well as the subsequent analysis of myosin expression by rt-PCR, q-PCR and western blotting for a variety of prostate cancer cell lines, I have decided to choose four isoforms as the most interesting candidates for further investigation: Myo1b, Myo9b, Myo10 and Myo18a. Myo1b and Myo10 are overexpressed in both metastatic prostate cancer and in the more highly metastatic PC3 cell lines, compared to LNCaP cells, and thus might be expected to contribute to the metastatic phenotype. Myo18a is overexpressed in PC3 cells, though not in metastatic prostate cancer tissues, but it worthy of further investigation as its overexpression may contribute to the PC3 cell phenotype.

Chapter 4
Role of myosins in prostate cancer cell migration

4.1 Introduction

After analysing expression of myosins in prostate cancer tissue and cell lines, I have decided to further focus on four myosin isoforms: Myo1b, Myo9b, Myo10 and Myo18a. Experiments focusing on Myo9b were started towards the end of the project, and due to time restrictions this myosin isoform could not have been fully investigated. General information about myosin domains and structure can be found in the introduction (section 1.3). The structure of myosins of interest is described in more detail below, since looking at structure of the protein can offer a valuable insight into its possible mechanism of action.

Myo1b belongs to class 1 and, like all the class 1 myosins, it has a basic myosin tail homology 1 (MyTH1) domain in its tail, which contains a pleckstrin homology (PH) domain-like fold (Figure 4.1) (Hokanson et al., 2006). The PH domain binds selectively to phosphatidyl inositol phospholipids (PIPs) (Lemmon and Ferguson, 2001; Tacon et al., 2004), and all of the class 1 myosins can bind to PIPs in vesicles and/or in the plasma membrane (Lin et al., 2005; Raposo et al., 1999; Ruppert et al., 1993; Salas-Cortes et al., 2005). Myo1b binds PtdIns(4,5)P_2 and PtdIns(3,4,5)P_3, with higher affinity for PtdIns(4,5)P_2 (Komaba and Coluccio, 2010).

Myo9b, which forms class 9 together with Myo9a, is not a very well-studied myosins isoform but certainly an interesting one. Myo9b contains a RhoGAP (GTPase activating protein) domain in its tail (Bement et al., 1994; Reinhard et al., 1995). The Rho family of small GTPases includes Rho, Rac and CDC42 which cycle between GTP-bound active and GDP-bound inactive states. GAPs partially control this by stimulating intrinsic GTP hydrolysing

activity of Rho GTPases, inhibiting them by facilitating the shift into inactive state (Jaffe and Hall, 2005). Rho GTPases are involved in actin reorganisation and various actomyosin-dependent processes, including regulation of the protrusion and retraction mechanisms (Ridley and Hall, 1992; Ridley et al., 2003). Head domain of Myo9b contains quite an unusual N-terminal extension of about 60 amino acids, only found in class 9 myosins, and its neck region contains 4 IQ motifs (Figure 4.1) (Wirth et al., 1996). Myo9b is highly expressed in leukocytes and shows low to moderate level of expression in various tissues including spleen, small intestine, testis, prostate, brain and others (Wirth et al., 1996).

Myo10, the only member of class 10, is widely expressed in vertebrate tissues, with high levels in developing brain, endothelia and many epithelia (Berg et al., 2000; Courson and Cheney, 2015). The tail of Myo10 has three PH (pleckstrin homology) domains, a myosin tail homology 4 (MyTH4) domain and a band 4.1/ezrin/radixin/moesin (FERM) domain (Figure 4.1) (Berg et al 2000). In myo10, the PH domains are responsible for binding of this myosin to PIPs, specifically to $PtdIns(3,4,5)P_3$ and $PtdIns(3,5)P_2$ and this is required for Myo10-induced filopodial formation (Plantard et al., 2010; Tacon et al., 2004), although the underlying molecular mechanism is unclear (Liu et al., 2012). The MyTH4 domain is involved in microtubule binding (Kerber and Cheney, 2011; Weber et al., 2004), which could mean that Myo10 acts as a potential motorised link between actin filaments and microtubules. The FERM domain binds β1, β3 and β5 integrins, receptors important for cell adhesion, and is thought to be required for transporting the integrins to the filopodia tips, which contributes to stability and functionality of the protrusions (Zhang et al., 2004). The initial sequence analysis of Myo10 identified a putative coiled-coil region in the tail, so the heavy chains were predicted to dimerise as a coiled coil. Our lab demonstrated that it is actually a stable single α-helix (SAH) (Knight et al., 2005), although more recently it has been suggested that the distal region of this sequence may allow Myo10 to form anti-parallel dimers (Lu et al., 2012).

Myo18a together with Myo18b forms class 18. An interesting feature of Myo18a is its ATP-insensitive actin binding site in its N-terminal domain (Figure 4.1), which suggests that Myo18a might act as a dynamic actin tether (Guzik-Lendrum et al., 2013; Isogawa et al., 2005). The N-terminal domain contains also a PDZ (PSD-95/Discs-Large/ZO-1) domain, known to act as a scaffold for holding signalling protein complexes together. Myo18a dimerises through a coiled-coil region in the tail, similarly to myosin 2. These two myosins share other similarities, such as two IQ motifs which bind essential and regulatory light chain (ELC and RLC) (Guzik-Lendrum et al., 2013). However, Myo18a does not form filaments like myosin 2 (see Section 1.3.2), as it lacks the repeating sequences of positive and negative charges along its coiled coils that promote the assembly of myosin tails into filaments in myosin 2 (Guzik-Lendrum et al., 2013).

In the second part of the study, I further investigated the putative role of Myo1b, Myo9b, Myo10 and Myo18a in prostate cancer. To find out more about the function of these myosin isoforms, I used RNA interference (RNAi) technology to knock down myosins in the highly metastatic PC3 cell line. I then determined the effects of the knockdown on the morphology and behaviour of PC3 cells. These included changes in cell shape and area, in organisation of actin cytoskeleton and changes in the status of filopodia and focal adhesions. Finally, I looked at endocytosis and migration in 2D and 3D-like environment.

Figure 4.1 Diagrammatic representations of Myo1b, Myo9b, Myo10 and Myo18a (adapted with permission from (Allsop and Peckham, 2011)). Detailed description of the structural features of each myosin in the main text.

4.2 Results

4.2.1 siRNA-mediated knockdown depletes myosin expression

I used siRNA to knock down the endogenous levels of four myosins Myo1b, Myo9b, Myo10 and Myo18a, in the highly metastatic PC3 cell line. As seen in Chapter 3 (Figure 3.3, 3.4), the PC3 cells normally express high levels of these myosins, and depletion can help determine how endogenous myosin expression affects cell morphology and behaviour. The efficiency of siRNA (SMARTpool and single reagents) knockdowns was confirmed by western blotting (Figure 4.2).

To establish the best time point for knockdown efficiency, I first ran a time-course experiment for Myo10 knockdown (Figure 4.2A). Levels of Myo10 were decreased by 90% after 72 hours and below the level of detection after 96 hours when using SMARTpool siRNA. Considering that the cells reached very high confluence after 96 hours, I used 72 hours as the standard time-point for analysis of any effects of knockdown, where I was better able to analyse cell shape in subconfluent cultures. I also confirmed that the depletion was efficient for the other myosin isoforms (Figure 4.2B). Figure 4.2B also shows that knockdown of a particular myosin did not affect levels of the remaining myosins, including NM2A, which confirms specificity of the knockdowns. Myo9b was the last myosin isoform analysed, and because of time restrictions its knockdown has been quantified separately, in comparison to GAPDH (Figure 4.2C). This also serves to show that GAPDH gave similar results to ERK as a loading control.
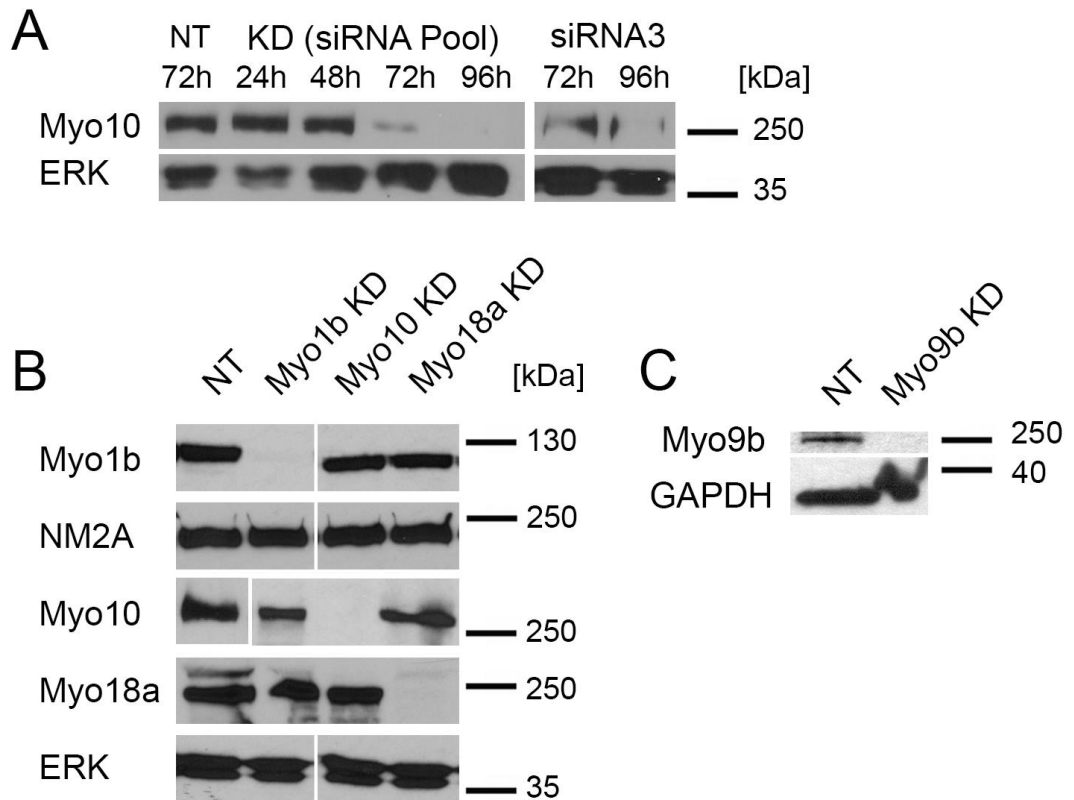
Figure 4.2 siRNA-mediated knockdown of myosins in highly metastatic PC3 cell line. A. Time-course experiment for knockdown of Myo10 using siGENOME SMARTpool siRNA (Thermo Scientific) after 24, 48, 72 and 96 hours; and with a single siRNA reagent (siRNA3) after 72 and 96 hours, analysed by immunoblotting. B. Knockdown of Myo1b, Myo10 and Myo18a in PC3 cell line using siGENOME SMARTpool siRNA after 72 hours, analysed by immunoblotting confirms that myosin levels are significantly reduced while levels of other myosins are not affected. C. Knockdown of Myo9b using siGENOME SMARTpool siRNA after 72 hours. Control cells were treated with non-targeting siRNA (NT). Molecular weight markers shown to the right. Total ERK (A, B) or GAPDH (C) were used as loading control.

4.2.2 Knockdown of Myo10 reduces the number of filopodia

Actin staining revealed that knockdown of myosins results in isoform-specific changes in cell morphology (Figure 4.3A). Most interestingly, knockdown of Myo10, but not the other myosins, significantly reduced the numbers of filopodia by more than 70% (to 4.2 ± 0.84 filopodia per cell, mean ± S.E.M., n=20) in comparison to control cells (13.1 ± 1.26 filopodia per cell, mean ± S.E.M., n=20, $p < 0.05$) (Figure 4.3B).

Knockdown of each of the myosins increased the cell spread area of PC3 cells significantly, by about 2-3 fold (Figure 4.3A, C). Cell shape was also changed, with Myo1b and Myo10 knockdown resulting in a more polygonal shape, and Myo9b and Myo18a knockdown resulting in a more rounded shape, with prominent membrane ruffles around the edges in case of Myo18a depletion, and an actin-rich area at the cell periphery in Myo9b-depleted cells (Figure 4.3A, arrows). These different results suggested that each myosin isoform affects the organisation of actin cytoskeleton in a distinct way.
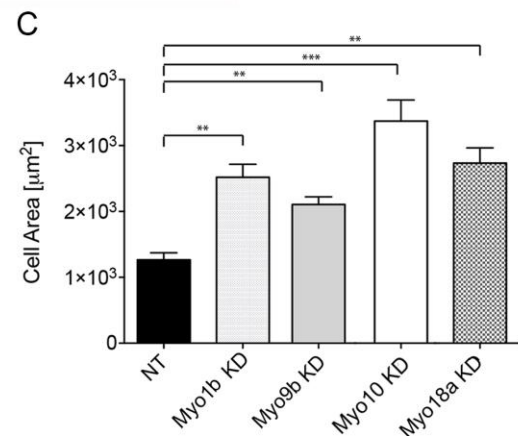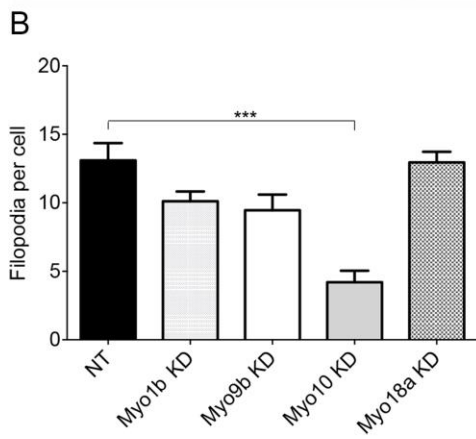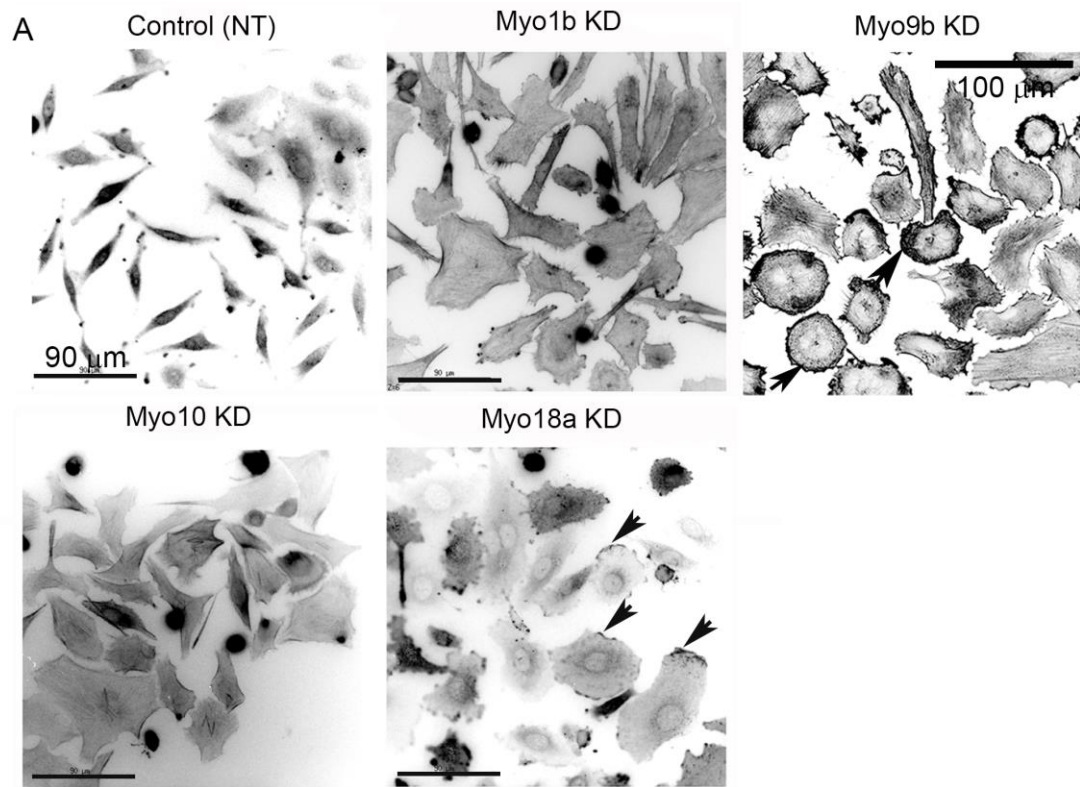
Figure 4.3 Knockdown of myosins affects morphology of PC3 cells.
A. Low power images of PC3 and myosin-depleted PC3 cells (after 72 h) stained for F-actin using fluorescent phalloidin to show changes in cell area. The fluorescent images are shown in reverse contrast for increased clarity. Arrows in the Myo9b KD picture indicate peripheral high density actin staining. Arrows in the Myo18a KD picture show numerous membrane ruffles. Scale bar = 90 µm or as shown. The images are representative of at least 3 separate experiments Control cells were treated with non-targeting siRNA (NT). B, C. Quantification of filopodial number (B) and cell area (C), bars represent mean + S.E. for n=20 cells from at least 3 separate experiments. Statistical analysis was performed using two-way ANOVA. Levels of significance are indicated by: $p < 0.05$ statistically significant (*), $p < 0.01$ very significant (**), $p < 0.001$ extremely significant (***).

To ensure that myosins were being inhibited specifically, and that the observed changes were not just a result of off-target effects, I also looked at the effect of individual siRNA reagents for Myo10 in PC3 cells. As shown by immunoblotting (Figure 4.2B), using individual siRNAs resulted in about 75% decrease in levels of Myo10, comparable to SMARTpool, which is a mix containing 25% of each of the 4 individual siRNA sequences. Furthermore, knockdown by individual reagents in PC3 cells resulted in similar phenotype changes (Figure 4.4A), including significantly decreased numbers of filopodia (Figure 4.4B) and an increase in cell area (Figure 4.4C). All types of treatment produces morphological changes similar to previous SMARTpool knockdown, with formation of actin stress fibres and loss of filopodia, which confirmed that the observed results are connected specifically to depletion of Myo10. This confirmed that the use of SMARTpool is efficiently and specifically knocking down the myosin of interest.
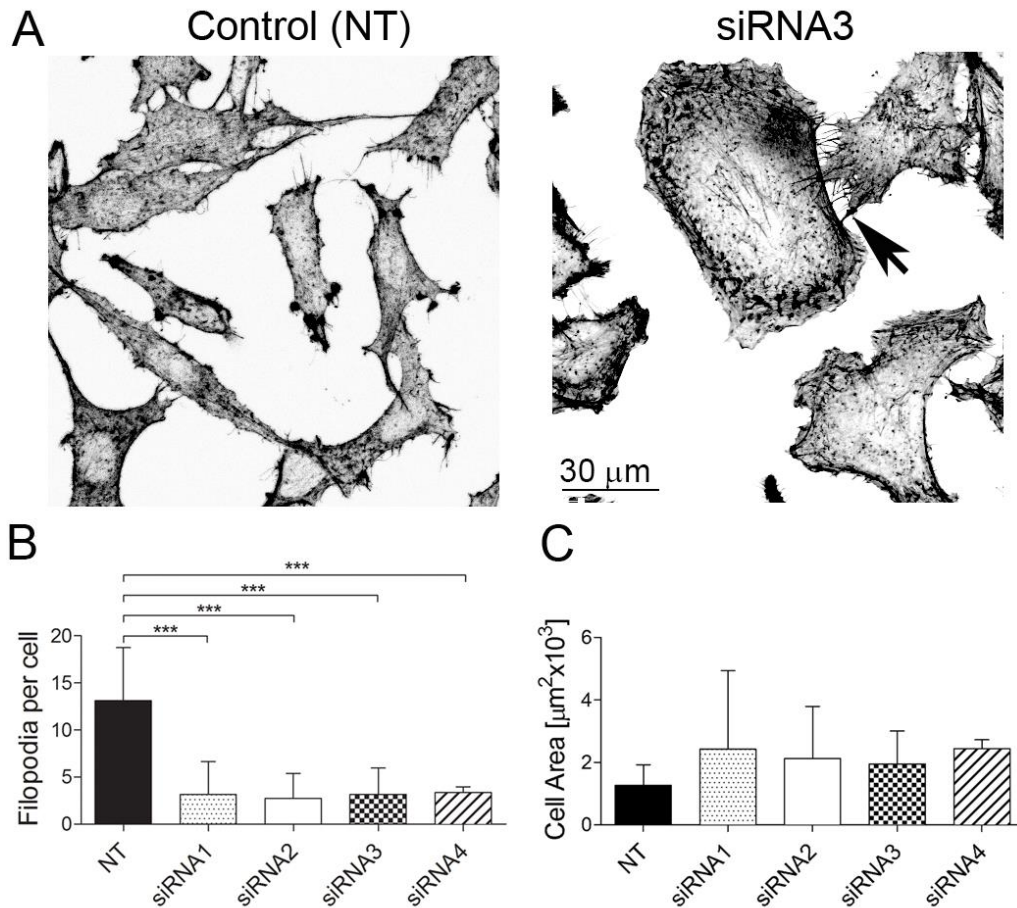
Figure 4.4 Knockdown of Myo10 by individual siRNA reagents.
A. Control and myosin-depleted PC3 cells (after 72 h) stained for F-actin using fluorescent phalloidin to show changes in cell area. The fluorescent images are shown in reverse contrast for increased clarity. Treatment with individual siRNA reagents (siRNA3 as an example) results in the same morphology changes as in case of SMARTpool, although some smaller cells with filopodia are also visible (arrow points to filopodia). Control cells were treated with non-targeting siRNA (NT). Scale bar = 30 μm. The images are representative of at least 3 separate experiments. B, C. Quantification of filopodial number (B) and cell area (C), bars represent mean + SD for n=20 cells from at least 3 separate experiments. Statistical analysis was performed using two-way ANOVA, $p < 0.001$ extremely significant (***).

4.2.3 Myo10 overexpression in prostate cancer cells increases the numbers of filopodia

Considering the striking reduction in filopodia number after Myo10 knockdown in PC3 cells, I then overexpressed Myo10 fused to GFP (Green Fluorescence Protein) (GFP-Myo10) to see whether increased levels of Myo10 will correlate with higher filopodia numbers. Myo10 overexpression has been shown to increase filopodia numbers in several cell lines (Berg and Cheney, 2002; Bohil et al., 2006), but not in prostate cancer cells. I overexpressed GFP-Myo10 in both PC3 cell line and the more benign LNCaP cells, characterised in Chapter 3 (Figure 4.5A). Similarly to endogenous Myo10, GFP-Myo10 localised to the tips of filopodia. Both cell lines overexpressing GFP-Myo10 showed increased numbers of filopodia in comparison to control cells. This was particularly visible in the LNCaP cell line where overexpression of GFP-Myo10 resulted in a significant increase, from 0.2 ± 0.6 filopodia per cell (mean $\pm$ SD, n=10) to an average of 9.2 ± 1.81 filopodia per cell, (mean $\pm$ SD, n=10, $p < 0.05$) (Figure 4.5B). These results confirmed that numbers of filopodia correlate with levels of Myo10.
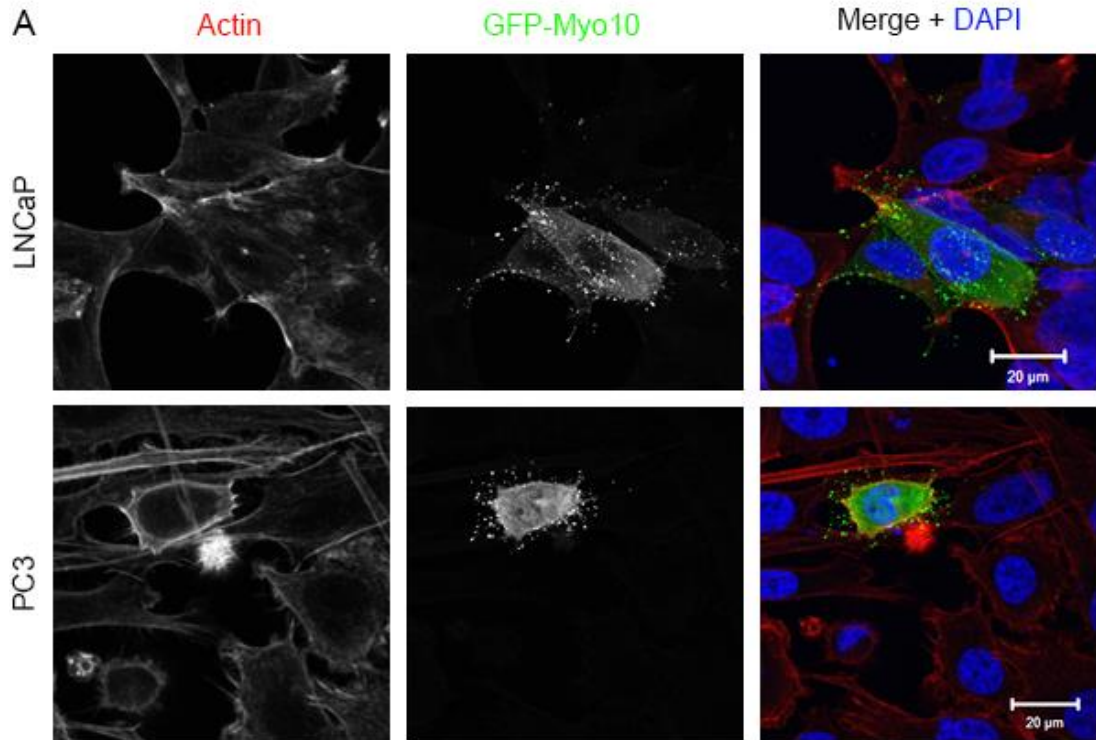
Figure 4.5 Overexpression of Myo10-EGFP results in increased number of filopodia in LNCaP and PC3 cell lines. A. LNCaP and PC3 cells stained for F-actin (AF546-phalloidin, red) and nuclei (DAPI, blue). Scale bar = 20 μm. The images are representative of at least 3 separate experiments. B. Bars represent mean + SD quantified for n = 10 cells, from 3 separate experiments. Statistical analysis was performed using two-way ANOVA, (**) is for $p < 0.01$.

4.2.4 Knockdown of Myo1b, Myo9b, Myo10 and Myo18a affects focal adhesions in PC3 cell line

Staining of myosin-depleted PC3 cells for actin and paxillin, a component of the focal adhesion complex (Turner, 2000), showed changes to focal adhesions and organisation of the F-actin cytoskeleton that depended on which myosin was knocked down. Control PC3 cells do not show prominent focal adhesions and typically contain low numbers of actin stress fibres (Figure 4.6A). After Myo1b depletion long stress fibres appeared throughout the cell and the ends of the stress fibres were associated with large, well-developed focal adhesions (Figure 4.6B, arrows). Myo9b-depleted PC3 cells were rounded, with numerous focal adhesions around the cell edges, some of them at the end of actin bundles (Figure 4.6C, arrows). Shorter, more central stress fibres were visible after knockdown of Myo10, and the ends of some of these stress fibres were associated with large focal adhesions (Figure 4.6D, arrows). In contrast, in Myo18a depleted cells, somewhat centripetal stress fibres were found in the lamella, where they were arranged parallel to the plasma membrane. Numerous prominent focal adhesions could be observed at the edges of the cell (Figure 4.6E, arrows). Moreover, a line profile analysis of the frequency of actin bundles in the lamella showed that the frequency of bundles was significantly reduced for Myo1b knockdown cells (2.1 ± 0.1 bundles per micron, mean ± S.E.M., n=9) compared to controls (2.6 ± 0.2 bundles per micron, mean ± S.E.M., n=9, p<0.5%). These results suggested to us that each myosin is able to affect the organisation of the actin cytoskeleton in a distinct way, and in particular to influence actin filament and focal adhesion formation.
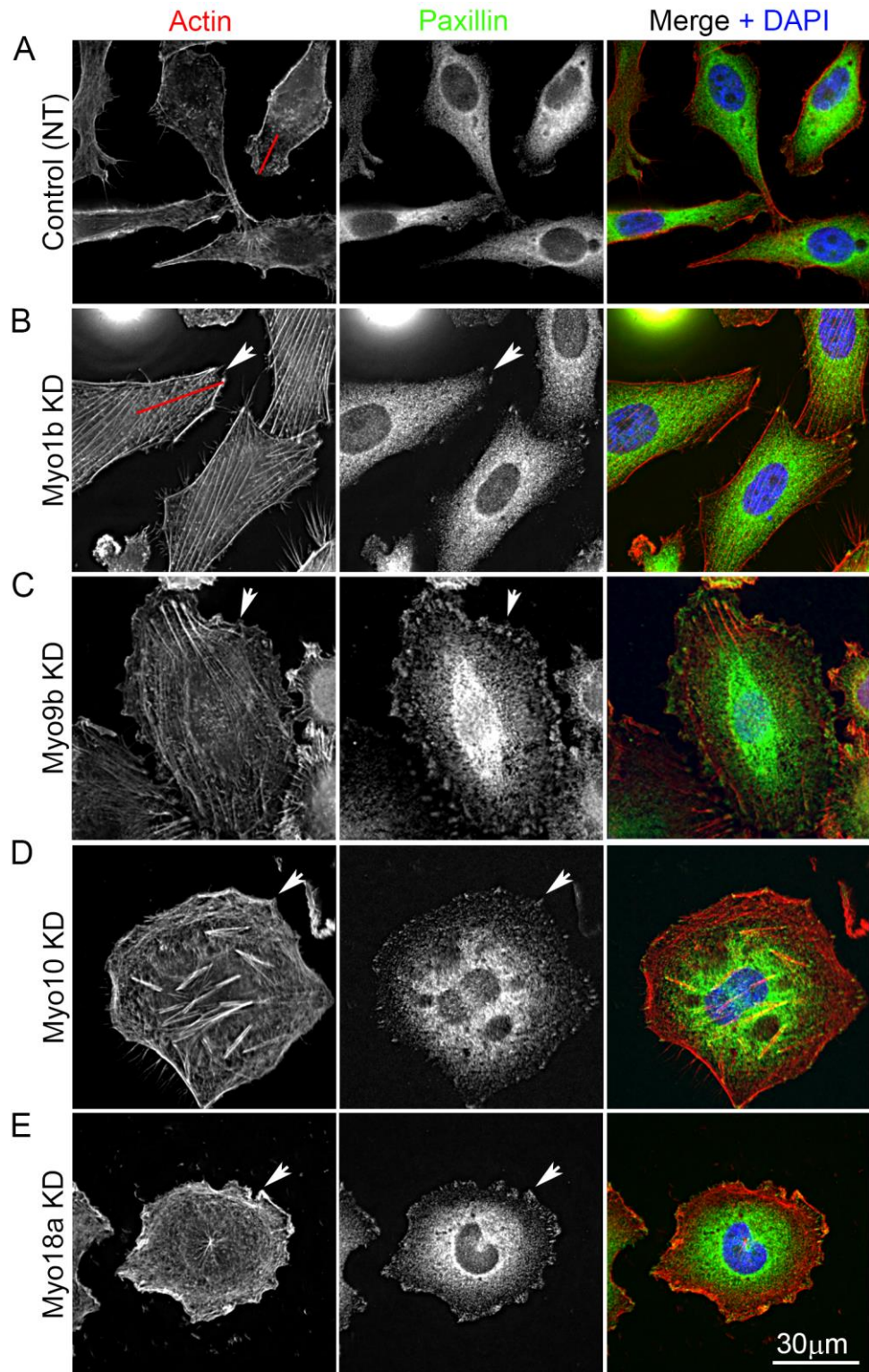
Figure 4.6 Effect of myosin knockdown on focal adhesions of PC3 cells. Control (A) and Myo1b (B), Myo9b (C), Myo10 (D) and Myo18a (E) knockdown PC3 cells stained for F-actin (phalloidin – red), paxillin (green) and nuclei (DAPI – blue). Arrows indicate large focal adhesions at the ends of F-actin bundles (arrowed) in knockdown cells. Scale bar = 30 µm. Red lines in (A, B) represent an example of line for the profile analysis of the frequency of actin bundles described in Section 4.2.4

4.2.5 Isoform-specific changes in NM2A organisation after silencing myosins

Staining of cells for actin filaments and non-muscle myosin 2a (NM2A), which is a component of stress fibres, revealed interesting, isoform-specific changes in each of the knockdowns. Control PC3 cells typically show a punctate distribution of NM2A filaments throughout the cell, with some co-localisation with actin filaments and the scarce stress fibres (Figure 4.7A, arrows and at higher magnification in Figure 4.8A). After Myo1b knockdown, NM2A filaments co-localised with the prominent long stress fibres (arrows in Figure 4.7B and Figure 4.8B). Following knockdown of Myo9b, visible stress fibres appeared across the whole cell area, with NM2A co-localising to the stress fibres. The cells also showed a distinctive actin-rich area at the cell periphery, from which NM2A was largely missing (Figure 4.7C, arrows in Figure 4.8C). Some co-localisation of actin and NM2A was also observed in Myo10-depleted PC3 cells (arrows in Figure 4.7D and Figure 4.8D).

But perhaps the most interesting changes appeared after knocking down Myo18a. The dense, centripetal actin filaments in the lamella were associated with a large visible increase in NM2A filaments (arrows in Figure 4.7E and Figure 4.8E). We found this trend really interesting, especially in light of the recent finding that Myo18a levels can affect the organisation of NM2A (Billington et al., 2015). It is worth noting that, as shown in section 4.2.1, knockdown of Myo1b, Myo10 and Myo18a did not affect the expression levels of NM2A (Figure 4.1B), and thus the changes in NM2A organisation we observed are not due to changes in NM2A expression levels. Finally, immunoblotting for phosphorylated light chain did not show any changes in levels of phosphorylation (Figure 4.9). This suggested that NM2A had not become activated by knockdown of Myo1b, Myo10 or Myo18a, but was being re-organised. Knockdown of Myo9b, however, seems to increase phosphorylation of myosin light chain, in agreement with Myo9b RhoGAP function and with what has been observed before for Myo9b knockout mice (Figure 4.9) (Hanley et al., 2010).
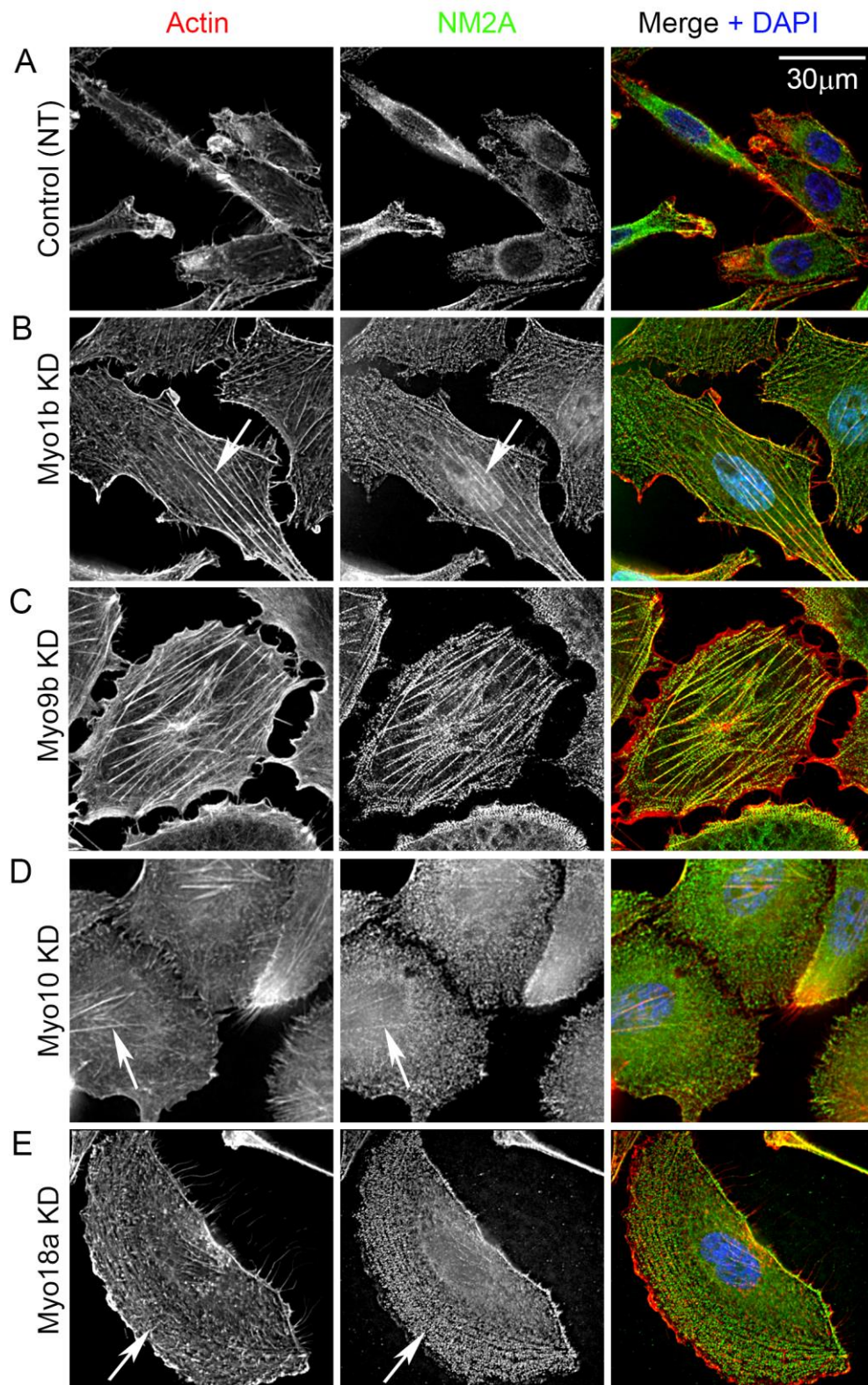
Figure 4.7 Effect of myosin knockdown on cytoskeleton and NM2A organisation in PC3 cells. Control (A) and Myo1b (B), Myo9b (C), Myo10 (D) and Myo18a (E) knockdown PC3 cells stained for F-actin (phalloidin – red), non-muscle myosin 2A (NM2A, green) and nuclei (DAPI – blue). The arrows indicate stress fibres and actin bundles in cells. Scale bar = 30 μm
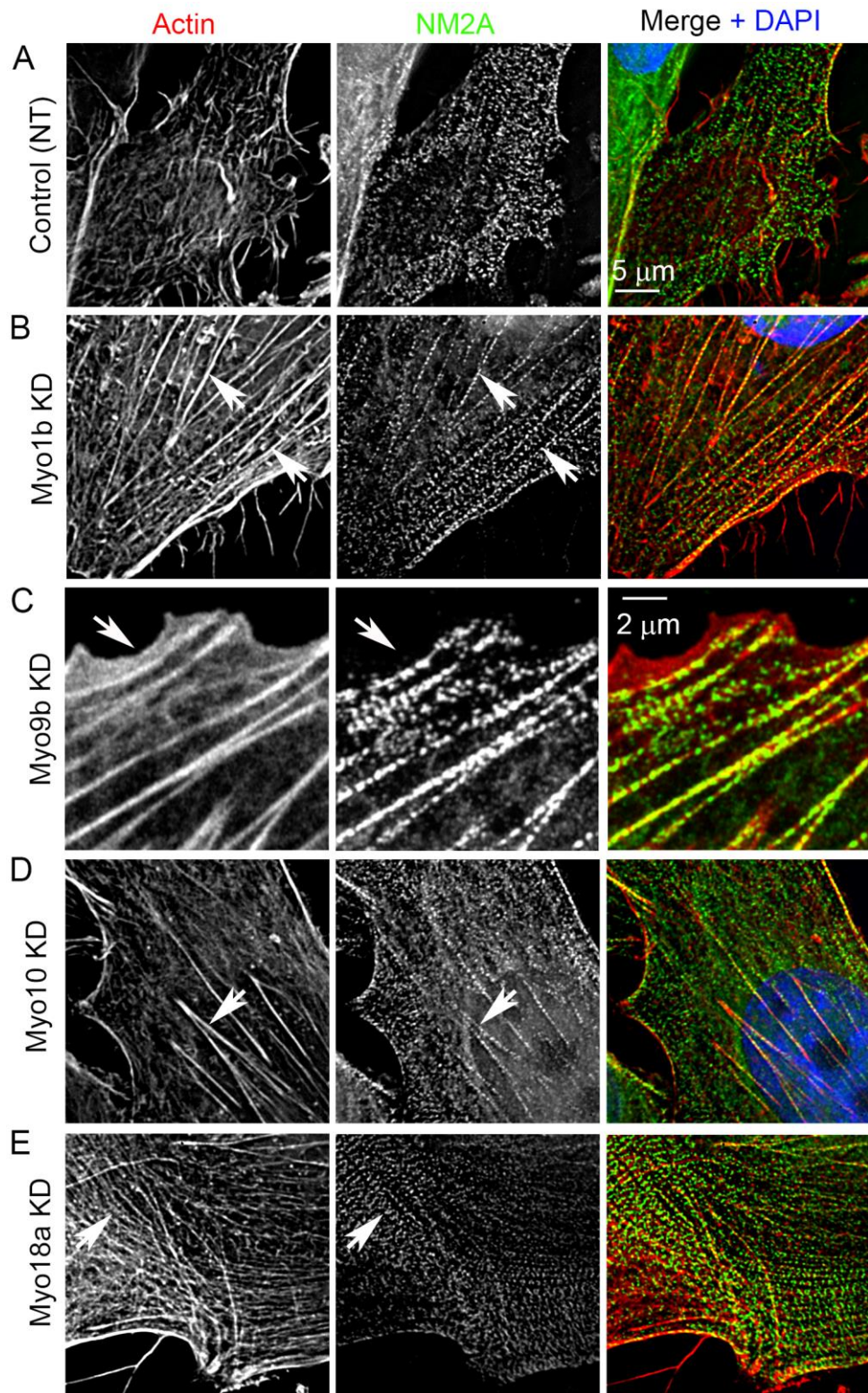
Figure 4.8 Effect of myosin knockdown on cytoskeleton and NM2A organisation in PC3 cells. Control (A) and Myo1b (B), Myo9b (C), Myo10 (D) and Myo18a (E) knockdown PC3 cells stained for F-actin (phalloidin – red), non-muscle myosin 2A (NM2A, green) and nuclei (DAPI – blue). The arrows indicate stress fibres and actin bundles in cells. Scale bar = 5 μm except for Myo9b KD (B) where the scale bar = 2 μm
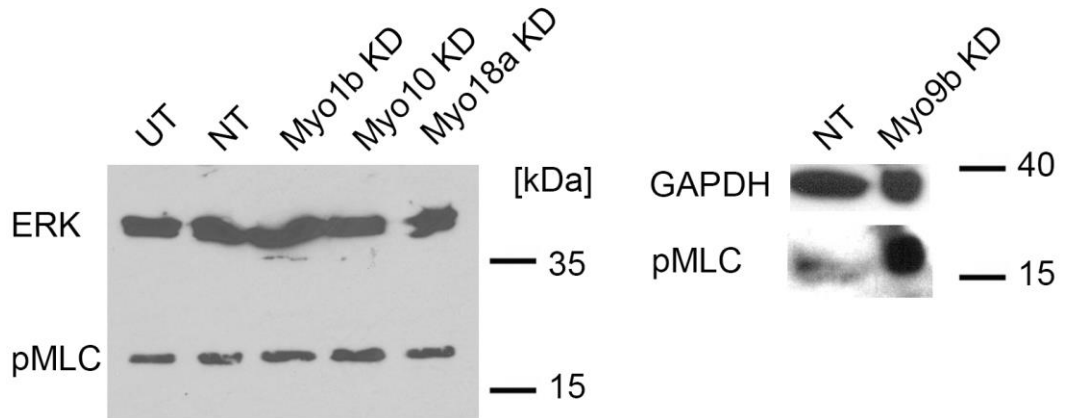
Figure 4.9 Levels of Phosphorylated Myosin Light Chain (pMLC) in PC3 cells. Levels of pMLC in control and Myo1b, Myo10 and Myo18a depleted PC3 cells, analysed by immunoblotting. Due to time restrictions, Myo9b knockdown has been analysed separately (I performed the experiment and Professor Michelle Peckham has done the immunoblotting). Control cells were treated with non-targeting siRNA (NT). Molecular weight markers shown to the right. Total ERK or GAPDH (Myo9b) were used as loading control.

4.2.6 Knockdown of myosins reduces cell migration in 2D and 3D-like environment

The changes to the actin cytoskeleton resulting from depletion of Myo1b, Myo9b, Myo10 and Myo18a raised the possibility that their depletion might also affect cell migration. Due to time restrictions, cell migration after Myo9b knockdown was not analysed during this project. As for the other myosin isoforms, overnight time-lapse microscopy and cell-tracking of HGF-stimulated PC3 cells in a 2D random migration assay showed that depletion of Myo10, but not Myo1b or Myo18a, affected cell migration speed, with tracks from Myo10-depleted cells visibly shorter than control cells (Figure 4.10A). Myo10 knockdown reduced cell speed significantly, by about 2 fold, from 0.49 ± 0.24 μm/min to 0.25 ± 0.1 μm/min (mean ± SD, n=50, p < 0.05) (Figure 4.10B). Directional persistence, defined as the ratio between displacement and the total path length, was not affected by knockdown of Myo1b or Myo10, but was significantly decreased in Myo18a depleted cells, by about 30% from 0.34 ± 0.18 to 0.26 ± 0.12 (mean ± SD, n=50, p < 0.05) (Figure 4.10C), suggesting a role for Myo18a in determining directionality of migration.

Using a circular invasion assay that closely mimics 3D invasion (Yu et al., 2012), I observed that control PC3 cells migrate freely into the matrix, whereas migration of myosin depleted cells is visibly decreased (Figure 4.10D). The control cells (NT, treated with non-targeting siRNA) migrated into cell-free area at the rate of about 26.5 ± 4.9 cells per square 250 μm x 250 μm (mean ± SD). For the same surface area, the rate for Myo1b knockdown cells was 2.6 ± 2.6, 1.4 ± 2.3 after Myo10 knockdown, and Myo18a knockdown resulted in 6.1 ± 5.2 cells on average migrating into the area (n=10 measured fields of view from at least 2 experiments). As represented by the pictures, inhibition of invasion into the cell-free Matrigel was most evident in the case of Myo10 (Figure 4.10D).
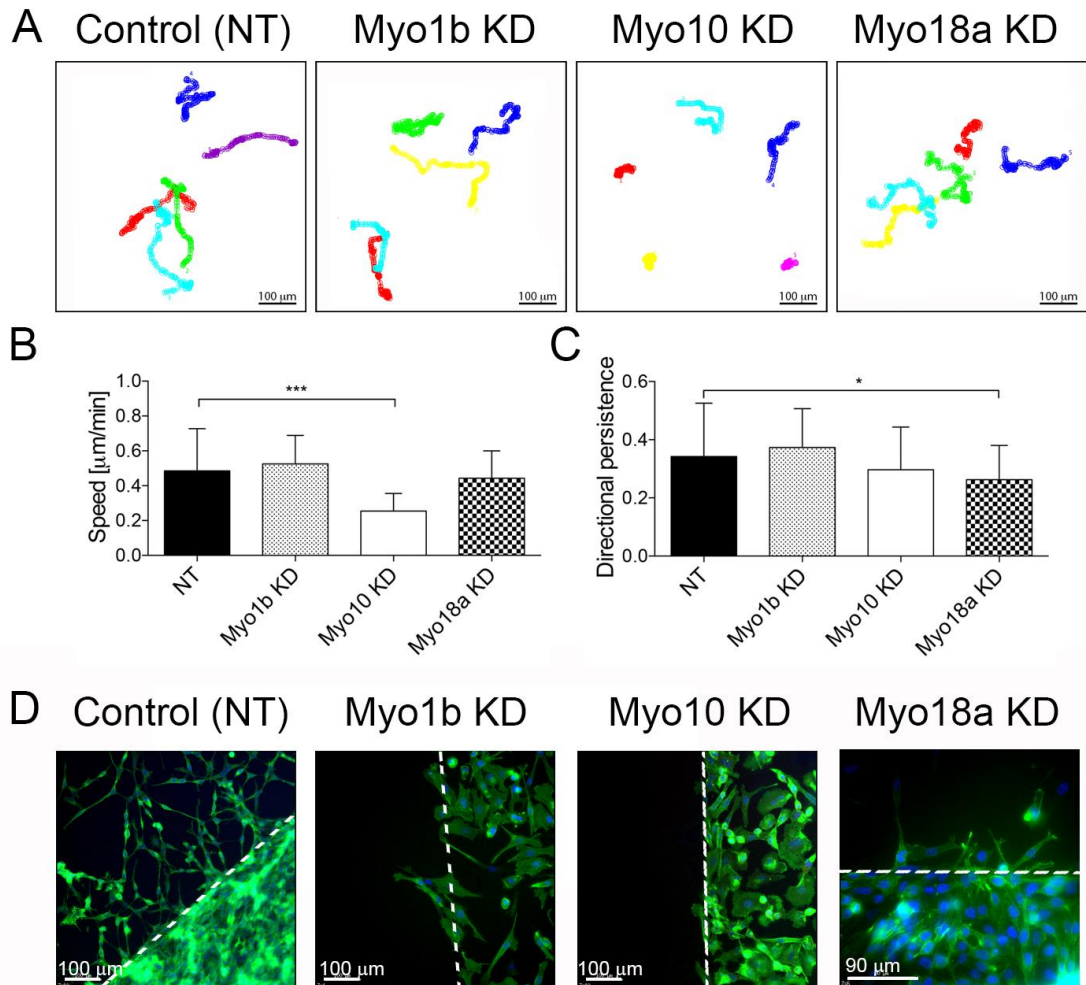
Figure 4.10 Effect of myosin knockdown on cell migration. A. Coloured lines show representative tracks for individual cells during an overnight time-lapse microscopy experiment for control (treated with non-targeting siRNA, NT) and Myo1b, Myo10 and Myo18a-depleted cells after HGF stimulation. Scale bar = 100 µm. B, C. Quantification of speed (B) and directional persistence (C) of cell migration, bars show mean + SD for n = 50 cells from at least 3 experiments (NT = control cells treated with non-targeting siRNA). Statistical analysis was performed using one-way ANOVA. Levels of significance are indicated as: p<0.05 for statistically significant (*), p<0.01 very significant (**), p<0.001 extremely significant (***). D. Circular invasion assay showing cells stained for actin filaments (phalloidin - green) and nuclei (DAPI - blue). Dashed line marks the border of cell-free space created by stoppers. Scale bars as shown. The images are representative of at least 3 separate experiments.

4.2.7 Knockdown of Myo1b affects endocytosis in PC3 cell line

As previously mentioned, Myo1b plays a role in endocytosis (Salas-Cortes et al., 2005), so I looked at this process in PC3 cells using immunostaining for EEA1 (early endosome antigen 1), a well-known marker for early endosomes (Figure 4.11A). As a control, I also tested endocytosis in cells depleted of Myo10, which is not thought to be involved in endocytosis. Knockdown of Myo1b, but not Myo10, resulted in noticeable decrease of EEA1-positive vesicles in PC3 cells. This is quantified in Figure 4.11B, confirming a statistically significant decrease of early endosomes in Myo1b-depleted cells, while endocytosis in Myo10 KD cells was not affected. Ideally, these results should be accompanied by assays looking at uptake of particles, but several attempts at experiments using fluorescent dextran or transferrin were unsuccessful and their outcomes inconclusive (data not shown).

4.2.8 Knocking down DCC, a Myo10 regulator, changes morphology of PC3 cells

As a further test of the involvement of Myo10 in the increase in filopodia, I investigated the effect of knockdown of one of its known binding partners. Myosins can be regulated by various factors and binding partners (see section 1.3.4), and Myo10 interacts with Deleted in Colon Cancer (DCC) (Zhu et al., 2007), which promotes movement of Myo10 along actin filaments and enhances Myo10-mediated elongation of basal filopodia (Liu et al., 2012). I silenced DCC in PC3 cells using siRNA (Figure 4.12A). Interestingly, analysis of immunostained PC3 cells after DCC knockdown showed an increase in cell area and loss of filopodia (quantified data not shown, representative images in Figure 4.12B, C). These effects are similar to depleting Myo10 and suggest a role for DCC in regulating Myo10 in prostate cancer cells. It would be interesting to see the effect of DCC on cell migration, although preferably efficiency of the knockdown should be optimised first, since knockdown of DCC reduced the protein levels only by about 60% in comparison to non-targeting control (Figute 4.12A).
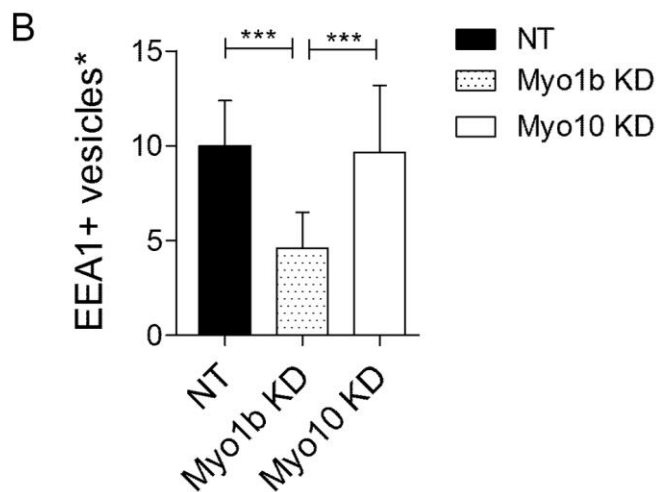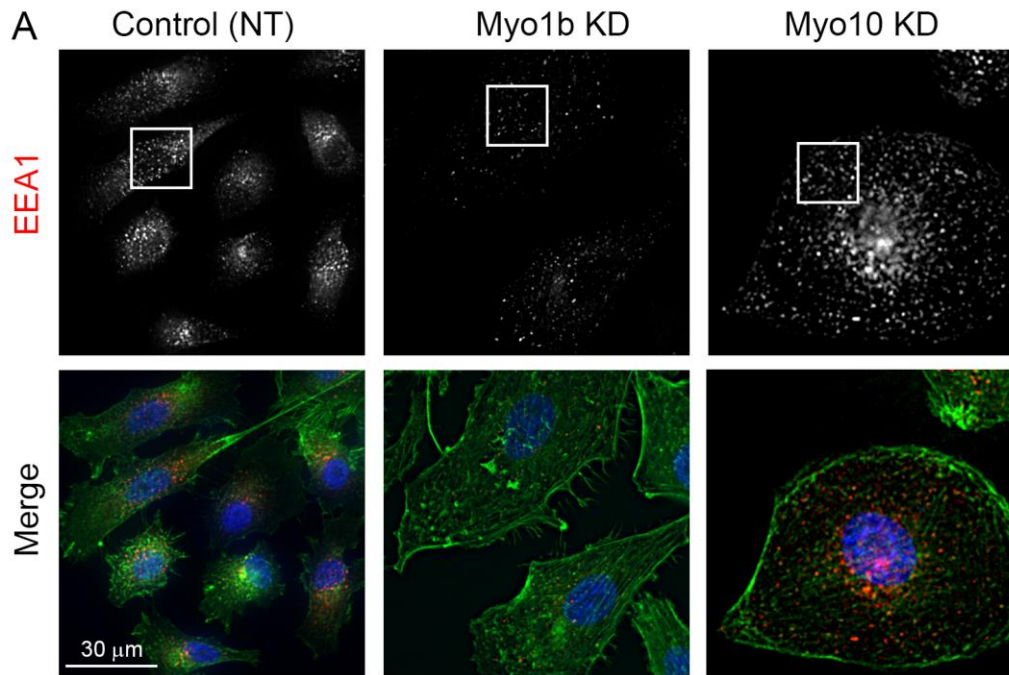
Figure 4.11 Knockdown of Myo1b affects endocytosis in PC3 cells.
A. PC3 cells stained for endosome marker, early endosome antigen (EEA1, red) actin filaments (phalloidin - green) and nuclei (DAPI - blue). White squares represent example areas where measurements were made for quantification (squares 20μm x 20 μm). Scale bar as shown. The images are representative of at least 3 separate experiments. B. EEA1-positive vesicles per square 20μm x 20 μm quantified. Bars show mean + SD for n=25 fields from at least 3 experiments. Statistical analysis was performed using one-way ANOVA. (***) is for $p < 0.001$.
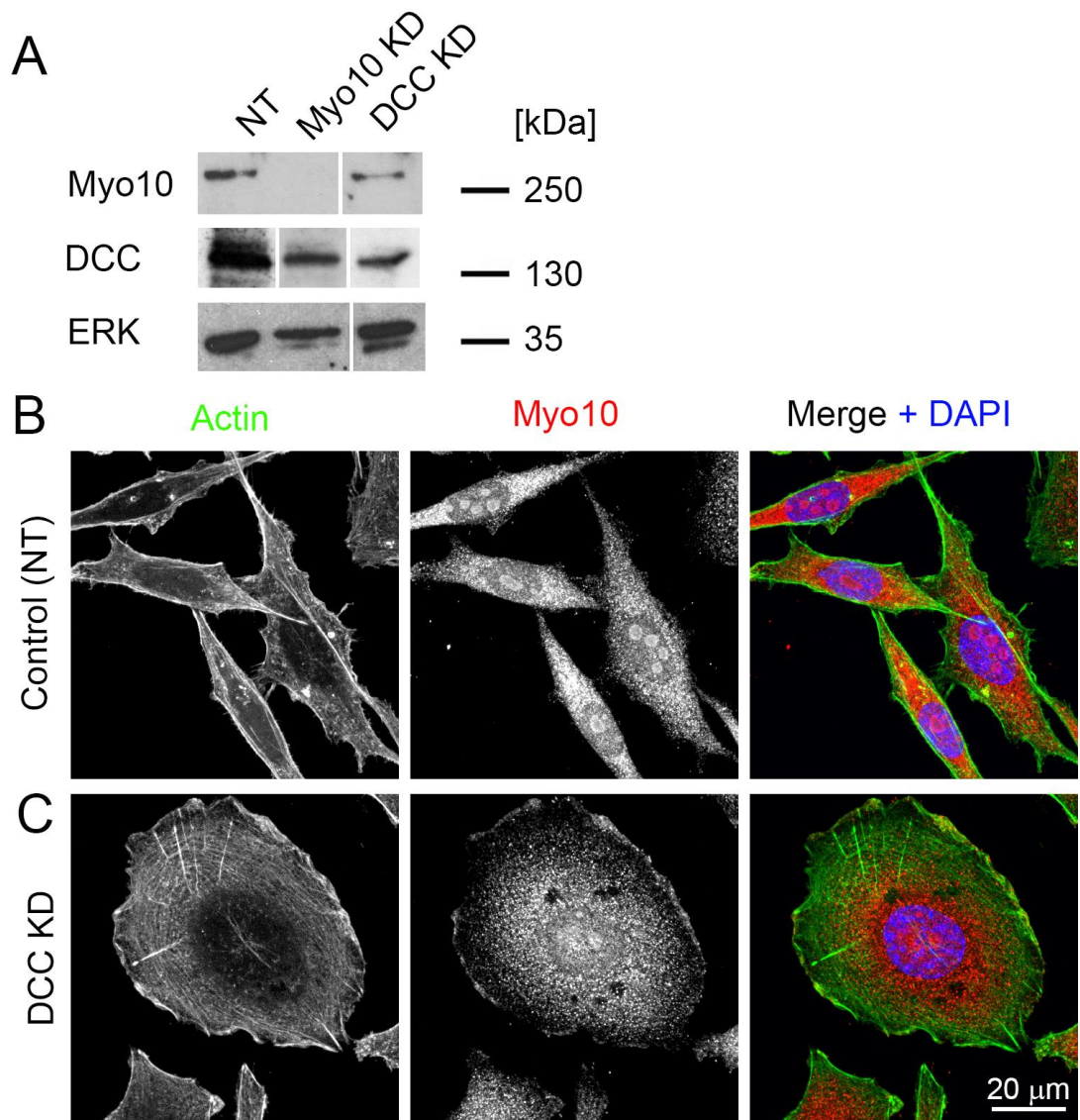
Figure 4.12 Knockdown of DCC affects the morphology of PC3 cells.
A. Knockdown of DCC and Myo10 in PC3 cells using siGENOME
SMARTpool siRNA after 72 hours, analysed by immunoblotting to confirm
efficiency. Control cells were treated with non-targeting siRNA (NT).
Molecular markers shown to the right. Total ERK was used as loading
control. B. PC3 cells stained for F-actin (phalloidin, green), Myo10 (red) and
nuclei (DAPI – blue). Scale bar = 20 μm. The images are representative of at
least 3 separate experiments.

Our functional studies relied primarily on siRNA technology and off-target effects cannot be fully excluded unless a rescue experiment is performed. However, two transient transfections (siRNA silencing and overexpression of GFP constructs) in succession are very challenging to complete successfully, and all my attempts resulted in very high cell death. In addition, siRNA-resistant constructs were not available for all the myosins of interest. I also found that four individual Myo10 siRNA sequences, each led to a similar phenotype (i.e. filopodia loss) (Figure 4.4), and this is distinct from the phenotype observed with Myo1b, Myo9b or Myo18a siRNA, arguing against off-target effects. Therefore, I concluded that it is unlikely that the off-target effects played a dominant role in mediating the biological effect of the knockdowns.

4.3 Discussion

The results presented here show that siRNA-mediated knockdown of Myo1b, Myo9b, Myo10 and Myo18a have isoform-specific effects on morphology and migration of PC3 cell line. High endogenous expression levels of Myo10 in PC3 cells are linked to high numbers of filopodia, and a more migratory phenotype as shown by immunostaining and cell migration assays. High levels of Myo1b influence cell morphology and actin organisation, with sparse long actin stress fibres appearing in Myo1b-depleted PC3 cells, but only contribute to cell migration in 3D, not 2D. High levels of Myo9b are linked to low levels of stress fibres and Myo9b knockdown increases the appearance of numerous focal adhesions. High expression levels of Myo18a affect cell morphology and organisation of NM2A, and contribute to 3D migration as well as to directional persistence of 2D cell migration. Overall, this subset of myosins might contribute to the migratory phenotype of PC3 cells, with Myo10 being the most important myosin for metastasis of prostate cancer.

Our knockdown and overexpression experiments confirm a clear relation between levels of Myo10 and numbers of filopodia, already observed in Chapter 3 when comparing different cell lines. Knockdown of DCC, Myo10 activator, also resulted in loss of filopodia, offering a further confirmation of this link. It has been shown previously that Myo10 is a strong promoter of filopodia formation. Overexpressing full-length Myo10 has been shown to increase the number and length of filopodia in previous studies, both for substrate attached filopodia, dependent on adhesion and Myo10's ability to bind integrins (Berg and Cheney, 2002; Watanabe et al., 2010; Zhang et al., 2004), and for dorsal filopodia, independently of adhesion or integrin binding (Bohil et al., 2006). It has been suggested that the Myo10 tail is mostly responsible for stimulating filopodia formation, through a variety of mechanisms. These include regulation of motor activity through a motor – tail interaction (Umeki et al., 2011) and/or transporting proteins that are important for filopodia formation, such as integrins (Bohil et al., 2006). More recent reports show that Myo10 is also required for the formation of other

actin-based protrusions such as invadopodia and podosomes (McMichael et al., 2010; Schoumacher et al., 2010).

Prostate cancer cells have been reported to exhibit motile responses to HGF (Parr et al., 2001; Wells et al., 2005). The reduction in PC3 cell migration in 2D HGF stimulated migration assays resulting from Myo10 knockdown, suggests that Myo10-dependent filopodia formation could be important for cell motility. As some cells lacking filopodia are still able to migrate (Lundquist, 2009), it has been suggested that filopodia are not essential for migration, but promote it, by exploring the environment, and enabling cells to decide where to go. Our experiments with PC3 cells, also show that filopodia are not absolutely required for cell migration, as even in the absence of filopodia, the Myo10-depleted cells were able to move in 2D migration assays, albeit more slowly than control cells.

The increase in cell area we observed when Myo10 is knocked down is consistent with that reported previously for other cell types (Bohil et al., 2006), where overexpression of Myo10 resulted in a significant reduction in cell area, and siRNA knockdown of Myo10 in HeLa cells resulted in a ~4 fold increase in cell area. It is unclear why Myo10 knockdown results in large central stress fibres, which have the appearance of thick bundles, reminiscent of bundles of actin in filopodia. However, fascin, an actin bundling protein found in filopodia is known to be overexpressed in PC3 cells (Darnel et al., 2009). Inhibition of fascin blocks filopodial formation (Huang et al., 2015). If levels of fascin remain high following Myo10 knockdown, but filopodia are unable to form, fascin may be able to bundle actin filaments in the cell body producing the large central stress fibres we observed.

Our finding that Myo10-dependent filopodia are likely to be important for cell migration agrees with the recent findings that Myo10-dependent filopodia are important for breast cancer metastasis (Arjonen et al., 2014; Cao et al., 2014). Myo10 was found to be upregulated in aggressive subtypes of breast carcinoma, and it was shown to be required for breast cancer cell adhesion,

migration and invasion *in vitro*, and to regulate dissemination of breast cancer cells *in vivo* in a mouse model (Arjonen et al., 2014; Cao et al., 2014). In this case, Myo10-induced cell adhesion, migration, and invasion were dependent on stabilization of filopodia that protrude into the matrix using the cell adhesion receptor β1 integrin.

One of these groups also reported a new link between Myo10 upregulation and mutant p53 expression (Arjonen et al., 2014). Mutant p53, a stable variant of p53 (resulting from gain-of-function mutations), is associated with increased metastasis, and overexpression of Myo10 is linked to expression of p53 in clinical breast cancer samples. Silencing of mutant p53 downregulated Myo10 expression levels, through the MAPK/ERK pathway, as inhibiting this pathway was also able to downregulate Myo10 expression levels. In addition, mutant p53 is also associated with an increase in the transcription factor ERG1 (early growth response protein 1), and ERG1 binds to the Myo10 promoter (Arjonen et al., 2014), thus providing a link between p53 and Myo10 expression levels. However, PC3 cells do not express p53, while they still have high levels of Myo10 expression (Carroll et al., 1993). Therefore, in these cells there must be some other mechanism by which Myo10 levels are increased.

We found that Myo18a affects PC3 cell morphology, migration and organisation of actin and NM2A, indicating that Myo18a contributes to cell motility. The large re-organisation of actin and NM2A induced by Myo18a knockdown may have two possible explanations; its interaction with non-muscle myosin 2 (NM2A) and its interaction with Myotonic dystrophy kinase-related Cdc42-binding kinase (MRCK; (Tan et al., 2008)) through the leucine rich adaptor protein LRAP35a. Myo18a associates with MRCK, which is linked to Cdc42, and works with ROCK to phosphorylate MYPT1 (myosin phosphatase target subunit-1). MYPT1 inhibits myosin light chain phosphatase (MCP1), thereby increasing MLC2 (myosin light chain 2) phosphorylation (Wilkinson et al., 2005), and should therefore increase the activity of NM2A and thus cell contractility. The association of MRCK with Myo18a is suggested to increase MLC2 phosphorylation, and increase

NM2A assembly in the lamella. MRCK knockdown resulted in a loss of lamellar NM2A –actin networks, while Rho mediated stress fibres remained. A similar effect was observed when Myo18a was depleted. However, this is not consistent with our finding that knockdown of Myo18a in PC3 cells results in an increase in NM2A filaments in the lamella.

Recently, Myo18a was additionally found to interact directly with NM2A *in vitro*, co-assembling into mixed bipolar filaments both *in vitro* and *in vivo* (Billington et al., 2015). Moreover, this interaction resulted in shorter NM2A filaments *in vitro* (Billington et al., 2015), suggesting that Myo18a is able to affect the size and organisation of NM2A filaments. NM2A filaments are ~314nm long, but mixed NM2A/Myo18a filaments are only 227 nm long. The failure to observe this *in vivo* using super-resolution microscopy was attributed to the low levels of Myo18a expression compared to NM2A. However, they pointed out that the ratio of Myo18a to NM2A could be higher in some cell types or subcellular locations (Billington et al., 2015), in which case effects on filament organisation might be observed. This suggests that the re-organisation of NM2A that we found to result from Myo18a knockdown results from a reduction in the direct interaction between Myo18a and NM2A, rather than changes in levels of light chain phosphorylation, or levels in NM2A expression.

Myo18a has also been identified as an interacting partner for the p21-activated kinase (PAK) though the βPIX/GIT1 complex (Hsu et al., 2010). That study showed that knockdown of Myo18a increased the size of focal adhesions, increased cell area and the cells became more rounded with dense, centripetal actin filaments, similar to the findings reported here. These authors suggested that when Myo18a is knocked down, PAK2 becomes relocalised to focal adhesions contributing to their increase in size and number, and the enlarged morphology observed, and that a lower focal adhesion turnover explains their lower motility. Consistent with these results, we also found that Myo18a knockdown increases the number of cell adhesions. Myo18a has also been reported to be required for cell migration in 2D and 3D (Hsu et al., 2014; Hsu et al., 2010; Tan et al., 2008), in

agreement with our findings that Myo18a knockdown affects directional persistence in 2D migration assays, and reduces migration in 3D migration.

High levels of Myo9b expression in PC3 cells are likely to contribute to lack of stress fibres, and thus to enhanced cell migration. The RhoGAP domain in Myo9b tail inhibits Rho, which reduces the downstream activity of ROCK (a Rho kinase). This in turn increases myosin light chain (MLC) phosphatase activity, resulting in lower levels of MLC phosphorylation, thus reducing actin stress fibre formation. This would mean that Myo9b knockdown, by increasing Rho activity, should increase stress fibre formation and MLC phosphorylation, and it's what was observed in this study. Genetic variation in Myo9b has recently been associated with an increased risk of esophageal adenocarcinoma, although its exact role remained undefined (Menke et al., 2012). Even though I did not look at cell migration of Myo9b-depleted cells in this project, such analysis was subsequently done by my group and showed that Myo9b knockdown significantly decreased cell migration in 2D and 3D, further confirming a potential role for Myo9b in motility of prostate cancer cells (Makowska et al., 2015).

Our screening data suggested that Myo1b might also play a role in metastasis, and knockdown of this myosin affects cell migration in 3D, cell shape and morphology, as well as endocytosis. Myo1b regulates actin assembly at various regions in the cell including the production of post-Golgi carriers (Almeida et al., 2011; Gillespie et al., 2001), endocytic organelle transport (Cordonnier et al., 2001; Raposo et al., 1999), and in maintaining cortical tension at the plasma membrane, where it specifically associates with dynamic, non-tropomyosin containing actin filaments (Coluccio and Geeves, 1999; Tang and Ostap, 2001). High endogenous levels of Myo1b in more highly metastatic cells might therefore increase cortical tension allowing cells to move through stiff extracellular matrices *in vivo*, perhaps explaining why knockdown of Myo1b affects migration in 3D, but not on a 2D surface.

Myo1b has been recently shown to regulate cell motility in human head and neck squamous cell carcinoma (HNSCC) (Ohmura et al., 2015). In this study, downregulation of Myo1b inhibited metastasis to lymph nodes in a model using nude mice. Consistent with our observations, Myo1b knockdown in HNSCC was shown not to affect the filopodia, and the authors suggested that Myo1b contributes to cancer cell motility through its role in the formation of large protrusions at the leading edges of cells (Ohmura et al., 2015). Epithelial to mesenchymal transition (EMT) is one of the mechanisms of cancer progression, including migration and invasion, the researchers also investigated the relation between Myo1b expression and some EMT-related molecules, but found no connection, concluding that Myo1b has a role in cell motility of HNSCC independent of major EMT transcription factors but through a different mechanism (Ohmura et al., 2015).

Myo1b has been associated with other types of protrusions than filopodia. Some of the protrusions where Myo1b has been observed seem to resemble tunnelling nanotubes, which have recently been observed in pancreatic cancer cells (Ware et al., 2015). It would be interesting to explore the role of Myo1b in these structures, especially that Myo1b plays a role in elongating membrane tubules (Almeida et al., 2011; Yamada et al., 2014). Although we did not see that Myo1b knockdown affects filopodia, Myo1b was reported to contribute to formation of so called 'repulsive filopodia' (Prosperi et al., 2015). Myo1b interacts with EphB2 receptor, and Eph receptors together with their ligands, ephrins, are important for cell segregation and cell repulsion (Astin et al., 2010). Myo1b is required to initiate the formation of long, thin EphB2-enriched filopodia at the interface of ephrinB1 and EphB2 cells (Prosperi et al., 2015). Myo1b may also regulate membrane tension by coupling cortical acto-NMM2 network to the plasma membrane (Diz-Munoz et al., 2010) and thus contributes to cell repulsion by regulating NMM2 distribution (Prosperi et al., 2015). Authors of this study speculate that similarly to its role for coupling the actin cytoskeleton to organelle membrane, Myo1b may couple mechanically the contractile acto-NMM2

fibres to the plasma membrane after its phosphorylation by EphB2 (Almeida et al., 2011; Prosperi et al., 2015; Yamada et al., 2014).

To conclude, these results show that Myo1b, Myo9b, Myo10 and Myo18a all contribute to the morphology and/or migration of highly metastatic PC3 cell line. Each myosin has an isoform-specific effect on actin organisation, and their increased expression in cells with high metastatic potential may allow them to work collectively. Together, they help generate a cell with multiple protrusions that is better able to migrate through a 3D matrix. In particular Myo10, which is important for filopodia in prostate cancer cells as well as in breast cancer, is likely to be important for metastasis in a broad range of tumours. Many different drugs have now been developed that can inhibit specific myosin isoforms including those in classes 1, 2, 5 and 6 (Bond et al., 2013), and our results additionally suggest that developing drugs to block specific myosin function could be useful in preventing metastasis. Importantly, these results emphasise that myosins not only use actin as tracks to walk along, but are able to actively drive actin organisation in cells.

Chapter 5
Myosins in other tissues

5.1 Introduction

After analysing myosins in prostate cancer in detail, two major questions have arisen: what is the myosin status in non-malignant prostate tissue and do myosins also play a role in other types of cancer. In this final experimental chapter, I have addressed both these questions: I have analysed a cell line representing benign prostate tissue and investigated myosins in a glioblastoma cell culture model.

5.1.1 Benign prostatic hyperplasia

One example of non-malignant prostate tissue is the BPH-1 cell line, which is derived from benign prostatic hyperplasia (BPH). This is a very common prostate disorder, affecting approximately 70% of men over the age of 70 (McVary, 2007). BPH is not considered to be a precursor of prostate cancer or a premalignant lesion, although the association between the two diseases remains unclear (Orsted and Bojesen, 2013). It is likely that although BPH does not increase the chances for prostate cancer development, it may increase the chance of diagnosing an incidental cancer (Chang et al., 2012).

5.1.2 Glioblastoma

Tumours of the central nervous system (CNS) can arise from several different cellular lineages that include glia, such as astrocytes and oligodendrocytes (Ostrom et al., 2014). Glioblastoma is the most common and most malignant of all glial tumours (grade IV astrocytoma), accounting for 60% of all of them (Ostrom et al., 2014). Malignant gliomas (glioblastomas) are primary brain tumours that are resistant to therapy and often have poor prognosis (Buckner et al., 2007; Stupp et al., 2007).

Interestingly, gliomas rarely metastasise outside the CNS, but they are capable of spreading long distances within the brain (Beadle et al., 2008; Burger and Kleihues, 1989). This limits effectiveness of local therapies and contributes to the high mortality rate seen in these tumours (Lim et al., 2007).

Moving glioma cells face particular mechanical constraints in the CNS environment they invade, which is packed tightly and has extracellular spaces in the sub-micrometre range (Thorne and Nicholson, 2006). The exact mode of migrating remains poorly understood. Migration of neural progenitor cells before they mature into neurons and glia provides some insight into the process: these cells utilise a unique, two-step mechanism not described in non-CNS-derived cells: continuous extension of a long finger of cytoplasm and separated, salutatory bursts of movements of the cell body (Bellion et al., 2005; Kakita and Goldman, 1999; Schaar and McConnell, 2005). However, changes in development of the brain can affect this process, so the mechanism of migration through adult brain has not been fully characterised (Beadle et al., 2008). It remains unclear whether invasion of the brain by human glioma cells occurs by mechanisms used by other non-CNS cells, such as carcinomas, the unique mechanism used by neural progenitor cells or in an entirely different way.

5.2 Results

5.2.1 Levels of myosins in Benign Prostatic Hyperplasia (BPH-1)

I first investigated the expression levels of different myosin isoforms in BPH-1 cell line. I focused on the myosins previously analysed in prostate cancer cell lines (Chapter 3) by immunoblotting Myo1b, NM2A, Myo6, Myo10 and Myo18a (Figure 5.1A). Myo9b was not involved in the analysis due to time constraints. I found that levels of Myo10 were quite high in BPH-1 cells, in comparison, about 50% of what I observed in the PC3 cell line. Myo1b expression was particularly high in the BPH-1 cell line, almost 2-fold higher than in PC3 cells. Levels of Myo6 and Myo18a were low, comparable to PC3 cell line (Figure 5.1A and B), and expression of Myo6 were still significantly higher in LNCaP cells than the other cell lines. Expression levels of NM2A (Figure 5.1) were similar across the examined cell lines (Section 3.2.4).

I also stained the BPH-1 cells for actin to investigate their overall morphology, in particular how actin is organised in these cells and the number of filopodia (Figure 5.1C). BPH-1 cells are adherent, rounded and grow in round-shaped colonies. Actin filaments are mostly found in bundles at the cell borders (Figure 5.1C). The cells display numerous protrusions and some ruffles, including protrusions that overlap with the neighbouring cells in the colonies. An analysis of filopodia number showed that BPH-1 cells have on average 8.1 ± 3.4 filopodia per cell (mean ± SD, n=20), although their ability of forming tight colonies can account for some inaccuracies in measurement. It is worth noting that this is on average 2 times less filopodia per cell than in PC3 cell line (15.35 ± 7.7, see Section 3.2.5), and this ratio correlates accurately with the expression levels of Myo10 in BPH-1 and PC3 cells.
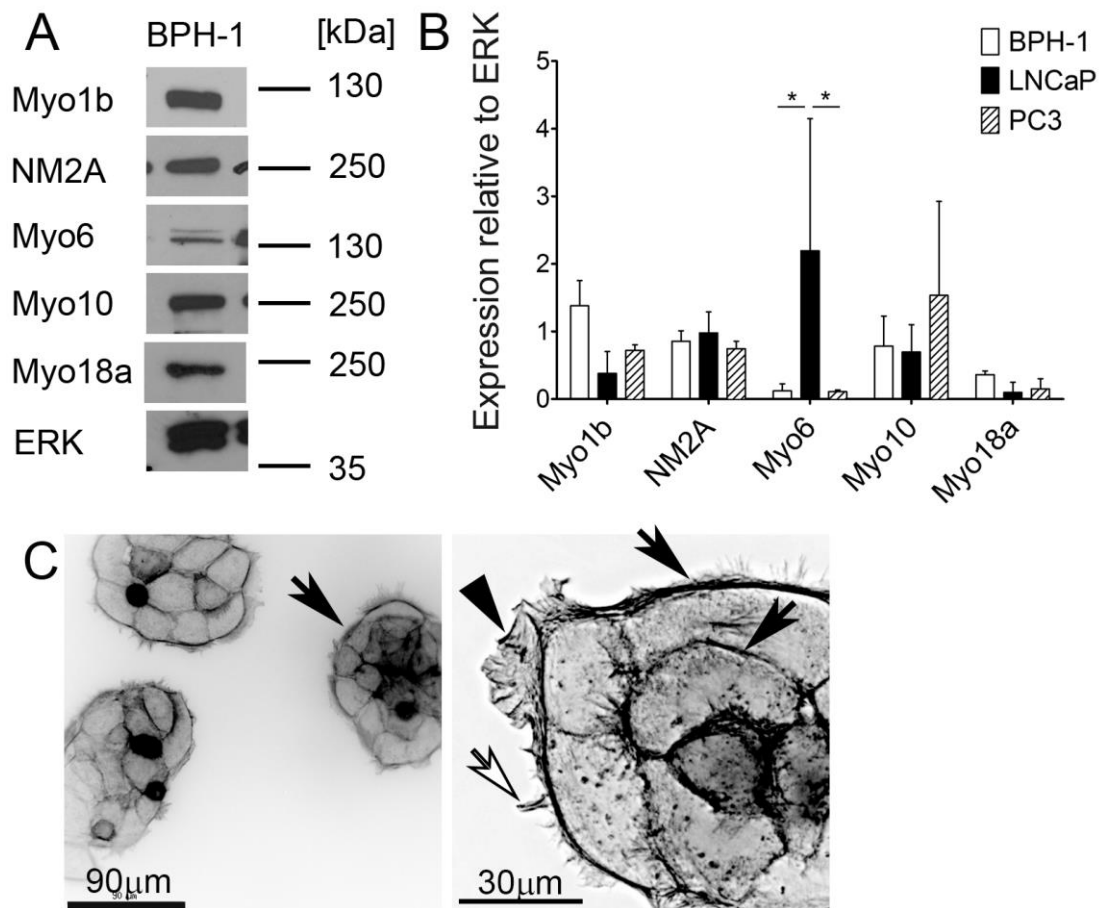
Figure 5.1 Myosins in BPH-1 cell line. A. Representative immunoblots for a range of myosins in BPH-1. Similar amounts of protein were loaded for each blot. Total ERK used as loading control. Molecular markers shown to the right. B. Quantification of expression relative to ERK, bars represent mean + SD for at least 3 experiments. Statistical analysis was performed using two-way ANOVA. Levels of significance indicated by: $p < 0.05$ statistically significant (*). Data from Figure 3.4 (LNCaP and PC3 cell lines) included for comparison. C. Low power (left) and high power (right) images of BPH-1 cells stained for F-actin using fluorescent phalloidin to show their morphology. The fluorescent images are shown in reverse contrast for increased clarity. Black arrows indicate actin bundles around the colonies and between cells. White arrow shows filopodia. Black arrowhead indicates a membrane protrusion. Scale bars as shown. The images are representative of at least 3 separate experiments.

5.2.2 Localisation of myosins in BPH-1 cell line

Next, I used immunostaining to look at the localisation of myosin isoforms in BPH-1 cell line. Similarly to PC3 cells, Myo10 in BPH-1 cells localised to the tips of filopodia and protrusions (arrows in Figure 5.2D and Figure 5.3D). Myo1b is localised close to the plasma membrane between neighbouring cells and in membrane ruffles (Figure 5.2A and arrow in Figure 5.3A). NM2A co-localised with F-actin bundles at the border of cells towards the edges of the colonies (arrows in Figure 5.2B and Figure 5.3B), unlike in prostate cancer cell lines LNCaP or PC3. Myo6 showed a somewhat diffuse staining in BPH-1 cells (Figure 5.2C and Figure 5.3C) and Myo18a localised to membrane ruffles at the border of colonies (arrows in Figure 5.2E and 5.3E). The nuclear staining observed for Myo18a was unexpected and may be non-specific.
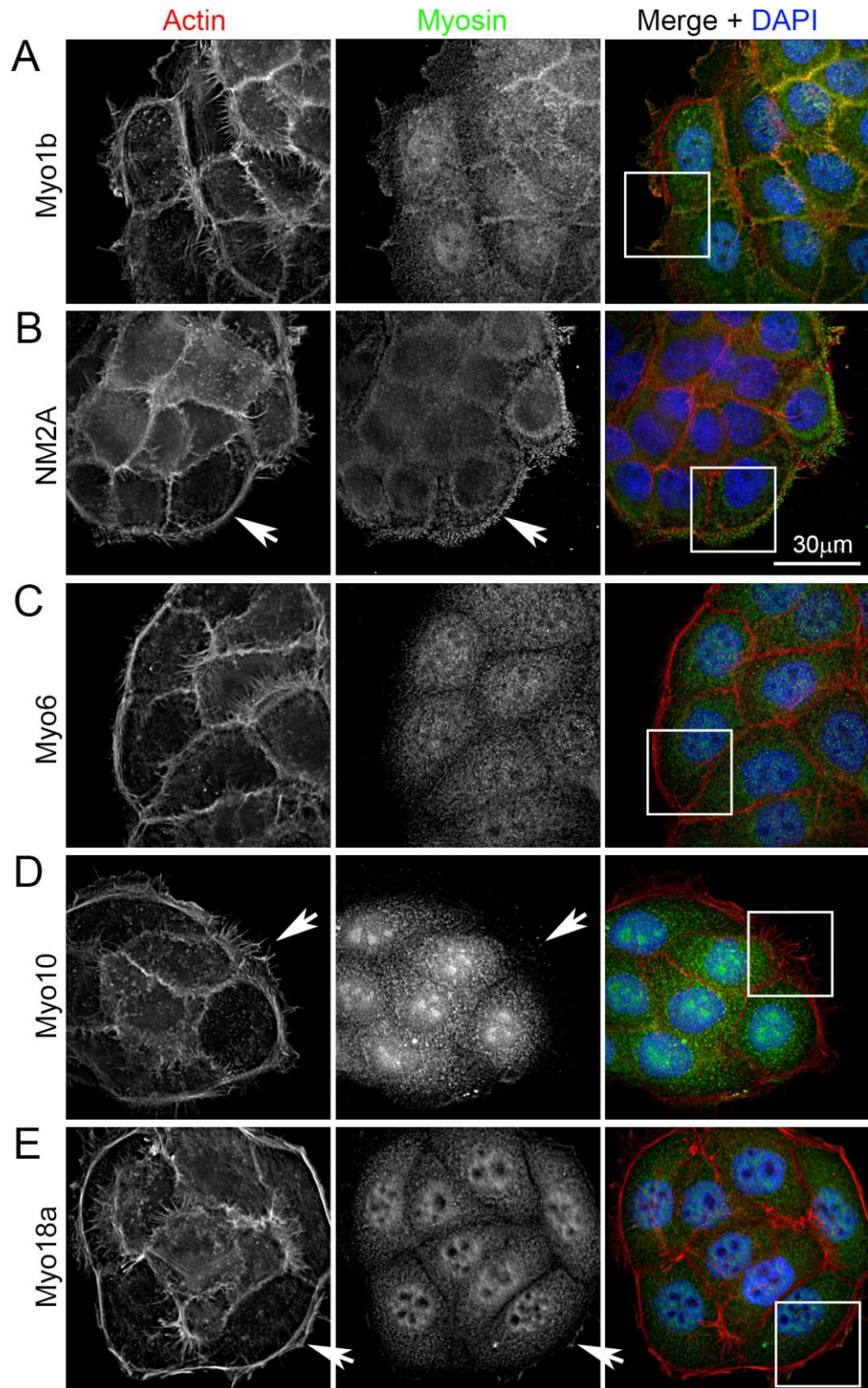
Figure 5.2 Localisation of myosins in BPH-1 cell line. BPH-1 cells stained for F-actin (AF546 phalloidin – red), nuclei (DAPI – blue) and myosins: 1b (A), NM2A (B), Myo6 (C), Myo10 (D) and Myo18a (E). Scale bar = 30 μm. White squares show areas zoomed in in Figure 5.3. The images are representative of at least 3 separate experiments.
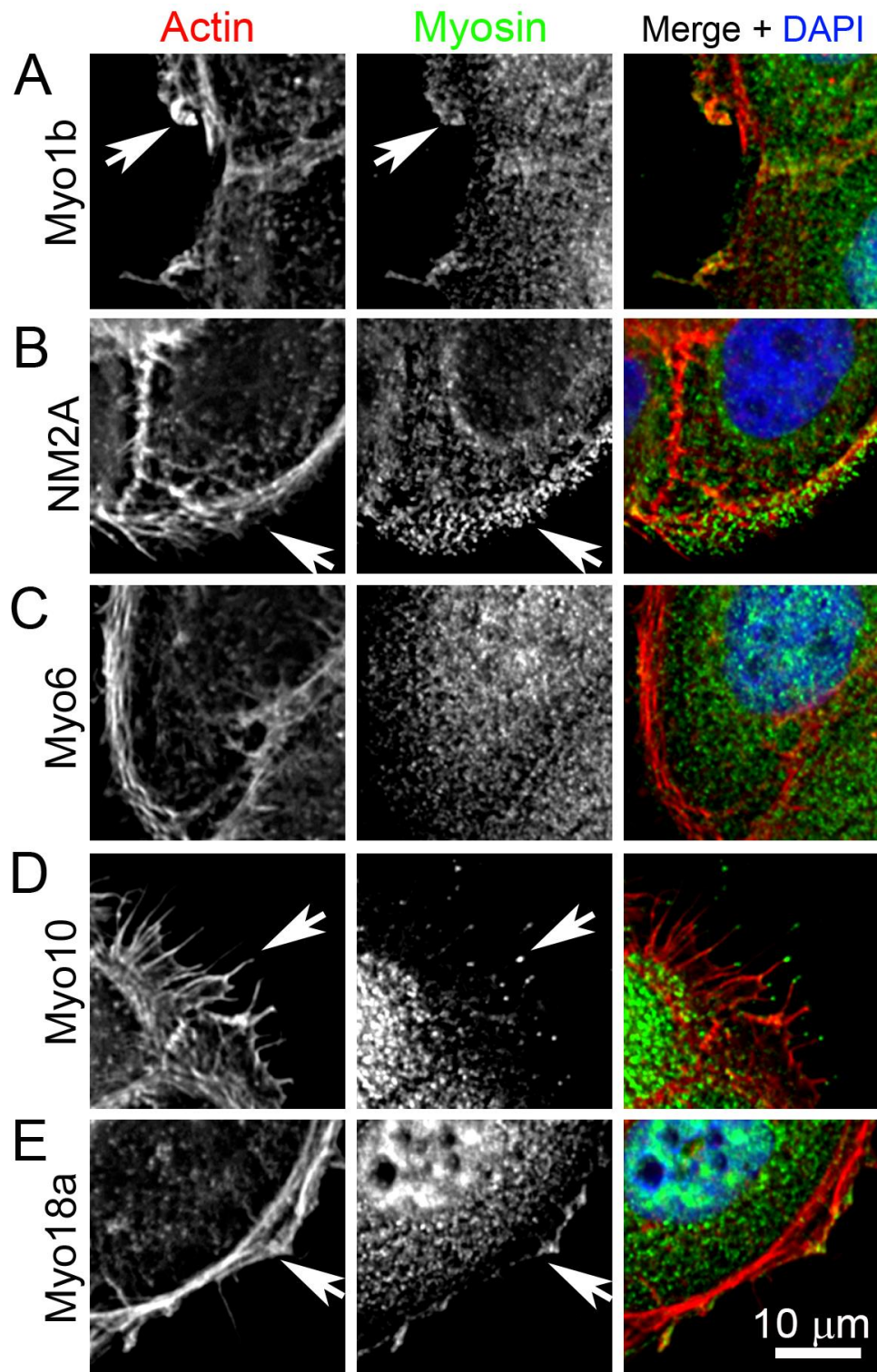
Figure 5.3 Localisation of myosins in BPH-1 cell line (zoomed in images from Figure 5.2). BPH-1 cells stained for F-actin (AF546 phalloidin – red), nuclei (DAPI – blue) and myosins: Myo1b (A), NM2A (B), Myo6 (C), Myo10 (D) and Myo18a (E). Scale bar = 10 μm. The images are representative of at least 3 separate experiments.

5.2.3 Knockdown of myosins in benign prostate cell line, BPH-1

When looking for potential therapeutic targets, it is crucial that they have effect over cancer cells while leaving normal, benign cells unaffected. While I already confirmed in the previous chapters that Myo1b, Myo10 and Myo18a are important for morphology and behaviour of malignant prostate cancer cells, I wanted to look at the effect of depleting benign prostate cells of these myosin isoforms. Using the same siRNA technology as described previously, I knocked down Myo1b, Myo10 and Myo18a in BPH-1 cells (Figure 5.4). Staining of BPH-1 cells for paxillin, part of the focal adhesion complex, revealed that control BPH-1 cells have numerous, well-developed focal adhesions (Figure 5.5A), in contrast to highly motile PC3 cells which do not show prominent focal adhesions (Chapter 4). The number or size of focal adhesions does not change following the knockdown of Myo1b, Myo10 or Myo18a (Figure 5.5B–D).

Staining the BPH-1 cells for NM2A and F-actin showed some changes after myosin knockdown, although not nearly as drastic as seen in cancer PC3 cells. Control BPH-1 cells show NM2A staining around the border of the cells and at the periphery of the colonies, where it co-localises with actin-rich areas. The cells at the border of the colony exhibit filopodia and wide protrusions, which contain actin and NM2A at their base, and only actin towards the edges (Figure 5.6A, arrows). After knockdown of Myo1b or Myo10 BPH-1 cells showed dense actin bundles at the edges of the cells (at the border between cells) and at the edge of the colonies, with NM2A co-localising with the actin-rich areas (Figure 5.6B and C). These bundles were more prominent in myosin-depleted cells than in control cells. After knockdown of Myo1b or Myo10, the cells maintained broad, short protrusions containing NM2A at their base. Some differences were visible in Myo10-depleted cells, namely they had noticeably increased cell area, although exact quantification was hindered due to the fact that BPH-1 cells grow in tight colonies and often overlap. Filopodia numbers following Myo10 knockdown decreased by about 35% and were unaffected in cells lacking Myo1b (data not shown).
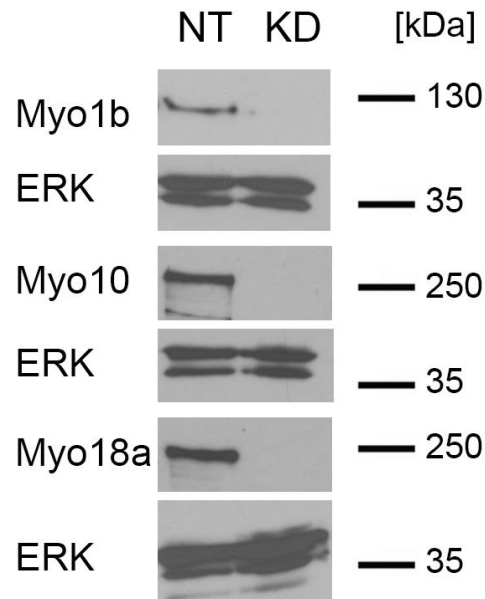
Figure 5.4 siRNA-mediated knockdown of myosins in BPH-1 cells.
Knockdown of Myo1b, Myo10 and Myo18a in BPH-1 cell line using siGENOME SMARTpool siRNA after 72 hours, analysed by immunoblotting. Control cells were treated with non-targeting siRNA (NT). Molecular weight markers shown to the right. Total ERK was used as loading control.

Consistent with what was observed in PC3 cells (Section 4.3.5), Myo18a knockdown in BPH-1 cells affected organisation of NM2A, increasing the formation of NM2A filaments (Figure 5.7). The filaments seemed to be associated along centripetal actin filaments (Figure 5.7A and B, arrows), however these were not as clearly visible as in Myo18a-depleted PC3 cells. The cells had broad protrusions at the border of the colonies, withNM2A filaments at their base and actin-rich, NM2A-free area towards the edge (Figure 5.7A and B, arrowheads). Interestingly, Myo18a knockdown slightly decreased the numbers of filopodia in BPH-1, by about 20%, although this was not statistically significant (data not shown).
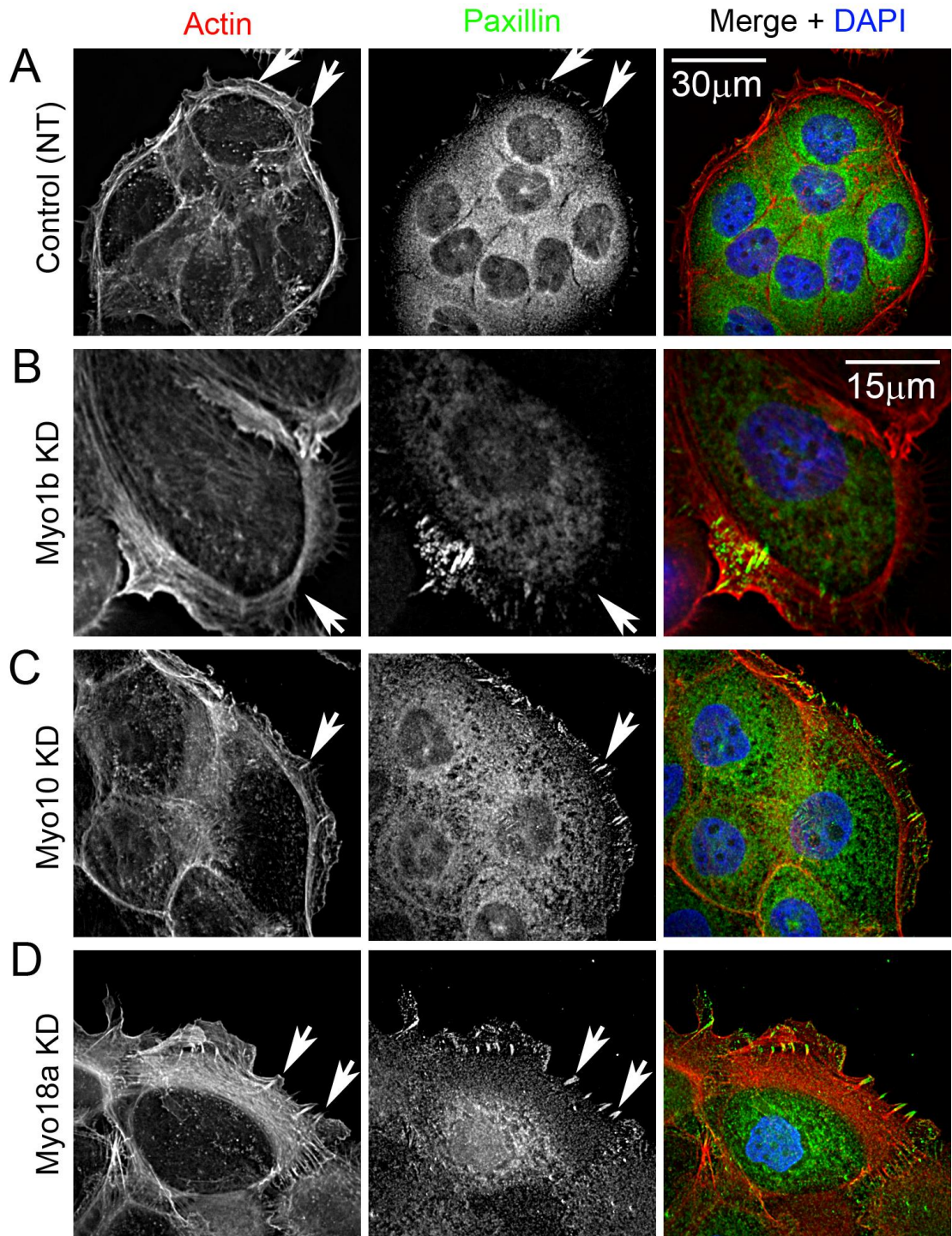
Figure 5.5 Knockdown of myosins in BPH-1 cells has no visible effect on focal adhesions. Control (A) and Myo1b (B), Myo10 (C) and Myo18a (D) knockdown BPH-1 cells stained for F-actin (phalloidin, red), paxillin (green) and nuclei (DAPI – blue). Arrows indicate large focal adhesions at the cell periphery. Control cells were treated with non-targeting siRNA (NT). Scale bar = 30 μm, expect for Myo1b panel (B), where the scale bar is 15 μm. The images are representative of at least 3 separate experiments.
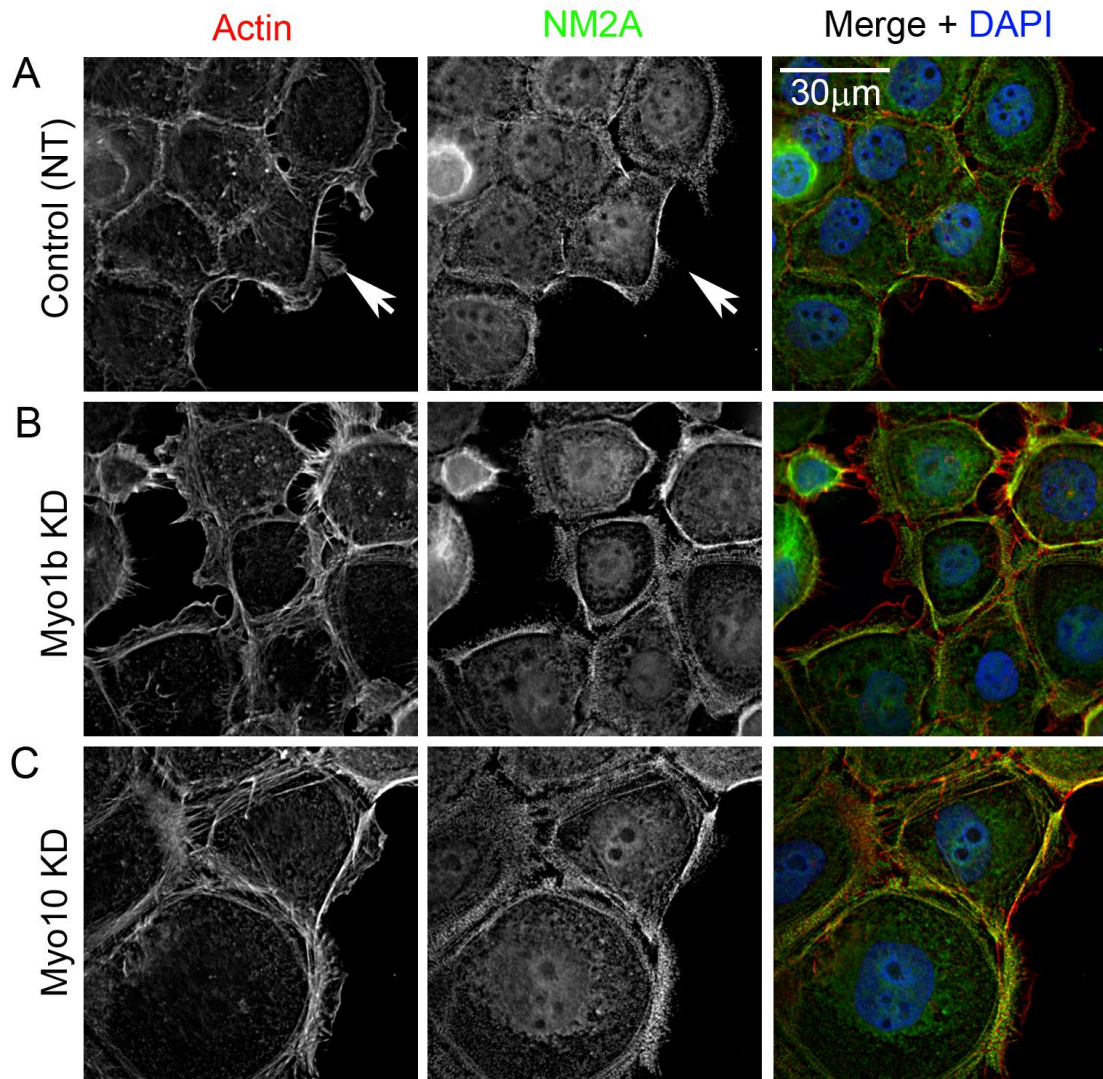
Figure 5.6 Effect of myosin knockdown on cytoskeleton and NM2A organisation in BPH-1 cells. Control (A) as well as Myo1b (B) and Myo10 (C) knockdown BPH-1 cells stained for F-actin (AF546-phalloidin – red), non-muscle myosin 2A (NM2A, green) and nuclei (DAPI – blue). The arrows in panel (A) indicate actin-rich protrusions. Control cells were treated with non-targeting siRNA (NT). Scale bar = 30 μm. The images are representative of at least 3 separate experiments.
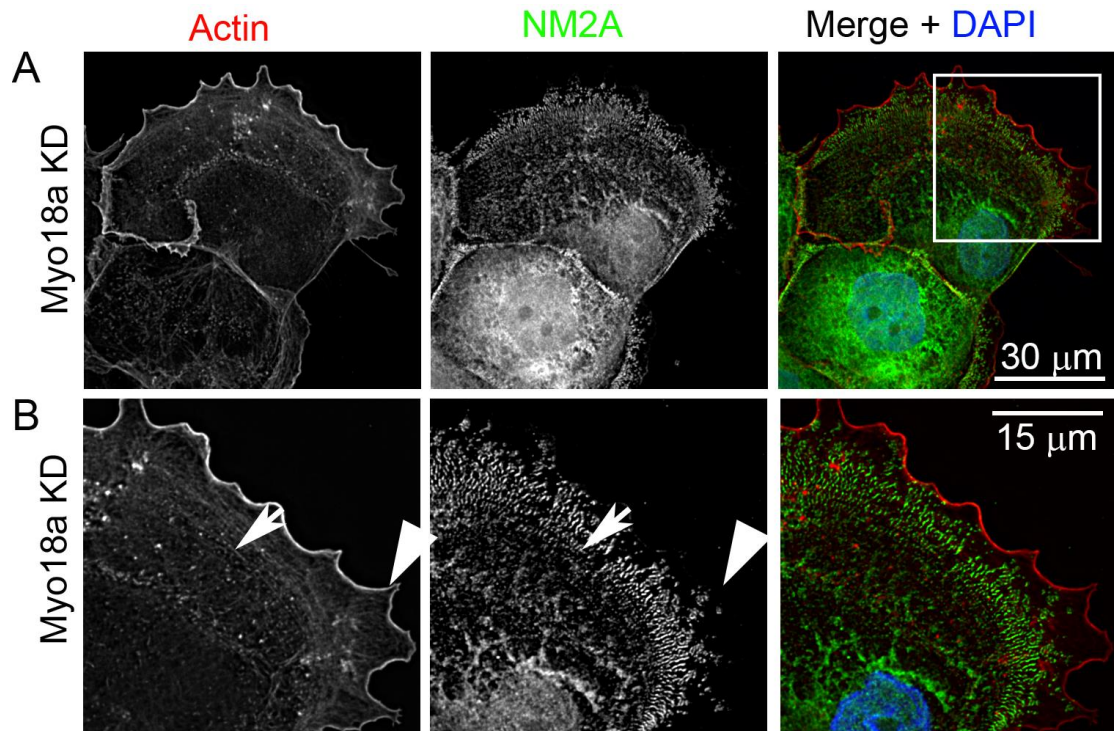
Figure 5.7 Effect of Myo18a knockdown on cytoskeleton and NM2A organisation in BPH-1 cells. BPH-1 cells after Myo18a knockdown, stained for F-actin (AF546-phalloidin – red), non-muscle myosin 2A (NM2A, green) and nuclei (DAPI – blue). White square in panel (A) shows the area zoomed into in panel (B). The arrows indicate centripetal actin bundles in cells, arrowheads point to actin-rich protrusions where NM2A is missing. Control cells for this experiment shown in Figure 5.6A. Scale bars as shown. The images are representative of at least 3 separate experiments.

5.2.4 Knockdown of Myo9a in benign prostate cell line, BPH-1

I next wanted to check if knockdown of any other myosin isoforms would have an effect on the benign cells. BPH-1 cells grow in connected colonies, so I looked at another myosin isoform which was not picked up by the general screen (see Chapter 3), Myo9a, which has a role in cell-cell junctions in epithelial cells (Omelchenko and Hall, 2012). In the preliminary screen, Myo9a has been shown by qPCR to be upregulated in the DU145 cell line (Figure 3.2), which also grows in rounded colonies. Interestingly, knocking down Myo9a brought quite drastic changes to BPH-1 cells, contrary to other myosins (Myo1b, Myo10 and Myo18a) examined in section 5.2.3. In contrast to control BPH-1 cells, which grow in tight colonies (Figure 5.8A), cells after Myo9a knockdown where much more scattered (Figure 5.8B). This is in agreement to what has been observed before that Myo9a regulates collective epithelial cell migration by targeting RhoGAP activity to cell-cell junctions (Omelchenko and Hall, 2012). Staining for paxillin showed that even though the cells have a different shape and actin organisation, numbers of focal adhesions remain comparable between controls (Figure 5.8C) and cells after Myo9a knockdown (Figure 5.8D).
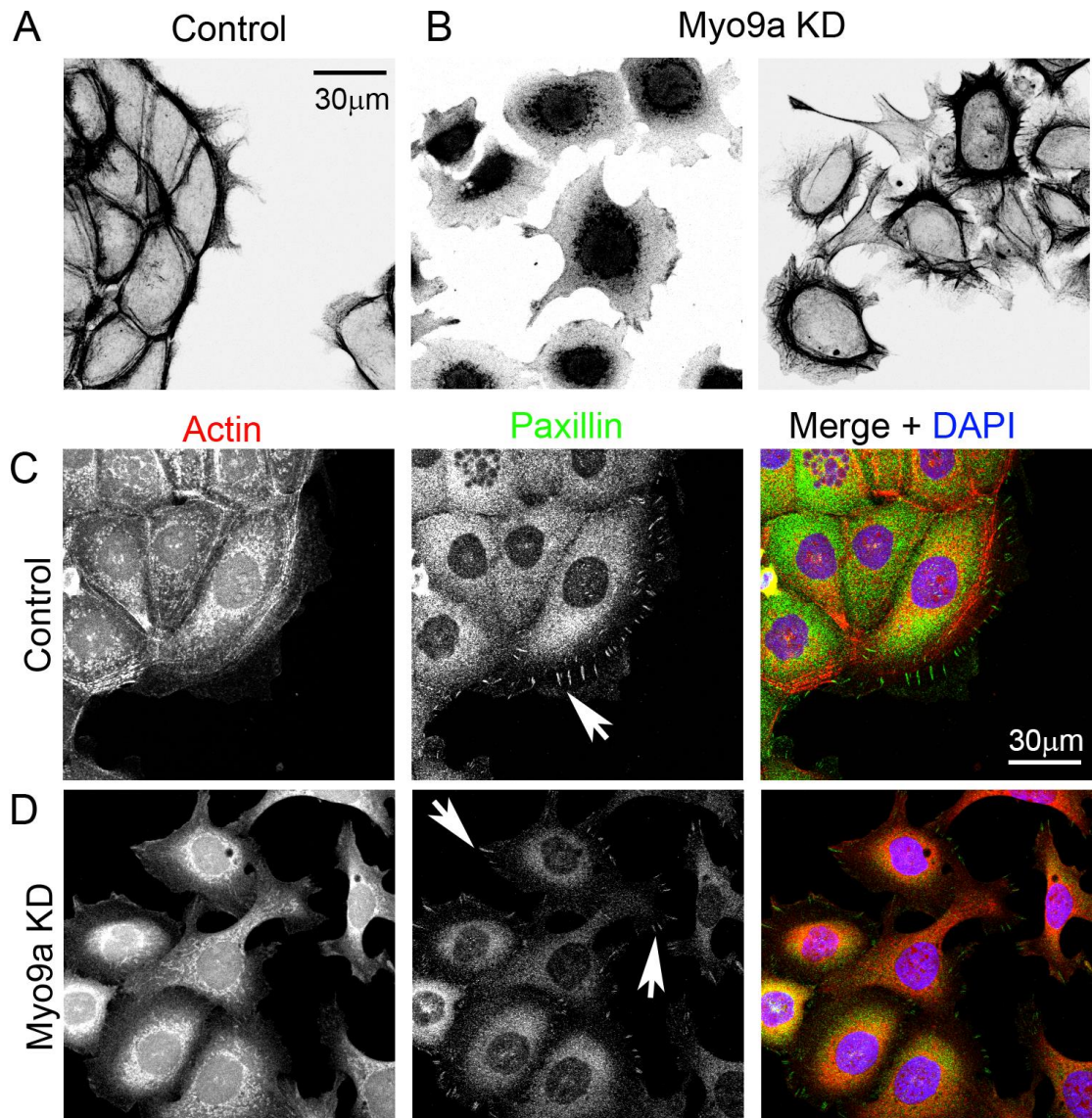
Figure 5.8 Effect of Myo9a knockdown on morphology of BPH-1 cells.
A, B. Images of control (A) and Myo9a knockdown (B) BPH-1 cells stained for F-actin using fluorescent phalloidin to show their morphology. The fluorescent images are shown in reverse contrast for increased clarity. Scale bar = 30 μm. C, D. Images of control (C) and Myo9a knockdown (D) cells stained for F-actin (AF546-phalloidin – red), paxillin (green) and nuclei (DAPI – blue). Arrows indicate large focal adhesions, present both in control and in the knockdown cells. Control cells were treated with non-targeting siRNA (NT). Scale bar = 30 μm. The images are representative of at least 3 separate experiments.

5.2.5 Myo10 is highly expressed in glioblastoma cell lines

Next, I investigated if Myo1b, Myo10 and Myo18a were upregulated in a brain cancer cell line, glioblastoma. Immunoblotting showed that among the three myosin isoforms upregulated in prostate cancer, only Myo10 was expressed at high levels in glioblastoma cell line (Figure 5.9A and B). I compared levels of Myo10 in prostate cancer cell lines and two glioblastoma cell lines: glioma p53$^{-/-}$PTEN$^{-/-}$ and glioma PTEN$^{-/-}$ (Figure 5.9B). So called "headless" Myo10 (Hdl-Myo10) isoform is expressed in the nervous system (Sousa et al., 2006). Hdl-Myo10 lacks a functional motor domain, has a molecular weight of 164 kDa, and it was recognised by the antibody in glioblastoma cell lines but not in prostate cancer (Figure 5.9B), in agreement with this isoform's expression pattern (Sousa et al., 2006). Interestingly, glioma p53$^{-/-}$PTEN$^{-/-}$ showed higher levels of Myo10 than glioma PTEN$^{-/-}$, while glioma PTEN$^{-/-}$ showed noticeably higher levels of Hdl-Myo10 in comparison to glioma p53$^{-/-}$PTEN$^{-/-}$ (Figure 5.9B). When stained for Myo10 and actin, glioblastoma p53$^{-/-}$PTEN$^{-/-}$ cells showed Myo10 localised at the end of their multiple actin-rich protrusions (Figure 5.9D). The glioma PTEN$^{-/-}$ cells also showed protrusions although longer and more sparse (Figure 5.9C). Both cell lines grow as a connected network.
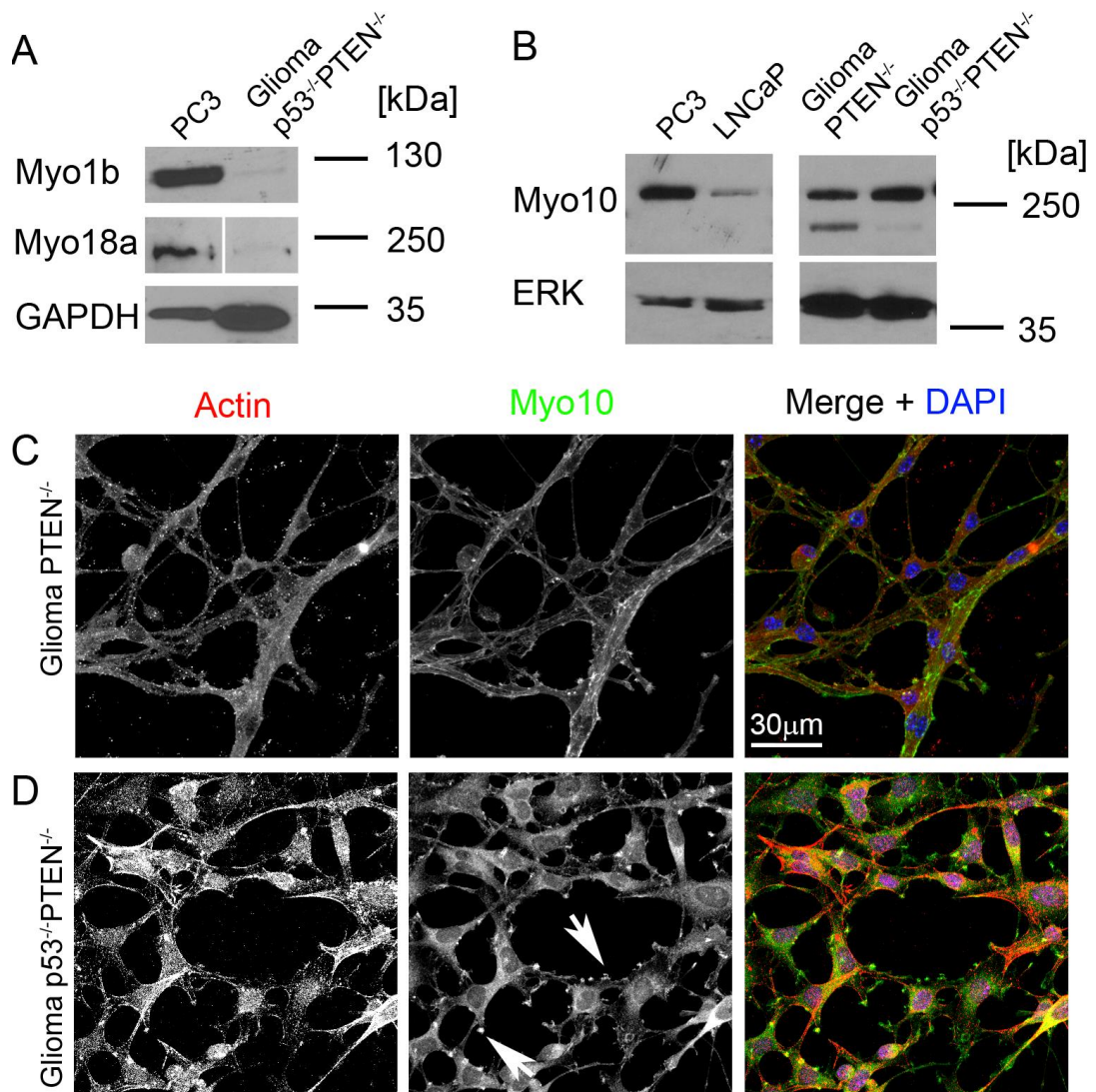
Figure 5.9 Myosins in p53$^{-/-}$PTEN$^{-/-}$ glioblastoma. A. Immunoblotting shows levels of Myo1b, Myo10 and Myo18a in the glioblastoma cell line. GAPDH used as loading control. B. glioblastoma cells stained for actin (AF546-phalloidin – red) and Myo10 (green). Arrow shows Myo10 punctae concentrated at the tips of protrusions. Scale bar = 30 μm. The images are representative of at least 3 separate experiments.

5.2.6 Knockdown of Myo10 in p53$^{-/-}$PTEN$^{-/-}$ glioblastoma reduces the number of protrusions and affects focal adhesions.

As Myo10, but not Myo1b or Myo18a, was expressed at relatively high levels, I used siRNA to deplete Myo10 expression only, in the glioblastoma cell line (Figure 5.10A), and examined the effects on the protrusions. Staining for F-actin showed that the shape of Myo10-depleted cells was altered, numbers of stress fibres increased, and the cell area was also slightly increased (Figure 5.10B, quantified in Figure 5.10C). Interestingly, knockdown of Myo10 in glioblastoma decreased the number of protrusions per cell (Figure 5.10B, quantified in Figure 5.10D), similarly to the phenotype changes seen in PC3 cells.

Staining of glioblastoma cells for actin and paxillin revealed that Myo10 depletion additionally affected focal adhesions in glioblastoma cells. Control cells show some focal adhesions at the tips of protrusions (Figure 5.11A). In contrast, after Myo10 knockdown, prominent actin stress fibres appeared in the large cells, with large, well-developed focal adhesions at their ends, suggesting a more adhesive phenotype (Figure 5.11B, arrows). These results suggest that the role of Myo10 in cell migration might be widespread among other types of cancer.
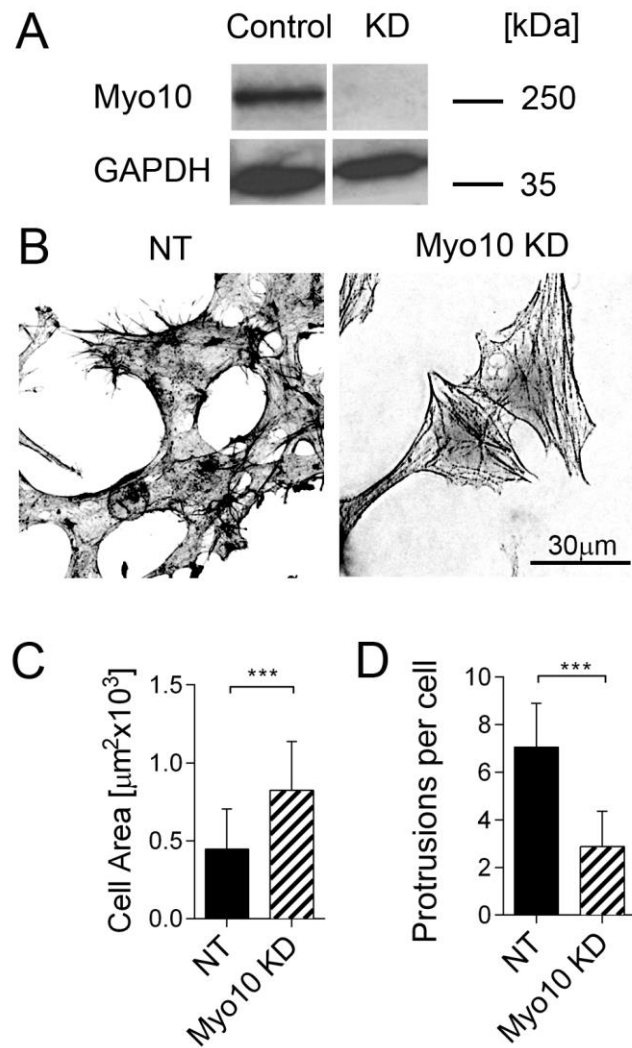
Figure 5.10 Knockdown of Myo10 affects morphology of p53$^{-/-}$PTEN$^{-/-}$ glioblastoma. A. Immunoblotting confirms that knockdown of Myo10 in p53$^{-/-}$PTEN$^{-/-}$ glioblastoma cell line using murine siGENOME SMARTpool siRNA for 72 hours noticeably reduced Myo10 protein level. Control cells were treated with non-targeting siRNA (NT). Molecular markers are shown to the right. GAPDH was used as loading control. B. Images of control (NT) and Myo10-depleted glioblastoma cells stained for F-actin using fluorescent phalloidin to show changes in morphology. The fluorescent images are shown in reverse contrast for increased clarity. Scale bar = 30 μm. The images are representative of at least 3 separate experiments. C, D. Quantification of filopodial number (C) and cell area (D). Bars show mean + SD for n=20 cells from at least 3 separate experiments. Statistical analysis was performed using two-way ANOVA. Levels of significance indicated by: (***) for p<0.001.
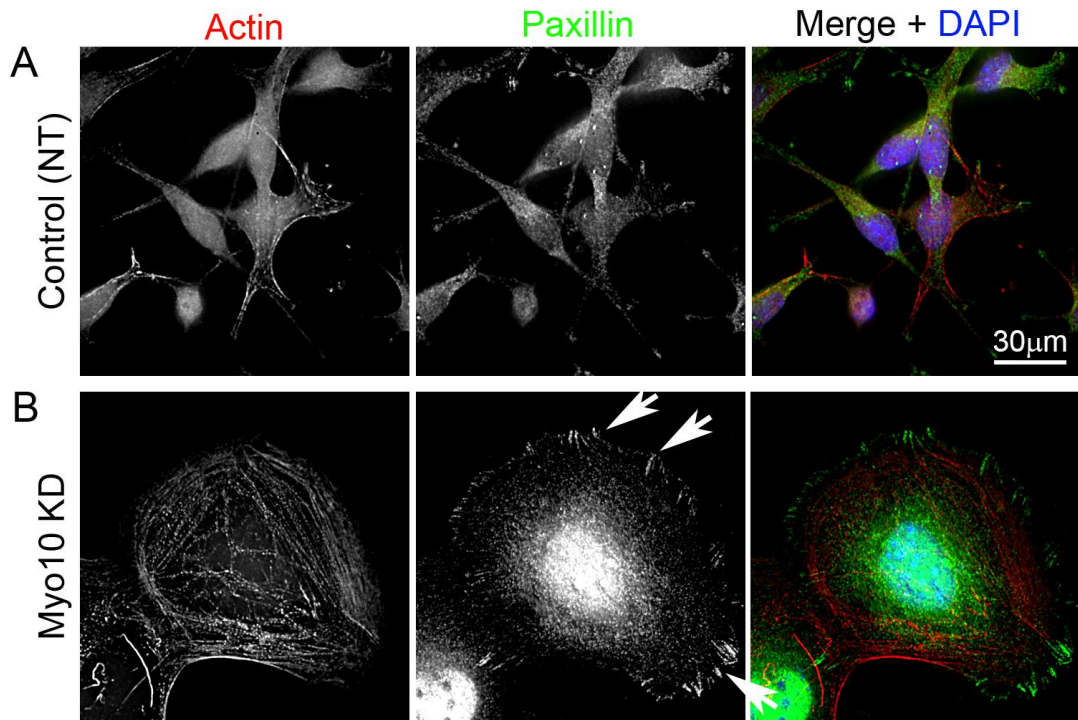
Figure 5.11 Knockdown of Myo10 affects focal adhesions of p53$^{-/-}$PTEN$^{-/-}$ glioblastoma. Control (A) and Myo10 knockdown (B) glioblastoma cells stained for F-actin (AF546 phalloidin, red) and paxillin (green). Arrows indicate large focal adhesions in knockdown cells. Control cells were treated with non-targeting siRNA (NT). Scale bar = 30 μm The images are representative of at least 3 separate experiments.

5.3 Discussion

The results presented here show that myosins are expressed and can be important in benign prostate tissue and glioblastoma. BPH-1, a benign prostatic hyperplasia cell line, shows high endogenous expression levels of some myosins when compared to prostate cancer cell lines. Levels of Myo1b are 1.5-fold higher than in PC3 cells, with Myo1b localising to membrane ruffles and actin-rich area between neighbouring cells. Levels of Myo10 are 2-fold lower in BPH-1 than in PC3 cells, and this number is reflected in numbers of filopodia: BPH-1 have on average half the number of filopodia seen in the PC3 cell line. High endogenous expression levels of Myo10 in another type of cancer, glioblastoma, are also associated with high numbers of protrusions. Knockdown of Myo10 in glioblastoma significantly decreases the numbers of filopodia, increases the cell area and affects focal adhesions. These changes are analogous to those observed in PC3 cells in Chapter 4 and suggest a broader role for Myo10 in cancer motility.

5.3.1 Benign prostatic hyperplasia

The BPH-1 cell line retains many characteristics of a benign prostate epithelium in terms of its morphology, enzymatic activity and testosterone metabolism (Hayward et al., 1995). However, one has to remember that this cell line is delivered from hyperplastic tissue, which means differences to normal prostate epithelium could be present. Other differences could occur because of the way the cell line has been established. For example, the primary cultures from which the cell line was derived showed very low levels of p53 (below detection level by immunofluorescence and western blotting), while BPH-1 cells show strong nuclear staining for p53 (Hayward et al., 1995). This upregulation and stabilisation of p53 is typical for SV40-immortalised cell lines – the SV40 large T antigen makes the p53 protein dysfunctional, as a result of sequestration to oncogene products (Ludlow, 1993), and it cannot be excluded that this changes the cell line behaviour.

The cell line shows no tumorigenic or metastatic potential when injected into nude mice (Hayward et al., 1995).

An unexpected observation in the BPH-1 cell line was the high level of expression of Myo1b, which was higher than in previously analysed in benign tissue (as shown in chapter 3: GEO analysis, Figure 3.1, and in 1535 NP, Figure 3.3 and 3.4). One could speculate that high proliferation of hyperplastic tissue requires intensive endocytosis, hence elevated expression of endocytosis-related proteins such as Myo1b. Since Myo1b was present in filopodia or tunnelling nanotubes in PC3 cells, it would be interesting to check if it plays a role in cell-cell transport, especially that in BPH-1 cells in localises particularly on the borders between cells. The BPH-1 cell line also showed relatively high numbers of filopodia (comparable to DU145 cells and 2-fold lower than in PC3 cells), which I did not expect to see in a cell line which has no metastatic potential.

On the other hand, knockdown of Myo1b or Myo10 did not result in large changes in the BPH-1 cells. The focal adhesion status remained unchanged, and although Myo10-depleted cells seemed to have increased cell area and decreased number of filopodia (by ~30%), the changes were not nearly as drastic as in the malignant PC3 cells. Together, these results suggest that Myo1b and Myo10 might play a different, possibly more important roles in cancer cells than benign prostate cells, making them good potential candidates for therapeutic targets. Further study of the myosin knockdown seems necessary to check whether other processes such as endocytosis are affected. On the other hand, after knockdown of Myo18a I observed increased formation of NM2A filaments, suggesting that Myo18a is still important for NM2A organisation in benign prostate cells.

In contrast to the myosin isoforms upregulated in prostate cancer, Myo9a seems to be important in BPH-1, particularly for cell-cell adhesion as previously shown in 16-HBE (human bronchial epithelium) cells (Omelchenko and Hall, 2012). Knockdown of Myo9a in 16-HBE cells caused increased scattering of epithelial cells, similar to what I observed in the

BPH-1 cell line, confirming that Myo9a is important for delivering RhoGAP activity to cell-cell junctions (Omelchenko and Hall, 2012). It would be interesting to check the effects of Myo9b knockdown on BPH-1 cells, but due to time restrictions this analysis was not performed.

5.3.2 Glioblastoma and its migration

Myo10 has been reported to be expressed in high levels in normal brain tissue (Berg and Cheney, 2002). Myo10 in neurons has been shown to regulate axonal pathfinding, outgrowth of neurites (neuronal projections, axons and dendrites) and related processes (Ju et al., 2014; Zhu et al., 2007). A Myo10 isoform expressed in the nervous system, "headless" Myo10 (Hdl-Myo10), which lacks a functional motor domain, has a role in dendritic spine development and in axon outgrowth (Sousa et al., 2006), where it has been reported to act as a dominant-negative regulator of full length Myo10 (Raines et al., 2012). A consequent study showed that the Hdl-Myo10 isoform could also serve as a scaffolding protein and increase retention of actin-remodelling protein VASP (vasodilator-stimulated phosphoprotein) in dendritic filopodia to promote their maturation into dendritic spines (Lin et al., 2013). In the glioma cell lines, I also observed the Hdl-Myo10 isoform, with higher levels in glioma PTEN$^{-/-}$ than in glioma p53$^{-/-}$PTEN$^{-/-}$, which could explain why PTEN$^{-/-}$ cells showed longer and less frequent, more "mature" protrusions than p53$^{-/-}$PTEN$^{-/-}$ glioma cells.

The role of myosins in glial cells has been less well studied, and has been focused around the study of malignant gliomas (incl. glioblastomas), primary brain tumours that often have poor prognosis (Buckner et al., 2007; Stupp et al., 2007). High mortality rates observed in these tumours can be contributed to the fact that although they rarely spread outside of the CNS, gliomas are able to invade within the brain very efficiently (Lim et al., 2007; Thorne and Nicholson, 2006). When gliomas invade the brain they typically migrate through white matter and infiltrate cortical and subcortical grey matter structures. For this process, but not for 2D migration, glioma cells have been

shown to require myosin 2 (Beadle et al., 2008; Gillespie et al., 2001). When carcinoma cells invade the brain, they do not infiltrate it but grow as a constrained, expansive mass (Beadle et al., 2008). This would suggest that gliomas use a different migration mechanism to carcinomas. The authors of this study claim the difference stems from the fact that carcinoma cells require formation of a broad lamellipodium to migrate and this is impossible in the restricted environment of the brain (Beadle et al., 2008). This argument does not seem convincing, since formation of a lamellipodium is mostly seen in migration on 2D, flat surfaces (Friedl and Wolf, 2003). Even glioma cells, when plated on a coverslip, form a broad lamellipodium and migrate much like epithelial cells, as reported by the same study (Beadle et al., 2008). In 2D environment, human and rat glioma cells migrate into a cell free zone with a velocity of 0.13 and 0.19 μm/min, a speed that is considerably lower than that observed for PC3 cells (Chapter 4, Figure 4.10), and although the authors also show much higher velocity of 0.5 μm/min for control glioma cells in a separate figure, this discrepancy is never explained. I was unable to observe motility for p53$^{-/-}$PTEN$^{-/-}$ glioblastoma cells despite several attempts. This could be due to cell line-specific differences or differences in experimental conditions: for example, the study describes glioma cells grown to confluence and migrating in a scratch assay, while in my knockdown experiments the cells were grown to 30-40% confluence.

Chapter 6. Discussion

I have presented a novel study that has investigated expression and potential roles of myosins in metastatic prostate cancer. The data show that a subset of myosins, including Myo1b, Myo9b and Myo10, is upregulated in localised and metastatic tumours. Myo1b, Myo9b, Myo10 and Myo18a contribute to the morphology and migration of a highly metastatic PC3 cell line. Myo10 promotes filopodia formation and has an evident contribution to cell migration, not only in prostate cancer but also in other types of cancer, including the highly invasive glioblastoma. High levels of Myo9b are linked to low levels of stress fibres. Myo1b and Myo18a influence cell morphology and actin organization, but have little effect on migration in 2D, while all 4 isoforms inhibit cell migration of PC3 cells in 3D invasion assays. Thus, changes in expression of several myosin isoforms may contribute to metastasis in prostate cancer, and myosins could potentially serve as therapeutic targets or diagnostic markers for metastatic disease.

Of all the myosins screened in this study, Myo10 emerges as possibly the most important isoform for migration of prostate cancer cells. Levels of Myo10 expression clearly correlated with numbers of filopodia in the different cell types that I investigated. There was also an evident link between Myo10 and cell migration and invasion. While filopodia are not necessarily essential for migration, high levels of Myo10 increase their numbers, and enhance migration and invasion of cancers. In breast cancer, high levels of Myo10 were shown to be important in transporting integrins to the filopodial tips for invasion (Arjonen et al., 2014). Thus our finding appears to broadly agree with the reports that Myo10 overexpression leads to metastasis in breast and lung cancer (Arjonen et al., 2014; Cao et al., 2014; Sun et al., 2015).

The breast cancer study also showed that mutant, but not wild type p53 was important for upregulating Myo10 expression levels through upregulation of

the MAPK/ERK pathway and increased levels of EGR1 transcription factor (Arjonen et al., 2014). Mutant p53 has been shown previously to drive random cell motility and increase invasiveness through enhancing recycling pathways of β1 integrins (Muller et al., 2009). Mutations of the TP53 tumour suppressor gene are one of the most common among cancers and mutant p53 promotes cell migration and metastasis (Oren and Rotter, 2010). In many types of human cancers, overexpression of mutant p53 is associated with a poor prognosis, consistent with the idea of a "gain of function" mutation, in contrast to loss of expression of WT p53 seen in other cancers (Selivanova and Ivaska, 2009). However, while p53 has a central role in preventing cancer in humans (Lane and Levine, 2010), we still do not fully understand how it functions.

In contrast to the breast cancer study, PC3 cells express high levels of Myo10, which are linked to numerous filopodia, high motility and invasiveness, even though they do not express mutant or wild type p53. Similarly, there are high levels of Myo10 in the p53$^{-/-}$PTEN$^{-/-}$ glioblastoma cell line, higher than in the PTEN$^{-/-}$ glioblastoma cells. In addition, an *in silico* analysis of the GEO cohort, previously used to examine myosin expression showed a significant drop of p53 levels in the metastatic tumours (Chapter 3, Figure 3.2). Loss of p53 alone may promote tumour initiation in some tissues, tumour progression in others, and in prostate cancer it is preferentially selected for in advanced prostate cancer, where it accelerates the progression of tumours (Chen et al., 2005). Thus, there must be a different mechanism by which levels of Myo10 are upregulated in those cells, which is p53-independent. This suggests that the described connection of Myo10 with p53 (Arjonen et al., 2014) is cancer type-specific or cell type-specific.

Previous reports have linked expression levels of other myosins to the p53 status of cells. For example, expression levels of Myo6 were shown to be upregulated by p53 (mRNA and protein) in some tumour cell lines such as H1299, RKO, and LS174T (Jung et al., 2006), through binding of p53 to the promoter of the MYO6 gene. However, in MCF7 cells, increasing p53

expression levels reduced Myo6 levels (Cho and Chen, 2010). In MCF7 and LNCaP cells, DNA damage increased expression of p53 and decreased Myo6 expression. We found that levels of Myo6 are high in LNCaP cells, which do express wt p53 and low in PC3 cells, which do not, suggesting that p53 may be regulating Myo6 expression levels in these cell types. However, these trends can also depend on the way the cell lines have initially been established (transformation method), or be more complex since p53 is involved in multiple cell signalling events (Cho and Chen, 2010).

RNAi mediated knockdown of NM2A predisposes mice to squamous cell carcinomas (SCC) (Schramek et al., 2014). This was shown to be related not only to actin-related processes, as in epithelial cells where NM2A is important for cell-cell adhesion, but was additionally linked to stabilisation of p53. In that study, knockdown of NM2A exacerbated SCC formation in mice in which TβRII (TGFβ receptor II), but had no effect in mice expressing mutant p53 in the skin epithelium. Knocking down NM2A function with blebbistatin prevented p53 accumulation in the nucleus.

Our results suggest that each myosin has a specific effect on actin organisation, and increasing their expression in cells with metastatic potential may allow them to work in concert to generate a torpedo-shaped cell with multiple protrusions that is better able to migrate through a 3D matrix and thus more able to metastasise *in vitro.* Alternative explanation to some of the changes observed after myosin knockdown could be that they are a secondary consequence of myosin loss. For example, changes to integrin transport after Myo10 knockdown could cause disrupted signalling and thus indirectly result changes in the actin organisation. Further studies will be necessary to rule out the unspecific results and discover the exact mechanisms behind the observed changes. What is more, how cancer cells move depends on their environment, and this is true in case of malignant gliomas (Beadle et al., 2008; Wong et al., 2015) but also for other types of cancer. It would therefore be interesting to study the role of myosins in assays that better reflect the 3D environment *in vivo,* for example looking at

glioma cell motility in an conditions similar to the particular extracellular environment found in the brain.

Several strategies could be used to utilise the role of myosins in therapy. One approach, for example, could be to target particular myosins, for example using small-molecule inhibitors. Small molecule myosin inhibitors, if selective and sufficiently potent, could be a useful resource for developing treatments for diseases involving myosin dysfunction or overactivity. So far, small-molecule inhibitors have been developed for myosins in class 2 (muscle and non-muscle) and classes: 1, 5 and 6 (Bond et al 2013). Most of the inhibitors operate by hindering ADP/Pi release by the myosin ATPase (Bond et al., 2013). Blebbistatin, the most well-known inhibitor, specific to non-muscle myosin 2, has been shown to inhibit migration, invasion and spreading of cancerous cells such as pancreatic adenocarcinoma and breast cancer in culture (Derycke et al., 2011; Duxbury et al., 2004). Despite efforts in the scientific field, there are not that many inhibitors and none of them have been applied or tested in therapeutic aspects. Limitations when using inhibitors include lack of specificity as well as the range of concentrations at which the compound would have to be available in the patient to work efficiently.

Additionally, small-molecule myosin inhibitors can serve as a useful tool for understanding myosin function. An interesting addition to the field would also be a complementary design of small-molecule myosin activators. Specific myosin inhibitors (and even activators) could provide valuable, complementary experiments to this study. One can imagine analysis of certain myosins, such as Myo10 and/or Myo9b, activated in the LNCaP cell line, effect of Myo6 activation in the PC3 cell line, or an experiment where several myosins could be inhibited in the PC3 cells at once. This approach could also be studied using established cell lines missing or overexpressing certain myosin isoforms, although the inhibitors offer an advantage of time-efficiency.

Rather than looking at particular molecules, a different tactic in cancer therapy is to take a broader, "blanket" approach. Although cancers are a group of diverse diseases, they can often be summarised by categories of dysfunctions such as the "hallmarks of cancer" (Hanahan and Weinberg, 2000). Besides, as shown by the example of Myo18a and NM2A, myosins can work together and they often have overlapping functions. This general approach can target proteins involved in regulatory processes or in cell migration, especially when targeting metastatic cancer. One example of a therapy that targets a cytoskeletal protein are the taxanes, such as docetaxel, which inhibit polymerisation of tubulin (Dreicer, 2006). Taxane-based chemotherapy is one of the few therapeutic options that have proven to be somewhat effective in metastatic castration-resistant prostate cancer, although for a very limited period of time (Dreicer, 2006). In general, prostatic adenocarcinoma tumours respond poorly to standard chemotherapeutic intervention (Augello et al., 2014; Berthold et al., 2005; Dreicer, 2006).

Another common strategy general across various types of cancer includes Heat shock protein 90 (Hsp90) as a potential therapeutic target. Hsp90 is an evolutionary conserved molecular chaperone that stabilises and activates many proteins essential for cell signalling and adaptive responses to stress (Zhao et al., 2005). Cancer cells can use the Hsp90 chaperone to protect mutated or overexpressed oncoproteins from misfolding and degradation, and it is often recognised as a crucial facilitator of cancer cell survival (Trepel et al., 2010). Hsp90 is therefore often upregulated in advanced cancers, and I have also observed this to be the case in the *in silico* analysis of the GEO profiles for prostate cancer (Figure 3.2).

Considerable progress has been made in the field of Hsp90 inhibitors, and even though none of them are approved, a number of inhibitors are currently undergoing clinical evaluation in cancer patients (Jhaveri and Modi, 2015; Trepel et al., 2010). Therapy can also target Hsp90 clients, such as protein kinases, involved in the proliferation and survival of cancer cells, which depend on chaperone activity of Hsp90 (Miyata et al., 2013). One example is

cell surface receptor tyrosine kinases, such as ErbB2/HER2 overexpressed in breast cancer which are targeted by Trastuzumab (Herceptin), monoclonal antibody drug which binds to ErbB2/HER2 and prevents the ErbB2/HER2-dependent progression of metastatic breast cancer (Sachdev and Jahanzeb, 2012). In prostate cancer, however, it seems that the tumour microenvironment and target complexity may complicate clinical efficacy. Initial preclinical observations suggested that castrate-resistant prostate cancer might respond well to IPI-504 (retaspimycin), a Hsp90 inhibitor therapy, since Hsp90 regulates the activity of androgen receptor (AR) (Saporita et al., 2007). However, the inhibitor was not effective in monotherapy of castration-resistant prostate cancer (Oh et al., 2011). This is similar to what has been reported for an analogous inhibitor, 17-AAG (Heath et al., 2008). These results could be explained by a study which showed that inhibition of Hsp90 by 17-AAG activates osteoclast Src kinase and promotes Src-dependent osteoclast maturation, and as a consequence, instead of acting against prostate cancer growth, Hsp90 inhibitor stimulates the growth of prostate carcinoma cells in the bone (Yano et al., 2008). By contrast, more promising results have been reported for multiple myeloma and for subtypes of breast cancer (Augello et al., 2014). These differences emphasise the value of choosing a cancer that is driven by an Hsp90 "client" protein (such as HER2 in breast cancer), as well as the importance of possible long-term impact of Hsp90 inhibitors on normal tissues (Augello et al., 2014; Yano et al., 2008).

Apart from the general chaperones, another protein that could potentially be targeted in therapy is myosin chaperone, UNC-45A. UNC-45A is an isoform of UNC-45 expressed in non-muscle cells, specific to non-muscle myosins, while UNC-45B is a chaperone specific to muscle (Price et al., 2002). Elevated levels of UNC-45A have been found in ovarian tumours, with higher levels exhibited by metastatic tumours (Bazzaro et al., 2007). Another study showed that not only is UNC-45A accumulation increased in breast carcinoma specimens and cell lines, but also its knockdown in cell lines decreases proliferation and invasion rates (Guo et al., 2011). UNC-45A also

co-localises with NM2A in the centrosome and regulates proliferation of HeLa cells (Jilani et al., 2015). However, my *in silico* analysis showed that UNC-45A was significantly decreased in metastatic prostate cancer and no reports exist on the role of myosin chaperones in prostate cancer. Future study of the regulatory mechanisms of UNC-45A expression and biological action could improve its potential function in prostate cancer.

Despite advances in early diagnosis, surgical techniques, systemic therapies, and patient care, modern anticancer therapy is still challenged greatly by metastatic dissemination. Metastasis frequently occurs prior to diagnosis of a primary tumour, which is why surgical excision is not curative. Continual empiricism in the treatment of cancer also seems unlikely to produce significant improvements and therefore understanding the mechanisms responsible for cancer metastasis should be a primary goal of research (Fidler, 2011). Indeed, incredible recent progress has been achieved in the field and new knowledge has been gained of the pathogenesis of metastasis on the systemic, cellular and molecular levels.

Multiple other approaches and strategies are being taken on by researchers in the fight against cancer metastasis. In case of prostate cancer, targeting the androgen receptor or subpopulations of cancer stem-like cells (Bhattacharya et al., 2015; Frame et al., 2013). More generally, it could also mean targeting stroma interaction and tumour-associated cells (Calvo and Sahai, 2011), inhibiting various molecules in signalling pathways involved in regulation of cell migration (Hotary et al., 2003; Vega et al., 2012; Wellbrock and Hurlstone, 2010), looking at aneuploidy or chromatin regulations (Donnelly et al., 2014; Zhu et al., 2015). To date, however, many of these approaches render inefficient.

This is partly because, depending on their molecular repertoire, tumour cells possess notable plasticity to change between different invasion modes and adjust migration mechanisms to cope with therapeutic challenge (Friedl and Wolf, 2003). The spectrum of adaptation responses observed for invasive migration implicates diverse mechanical and signalling programs in cancer

cell migration that adapt to molecular challenge during disease progression and, possibly, during therapeutic challenge (Alexander and Friedl, 2012). This means that there is still an urgent need to improve our understanding of cancer metastasis. We believe myosins might be an attractive object of study in this context, because of their ubiquity and multiple specific functions, some possibly dysregulated in cancer. This might present an opportunity for myosins to serve as 'crucial points' of the network of interactions involved in metastasis. An ideal therapy would not leave the cancerous cell an option to omit the challenge, but compensatory changes negating the effect would be available in normal cells. This is why it would be interesting to expand this study to check whether the analysed subset of myosins could be potential targets for therapy in other types of cancer or more specifically in prostate cancer.

Bibliography

Abounit, S., and Zurzolo, C. (2012). Wiring through tunneling nanotubes--from electrical signals to organelle transfer. Journal of cell science *125*, 1089-1098.

Akhmanova, A., and Hammer, J.A., 3rd (2010). Linking molecular motors to membrane cargo. Current opinion in cell biology *22*, 479-487.

Albertsen, P.C., Hanley, J.A., and Fine, J. (2005). 20-year outcomes following conservative management of clinically localized prostate cancer. JAMA : the journal of the American Medical Association *293*, 2095-2101.

Albuschies, J., and Vogel, V. (2013). The role of filopodia in the recognition of nanotopographies. Scientific reports *3*, 1658.

Alexander, S., and Friedl, P. (2012). Cancer invasion and resistance: interconnected processes of disease progression and therapy failure. Trends in molecular medicine *18*, 13-26.

Allsop, G., and Peckham, M. (2011). Cytoskeleton and Cell Motility. Comprehensive Biotechnology. .

Almeida, C.G., Yamada, A., Tenza, D., Louvard, D., Raposo, G., and Coudrier, E. (2011). Myosin 1b promotes the formation of post-Golgi carriers by regulating actin assembly and membrane remodelling at the trans-Golgi network. Nature cell biology *13*, 779-789.

Ankrett, R.J., Rowe, A.J., Cross, R.A., Kendrick-Jones, J., and Bagshaw, C.R. (1991). A folded (10 S) conformer of myosin from a striated muscle and its implications for regulation of ATPase activity. Journal of molecular biology *217*, 323-335.

Arjonen, A., Kaukonen, R., and Ivaska, J. (2011). Filopodia and adhesion in cancer cell motility. Cell adhesion & migration *5*, 421-430.

Arjonen, A., Kaukonen, R., Mattila, E., Rouhi, P., Hognas, G., Sihto, H., Miller, B.W., Morton, J.P., Bucher, E., Taimen, P.*, et al.* (2014). Mutant p53-associated myosin-X upregulation promotes breast cancer invasion and metastasis. The Journal of clinical investigation *124*, 1069-1082.

Aschenbrenner, L., Lee, T., and Hasson, T. (2003). Myo6 facilitates the translocation of endocytic vesicles from cell peripheries. Molecular biology of the cell *14*, 2728-2743.

Astin, J.W., Batson, J., Kadir, S., Charlet, J., Persad, R.A., Gillatt, D., Oxley, J.D., and Nobes, C.D. (2010). Competition amongst Eph receptors regulates contact inhibition of locomotion and invasiveness in prostate cancer cells. Nature cell biology *12*, 1194-1204.

Augello, M.A., Den, R.B., and Knudsen, K.E. (2014). AR function in promoting metastatic prostate cancer. Cancer metastasis reviews *33*, 399-411.

Bazzaro, M., Santillan, A., Lin, Z., Tang, T., Lee, M.K., Bristow, R.E., Shih Ie, M., and Roden, R.B. (2007). Myosin II co-chaperone general cell UNC-45 overexpression is associated with ovarian cancer, rapid proliferation, and motility. The American journal of pathology *171*, 1640-1649.

Beach, J.R., Licate, L.S., Crish, J.F., and Egelhoff, T.T. (2011). Analysis of the role of Ser1/Ser2/Thr9 phosphorylation on myosin II assembly and function in live cells. BMC cell biology *12*, 52.

Beadle, C., Assanah, M.C., Monzo, P., Vallee, R., Rosenfeld, S.S., and Canoll, P. (2008). The role of myosin II in glioma invasion of the brain. Molecular biology of the cell *19*, 3357-3368.

Bellion, A., Baudoin, J.P., Alvarez, C., Bornens, M., and Metin, C. (2005). Nucleokinesis in tangentially migrating neurons comprises two alternating phases: forward migration of the Golgi/centrosome associated with centrosome splitting and myosin contraction at the rear. The Journal of neuroscience : the official journal of the Society for Neuroscience *25*, 5691-5699.

Bement, W.M., Hasson, T., Wirth, J.A., Cheney, R.E., and Mooseker, M.S. (1994). Identification and overlapping expression of multiple unconventional myosin genes in vertebrate cell types. Proceedings of the National Academy of Sciences of the United States of America *91*, 11767.

Berg, J.S., and Cheney, R.E. (2002). Myosin-X is an unconventional myosin that undergoes intrafilopodial motility. Nature cell biology *4*, 246-250.

Berg, J.S., Derfler, B.H., Pennisi, C.M., Corey, D.P., and Cheney, R.E. (2000). Myosin-X, a novel myosin with pleckstrin homology domains, associates with regions of dynamic actin. Journal of cell science *113 Pt 19*, 3439-3451.

Berg, J.S., Powell, B.C., and Cheney, R.E. (2001). A millennial myosin census. Molecular biology of the cell *12*, 780-794.

Berthold, D.R., Sternberg, C.N., and Tannock, I.F. (2005). Management of advanced prostate cancer after first-line chemotherapy. Journal of clinical oncology : official journal of the American Society of Clinical Oncology *23*, 8247-8252.

Bhattacharya, S., Hirmand, M., Phung, and van Os, S. (2015). Development of enzalutamide for metastatic castration-resistant prostate cancer. Annals of the New York Academy of Sciences.

Billington, N., Beach, J.R., Heissler, S.M., Remmert, K., Guzik-Lendrum, S., Nagy, A., Takagi, Y., Shao, L., Li, D., Yang, Y.*, et al.* (2015). Myosin 18A coassembles with nonmuscle myosin 2 to form mixed bipolar filaments. Current biology : CB *25*, 942-948.

Billington, N., Wang, A., Mao, J., Adelstein, R.S., and Sellers, J.R. (2013). Characterization of three full-length human nonmuscle myosin II paralogs. The Journal of biological chemistry *288*, 33398-33410.

Bishr, M., and Saad, F. (2013). Overview of the latest treatments for castration-resistant prostate cancer. Nature reviews Urology *10*, 522-528.

Bohil, A.B., Robertson, B.W., and Cheney, R.E. (2006). Myosin-X is a molecular motor that functions in filopodia formation. Proceedings of the National Academy of Sciences of the United States of America *103*, 12411-12416.

Bond, L.M., Tumbarello, D.A., Kendrick-Jones, J., and Buss, F. (2013). Small-molecule inhibitors of myosin proteins. Future medicinal chemistry *5*, 41-52.

Bresnick, A.R. (1999). Molecular mechanisms of nonmuscle myosin-II regulation. Current opinion in cell biology *11*, 26-33.

Bright, R.K., Vocke, C.D., Emmert-Buck, M.R., Duray, P.H., Solomon, D., Fetsch, P., Rhim, J.S., Linehan, W.M., and Topalian, S.L. (1997). Generation and genetic characterization of immortal human prostate epithelial cell lines derived from primary cancer specimens. Cancer research *57*, 995-1002.

Bubendorf, L., Schopfer, A., Wagner, U., Sauter, G., Moch, H., Willi, N., Gasser, T.C., and Mihatsch, M.J. (2000). Metastatic patterns of prostate cancer: an autopsy study of 1,589 patients. Human pathology *31*, 578-583.

Buckner, J.C., Brown, P.D., O'Neill, B.P., Meyer, F.B., Wetmore, C.J., and Uhm, J.H. (2007). Central nervous system tumors. Mayo Clinic proceedings *82*, 1271-1286.

Burger, P.C., and Kleihues, P. (1989). Cytologic composition of the untreated glioblastoma with implications for evaluation of needle biopsies. Cancer *63*, 2014-2023.

Buss, F., and Kendrick-Jones, J. (2008). How are the cellular functions of myosin VI regulated within the cell? Biochemical and biophysical research communications *369*, 165-175.

Buss, F., and Kendrick-Jones, J. (2011). Multifunctional myosin VI has a multitude of cargoes. Proceedings of the National Academy of Sciences of the United States of America *108*, 5927-5928.

Buss, F., Kendrick-Jones, J., Lionne, C., Knight, A.E., Cote, G.P., and Paul Luzio, J. (1998). The localization of myosin VI at the golgi complex and leading edge of fibroblasts and its phosphorylation and recruitment into membrane ruffles of A431 cells after growth factor stimulation. The Journal of cell biology *143*, 1535-1545.

Calvo, F., and Sahai, E. (2011). Cell communication networks in cancer invasion. Current opinion in cell biology *23*, 621-629.

Cao, R., Chen, J., Zhang, X., Zhai, Y., Qing, X., Xing, W., Zhang, L., Malik, Y.S., Yu, H., and Zhu, X. (2014). Elevated expression of myosin X in tumours contributes to breast cancer aggressiveness and metastasis. British journal of cancer *111*, 539-550.

Carroll, A.G., Voeller, H.J., Sugars, L., and Gelmann, E.P. (1993). p53 oncogene mutations in three human prostate cancer cell lines. The Prostate *23*, 123-134.

Chandran, U.R., Ma, C., Dhir, R., Bisceglia, M., Lyons-Weiler, M., Liang, W., Michalopoulos, G., Becich, M., and Monzon, F.A. (2007). Gene expression profiles of prostate cancer reveal involvement of multiple molecular pathways in the metastatic process. BMC cancer *7*, 64.

Chang, R.T., Kirby, R., and Challacombe, B.J. (2012). Is there a link between BPH and prostate cancer? The Practitioner *256*, 13-16, 12.

Chen, Z., Trotman, L.C., Shaffer, D., Lin, H.K., Dotan, Z.A., Niki, M., Koutcher, J.A., Scher, H.I., Ludwig, T., Gerald, W.*, et al.* (2005). Crucial role of p53-dependent cellular senescence in suppression of Pten-deficient tumorigenesis. Nature *436*, 725-730.

Cho, S.J., and Chen, X. (2010). Myosin VI is differentially regulated by DNA damage in p53- and cell type-dependent manners. The Journal of biological chemistry *285*, 27159-27166.

Coluccio, L.M. (2008). Myosins. A superfamily of molecular motors (Springer).

Coluccio, L.M., and Geeves, M.A. (1999). Transient kinetic analysis of the 130-kDa myosin I (MYR-1 gene product) from rat liver. A myosin I designed for maintenance of tension? The Journal of biological chemistry *274*, 21575-21580.

Cordonnier, M.N., Dauzonne, D., Louvard, D., and Coudrier, E. (2001). Actin filaments and myosin I alpha cooperate with microtubules for the movement of lysosomes. Molecular biology of the cell *12*, 4013-4029.

Courson, D.S., and Cheney, R.E. (2015). Myosin-X and disease. Experimental cell research *334*, 10-15.

Craig, R., Smith, R., and Kendrick-Jones, J. (1983). Light-chain phosphorylation controls the conformation of vertebrate non-muscle and smooth muscle myosin molecules. Nature *302*, 436-439.

Craig, R., and Woodhead, J.L. (2006). Structure and function of myosin filaments. Current opinion in structural biology *16*, 204-212.

D'Amico, A.V., Whittington, R., Malkowicz, S.B., Schultz, D., Blank, K., Broderick, G.A., Tomaszewski, J.E., Renshaw, A.A., Kaplan, I., Beard, C.J.*, et al.* (1998). Biochemical outcome after radical prostatectomy, external beam radiation therapy, or interstitial radiation therapy for clinically localized prostate cancer. JAMA : the journal of the American Medical Association *280*, 969-974.

Dahan, I., Yearim, A., Touboul, Y., and Ravid, S. (2012). The tumor suppressor Lgl1 regulates NMII-A cellular distribution and focal adhesion morphology to optimize cell migration. Molecular biology of the cell *23*, 591-601.

Darnel, A.D., Behmoaram, E., Vollmer, R.T., Corcos, J., Bijian, K., Sircar, K., Su, J., Jiao, J., Alaoui-Jamali, M.A., and Bismar, T.A. (2009). Fascin regulates prostate cancer cell invasion and is associated with metastasis and biochemical failure in prostate cancer. Clinical cancer research : an official journal of the American Association for Cancer Research *15*, 1376-1383.

De La Cruz, E.M., and Ostap, E.M. (2004). Relating biochemistry and function in the myosin superfamily. Current opinion in cell biology *16*, 61-67.

De Marzo, A.M., Knudsen, B., Chan-Tack, K., and Epstein, J.I. (1999). E-cadherin expression as a marker of tumor aggressiveness in routinely processed radical prostatectomy specimens. Urology *53*, 707-713.

Derycke, L., Stove, C., Vercoutter-Edouart, A.S., De Wever, O., Dolle, L., Colpaert, N., Depypere, H., Michalski, J.C., and Bracke, M. (2011). The role of non-muscle myosin IIA in aggregation and invasion of human MCF-7 breast cancer cells. The International journal of developmental biology *55*, 835-840.

Diz-Munoz, A., Krieg, M., Bergert, M., Ibarlucea-Benitez, I., Muller, D.J., Paluch, E., and Heisenberg, C.P. (2010). Control of directed cell migration in vivo by membrane-to-cortex attachment. PLoS biology *8*, e1000544.

Doctor, S.M., Tsao, C.K., Godbold, J.H., Galsky, M.D., and Oh, W.K. (2014). Is prostate cancer changing?: evolving patterns of metastatic castration-resistant prostate cancer. Cancer *120*, 833-839.

Dong, W., Wang, L., and Shen, R. (2013). MYO5B is epigenetically silenced and associated with MET signaling in human gastric cancer. Digestive diseases and sciences *58*, 2038-2045.

Donnelly, N., Passerini, V., Durrbaum, M., Stingele, S., and Storchova, Z. (2014). HSF1 deficiency and impaired HSP90-dependent protein folding are hallmarks of aneuploid human cells. The EMBO journal *33*, 2374-2387.

Dose, A.C., and Burnside, B. (2002). A class III myosin expressed in the retina is a potential candidate for Bardet-Biedl syndrome. Genomics *79*, 621-624.

Dreicer, R. (2006). Chemotherapy for advanced prostate cancer: docetaxel and beyond. Hematology/oncology clinics of North America *20*, 935-946, x.

Du, M., Wang, G., Ismail, T.M., Gross, S., Fernig, D.G., Barraclough, R., and Rudland, P.S. (2012). S100P dissociates myosin IIA filaments and focal adhesion sites to reduce cell adhesion and enhance cell migration. The Journal of biological chemistry *287*, 15330-15344.

Duhoux, F.P., Ameye, G., Libouton, J.M., Bahloula, K., Iossifidis, S., Chantrain, C.F., Demoulin, J.B., and Poirel, H.A. (2011). The t(11;19)(q23;p13) fusing MLL with MYO1F is recurrent in infant acute myeloid leukemias. Leukemia research *35*, e171-172.

Dulyaninova, N.G., and Bresnick, A.R. (2013). The heavy chain has its day: regulation of myosin-II assembly. Bioarchitecture *3*, 77-85.

Dunn, T.A., Chen, S., Faith, D.A., Hicks, J.L., Platz, E.A., Chen, Y., Ewing, C.M., Sauvageot, J., Isaacs, W.B., De Marzo, A.M.*, et al.* (2006). A novel role of myosin VI in human prostate cancer. The American journal of pathology *169*, 1843-1854.

Duxbury, M.S., Ashley, S.W., and Whang, E.E. (2004). Inhibition of pancreatic adenocarcinoma cellular invasiveness by blebbistatin: a novel myosin II inhibitor. Biochemical and biophysical research communications *313*, 992-997.

Etzioni, R., Penson, D.F., Legler, J.M., di Tommaso, D., Boer, R., Gann, P.H., and Feuer, E.J. (2002). Overdiagnosis due to prostate-specific antigen screening: lessons from U.S. prostate cancer incidence trends. Journal of the National Cancer Institute *94*, 981-990.

Fidler, I.J. (2003). The pathogenesis of cancer metastasis: the 'seed and soil' hypothesis revisited. Nature reviews Cancer *3*, 453-458.

Fidler, I.J. (2011). The biology of cancer metastasis. Seminars in cancer biology *21*, 71.

Fife, C.M., McCarroll, J.A., and Kavallaris, M. (2014). Movers and shakers: cell cytoskeleton in cancer metastasis. British journal of pharmacology *171*, 5507-5523.

Foth, B.J., Goedecke, M.C., and Soldati, D. (2006). New insights into myosin evolution and classification. Proceedings of the National Academy of Sciences of the United States of America *103*, 3681-3686.

Frame, F.M., Pellacani, D., Collins, A.T., Simms, M.S., Mann, V.M., Jones, G.D., Meuth, M., Bristow, R.G., and Maitland, N.J. (2013). HDAC inhibitor confers radiosensitivity to prostate stem-like cells. British journal of cancer *109*, 3023-3033.

Friedl, P., and Wolf, K. (2003). Tumour-cell invasion and migration: diversity and escape mechanisms. Nature reviews Cancer *3*, 362-374.

Geisbrecht, E.R., and Montell, D.J. (2002). Myosin VI is required for E-cadherin-mediated border cell migration. Nature cell biology *4*, 616-620.

Gillespie, P.G., Albanesi, J.P., Bahler, M., Bement, W.M., Berg, J.S., Burgess, D.R., Burnside, B., Cheney, R.E., Corey, D.P., Coudrier, E.*, et al.* (2001). Myosin-I nomenclature. The Journal of cell biology *155*, 703-704.

Goc, A., Al-Husein, B., Kochuparambil, S.T., Liu, J., Heston, W.W., and Somanath, P.R. (2011). PI3 kinase integrates Akt and MAP kinase signaling pathways in the regulation of prostate cancer. International journal of oncology *38*, 267-277.

Goode, B.L., Drubin, D.G., and Barnes, G. (2000). Functional cooperation between the microtubule and actin cytoskeletons. Current opinion in cell biology *12*, 63-71.

Grabowska, M.M., DeGraff, D.J., Yu, X., Jin, R.J., Chen, Z., Borowsky, A.D., and Matusik, R.J. (2014). Mouse models of prostate cancer: picking the best model for the question. Cancer metastasis reviews *33*, 377-397.

Guo, W., Chen, D., Fan, Z., and Epstein, H.F. (2011). Differential turnover of myosin chaperone UNC-45A isoforms increases in metastatic human breast cancer. Journal of molecular biology *412*, 365-378.

Gupta, G.P., and Massague, J. (2006). Cancer metastasis: building a framework. Cell *127*, 679-695.

Guzik-Lendrum, S., Heissler, S.M., Billington, N., Takagi, Y., Yang, Y., Knight, P.J., Homsher, E., and Sellers, J.R. (2013). Mammalian myosin-18A, a highly divergent myosin. The Journal of biological chemistry *288*, 9532-9548.

Hallett, R.M., Dvorkin-Gheva, A., Bane, A., and Hassell, J.A. (2012). A gene signature for predicting outcome in patients with basal-like breast cancer. Scientific reports *2*, 227.

Hanahan, D., and Weinberg, R.A. (2000). The hallmarks of cancer. Cell *100*, 57-70.

Hanahan, D., and Weinberg, R.A. (2011). Hallmarks of cancer: the next generation. Cell *144*, 646-674.

Hanley, P.J., Xu, Y., Kronlage, M., Grobe, K., Schon, P., Song, J., Sorokin, L., Schwab, A., and Bahler, M. (2010). Motorized RhoGAP myosin IXb (Myo9b) controls cell shape and motility. Proceedings of the National Academy of Sciences of the United States of America *107*, 12145-12150.

Hartman, M.A., and Spudich, J.A. (2012). The myosin superfamily at a glance. Journal of cell science *125*, 1627-1632.

Hayward, S.W., Dahiya, R., Cunha, G.R., Bartek, J., Deshpande, N., and Narayan, P. (1995). Establishment and characterization of an immortalized but non-transformed human prostate epithelial cell line: BPH-1. In vitro cellular & developmental biology Animal *31*, 14-24.

Heath, E.I., Hillman, D.W., Vaishampayan, U., Sheng, S., Sarkar, F., Harper, F., Gaskins, M., Pitot, H.C., Tan, W., Ivy, S.P.*, et al.* (2008). A phase II trial of 17-allylamino-17-demethoxygeldanamycin in patients with hormone-refractory metastatic prostate cancer. Clinical cancer research : an official journal of the American Association for Cancer Research *14*, 7940-7946.

Heckman, C.A., and Plummer, H.K., 3rd (2013). Filopodia as sensors. Cellular signalling *25*, 2298-2311.

Hokanson, D.E., Laakso, J.M., Lin, T., Sept, D., and Ostap, E.M. (2006). Myo1c binds phosphoinositides through a putative pleckstrin homology domain. Molecular biology of the cell *17*, 4856-4865.

Holly, J.M., Zeng, L., and Perks, C.M. (2013). Epithelial cancers in the post-genomic era: should we reconsider our lifestyle? Cancer metastasis reviews *32*, 673-705.

Horoszewicz, J.S., Leong, S.S., Kawinski, E., Karr, J.P., Rosenthal, H., Chu, T.M., Mirand, E.A., and Murphy, G.P. (1983). LNCaP model of human prostatic carcinoma. Cancer research *43*, 1809-1818.

Hoskin, P.J., Rojas, A.M., Ostler, P.J., Hughes, R., Lowe, G.J., and Bryant, L. (2013). Quality of life after radical radiotherapy for prostate cancer: longitudinal study from a randomised trial of external beam radiotherapy alone or in combination with high dose rate brachytherapy. Clinical oncology (Royal College of Radiologists (Great Britain)) *25*, 321-327.

Hotary, K.B., Allen, E.D., Brooks, P.C., Datta, N.S., Long, M.W., and Weiss, S.J. (2003). Membrane type I matrix metalloproteinase usurps tumor growth control imposed by the three-dimensional extracellular matrix. Cell *114*, 33-45.

Hsu, R.M., Hsieh, Y.J., Yang, T.H., Chiang, Y.C., Kan, C.Y., Lin, Y.T., Chen, J.T., and Yu, J.S. (2014). Binding of the extreme carboxyl-terminus of PAK-interacting exchange factor beta (betaPIX) to myosin 18A (MYO18A) is required for epithelial cell migration. Biochimica et biophysica acta *1843*, 2513-2527.

Hsu, R.M., Tsai, M.H., Hsieh, Y.J., Lyu, P.C., and Yu, J.S. (2010). Identification of MYO18A as a novel interacting partner of the PAK2/betaPIX/GIT1 complex and its potential function in modulating epithelial cell migration. Molecular biology of the cell *21*, 287-301.

Huang, F.K., Han, S., Xing, B., Huang, J., Liu, B., Bordeleau, F., Reinhart-King, C.A., Zhang, J.J., and Huang, X.Y. (2015). Targeted inhibition of fascin function blocks tumour invasion and metastatic colonization. Nature communications *6*, 7465.

Hurt, E.M., Kawasaki, B.T., Klarmann, G.J., Thomas, S.B., and Farrar, W.L. (2008). CD44+ CD24(-) prostate cells are early cancer progenitor/stem cells that provide a model for patients with poor prognosis. British journal of cancer *98*, 756-765.

Ikebe, M., and Hartshorne, D.J. (1985). Phosphorylation of smooth muscle myosin at two distinct sites by myosin light chain kinase. The Journal of biological chemistry *260*, 10027-10031.

Isogawa, Y., Kon, T., Inoue, T., Ohkura, R., Yamakawa, H., Ohara, O., and Sutoh, K. (2005). The N-terminal domain of MYO18A has an ATP-insensitive actin-binding site. Biochemistry *44*, 6190-6196.

Iwanicki, M.P., Davidowitz, R.A., Ng, M.R., Besser, A., Muranen, T., Merritt, M., Danuser, G., Ince, T.A., and Brugge, J.S. (2011). Ovarian cancer spheroids use myosin-generated force to clear the mesothelium. Cancer discovery *1*, 144-157.

Jacobs, K., Van Gele, M., Forsyth, R., Brochez, L., Vanhoecke, B., De Wever, O., and Bracke, M. (2010). P-cadherin counteracts myosin II-B function: implications in melanoma progression. Molecular cancer *9*, 255.

Jacquemet, G., Hamidi, H., and Ivaska, J. (2015). Filopodia in cell adhesion, 3D migration and cancer cell invasion. Current opinion in cell biology *36*, 23-31.

Jaffe, A.B., and Hall, A. (2005). Rho GTPases: biochemistry and biology. Annual review of cell and developmental biology *21*, 247-269.

Jemal, A., Bray, F., Center, M.M., Ferlay, J., Ward, E., and Forman, D. (2011). Global cancer statistics. CA: a cancer journal for clinicians *61*, 69-90.

Jhaveri, K., and Modi, S. (2015). Ganetespib: research and clinical development. OncoTargets and therapy *8*, 1849-1858.

Jilani, Y., Lu, S., Lei, H., Karnitz, L.M., and Chadli, A. (2015). UNC45A localizes to centrosomes and regulates cancer cell proliferation through ChK1 activation. Cancer letters *357*, 114-120.

Ju, X.D., Guo, Y., Wang, N.N., Huang, Y., Lai, M.M., Zhai, Y.H., Guo, Y.G., Zhang, J.H., Cao, R.J., Yu, H.L.*, et al.* (2014). Both Myosin-10 isoforms are required for radial neuronal migration in the developing cerebral cortex. Cerebral cortex (New York, NY : 1991) *24*, 1259-1268.

Jung, E.J., Liu, G., Zhou, W., and Chen, X. (2006). Myosin VI is a mediator of the p53-dependent cell survival pathway. Molecular and cellular biology *26*, 2175-2186.

Kaighn, M.E., Kirk, D., Szalay, M., and Lechner, J.F. (1981). Growth control of prostatic carcinoma cells in serum-free media: interrelationship of hormone response, cell density, and nutrient media. Proceedings of the National Academy of Sciences of the United States of America *78*, 5673-5676.

Kakita, A., and Goldman, J.E. (1999). Patterns and dynamics of SVZ cell migration in the postnatal forebrain: monitoring living progenitors in slice preparations. Neuron *23*, 461-472.

Kawauchi, T. (2012). Cell Adhesion and Its Endocytic Regulation in Cell Migration during Neural Development and Cancer Metastasis. International journal of molecular sciences *13*, 4564-4590.

Kelley, P.M., Weston, M.D., Chen, Z.Y., Orten, D.J., Hasson, T., Overbeck, L.D., Pinnt, J., Talmadge, C.B., Ing, P., Mooseker, M.S.*, et al.* (1997). The genomic structure of the gene defective in Usher syndrome type Ib (MYO7A). Genomics *40*, 73-79.

Kerber, M.L., and Cheney, R.E. (2011). Myosin-X: a MyTH-FERM myosin at the tips of filopodia. Journal of cell science *124*, 3733-3741.

Kim, S.V., and Flavell, R.A. (2008). Myosin I: from yeast to human. Cellular and molecular life sciences : CMLS *65*, 2128-2137.

Knight, P.J., Thirumurugan, K., Xu, Y., Wang, F., Kalverda, A.P., Stafford, W.F., 3rd, Sellers, J.R., and Peckham, M. (2005). The predicted coiled-coil domain of myosin 10 forms a novel elongated domain that lengthens the head. The Journal of biological chemistry *280*, 34702-34708.

Komaba, S., and Coluccio, L.M. (2010). Localization of myosin 1b to actin protrusions requires phosphoinositide binding. The Journal of biological chemistry *285*, 27686-27693.

Krendel, M., and Mooseker, M.S. (2005). Myosins: tails (and heads) of functional diversity. Physiology (Bethesda, Md) *20*, 239-251.

Kriajevska, M.V., Cardenas, M.N., Grigorian, M.S., Ambartsumian, N.S., Georgiev, G.P., and Lukanidin, E.M. (1994). Non-muscle myosin heavy chain as a possible target for protein encoded by metastasis-related mts-1 gene. The Journal of biological chemistry *269*, 19679-19682.

Lan, L., Han, H., Zuo, H., Chen, Z., Du, Y., Zhao, W., Gu, J., and Zhang, Z. (2010). Upregulation of myosin Va by Snail is involved in cancer cell migration and metastasis. International journal of cancer Journal international du cancer *126*, 53-64.

Lane, D., and Levine, A. (2010). p53 Research: the past thirty years and the next thirty years. Cold Spring Harbor perspectives in biology *2*, a000893.

Lemmon, M.A., and Ferguson, K.M. (2001). Molecular determinants in pleckstrin homology domains that allow specific recognition of phosphoinositides. Biochemical Society transactions *29*, 377-384.

Lim, D.A., Cha, S., Mayo, M.C., Chen, M.H., Keles, E., VandenBerg, S., and Berger, M.S. (2007). Relationship of glioblastoma multiforme to neural stem cell regions predicts invasive and multifocal tumor phenotype. Neuro-oncology *9*, 424-429.

Lin, T., Tang, N., and Ostap, E.M. (2005). Biochemical and motile properties of Myo1b splice isoforms. The Journal of biological chemistry *280*, 41562-41567.

Lin, W.H., Hurley, J.T., Raines, A.N., Cheney, R.E., and Webb, D.J. (2013). Myosin X and its motorless isoform differentially modulate dendritic spine development by regulating trafficking and retention of vasodilator-stimulated phosphoprotein. Journal of cell science *126*, 4756-4768.

Liu, Y., Peng, Y., Dai, P.G., Du, Q.S., Mei, L., and Xiong, W.C. (2012). Differential regulation of myosin X movements by its cargos, DCC and neogenin. Journal of cell science *125*, 751-762.

Long, R.M., Morrissey, C., Fitzpatrick, J.M., and Watson, R.W. (2005). Prostate epithelial cell differentiation and its relevance to the understanding of prostate cancer therapies. Clinical science (London, England : 1979) *108*, 1-11.

Lu, Q., Ye, F., Wei, Z., Wen, Z., and Zhang, M. (2012). Antiparallel coiled-coil-mediated dimerization of myosin X. Proceedings of the National Academy of Sciences of the United States of America *109*, 17388-17393.

Ludlow, J.W. (1993). Interactions between SV40 large-tumor antigen and the growth suppressor proteins pRB and p53. FASEB journal : official publication of the Federation of American Societies for Experimental Biology *7*, 866-871.

Lundquist, E.A. (2009). The finer points of filopodia. PLoS biology *7*, e1000142.

Ma, J., and Waxman, D.J. (2009). Dominant effect of antiangiogenesis in combination therapy involving cyclophosphamide and axitinib. Clinical cancer research : an official journal of the American Association for Cancer Research *15*, 578-588.

Maddugoda, M.P., Crampton, M.S., Shewan, A.M., and Yap, A.S. (2007). Myosin VI and vinculin cooperate during the morphogenesis of cadherin cell cell contacts in mammalian epithelial cells. The Journal of cell biology *178*, 529-540.

Makowska, K.A., Hughes, R.E., White, K.J., Wells, C.M., and Peckham, M. (2015). Specific Myosins Control Actin Organization, Cell Morphology, and Migration in Prostate Cancer Cells. Cell Reports.

Mazzolini, R., Rodrigues, P., Bazzocco, S., Dopeso, H., Ferreira, A.M., Mateo-Lozano, S., Andretta, E., Woerner, S.M., Alazzouzi, H., Landolfi, S.*,*

et al. (2013). Brush border myosin Ia inactivation in gastric but not endometrial tumors. International journal of cancer Journal international du cancer *132*, 1790-1799.

McConnell, R.E., and Tyska, M.J. (2010). Leveraging the membrane - cytoskeleton interface with myosin-1. Trends in cell biology *20*, 418-426.

McMichael, B.K., Cheney, R.E., and Lee, B.S. (2010). Myosin X regulates sealing zone patterning in osteoclasts through linkage of podosomes and microtubules. The Journal of biological chemistry *285*, 9506-9515.

McVary, K.T. (2007). A review of combination therapy in patients with benign prostatic hyperplasia. Clinical therapeutics *29*, 387-398.

Menke, V., Van Zoest, K.P., Moons, L.M., Pot, R.G., Siersema, P.D., Kuipers, E.J., and Kusters, J.G. (2012). Myo9B is associated with an increased risk of Barrett's esophagus and esophageal adenocarcinoma. Scandinavian journal of gastroenterology *47*, 1422-1428.

Mitas, M., Mikhitarian, K., Walters, C., Baron, P.L., Elliott, B.M., Brothers, T.E., Robison, J.G., Metcalf, J.S., Palesch, Y.Y., Zhang, Z.*, et al.* (2001). Quantitative real-time RT-PCR detection of breast cancer micrometastasis using a multigene marker panel. International journal of cancer Journal international du cancer *93*, 162-171.

Miyata, Y., Nakamoto, H., and Neckers, L. (2013). The therapeutic target Hsp90 and cancer hallmarks. Current pharmaceutical design *19*, 347-365.

Mori, K., Matsuda, K., Furusawa, T., Kawata, M., Inoue, T., and Obinata, M. (2005). Subcellular localization and dynamics of MysPDZ (Myo18A) in live mammalian cells. Biochemical and biophysical research communications *326*, 491-498.

Muller, P.A., Caswell, P.T., Doyle, B., Iwanicki, M.P., Tan, E.H., Karim, S., Lukashchuk, N., Gillespie, D.A., Ludwig, R.L., Gosselin, P.*, et al.* (2009). Mutant p53 drives invasion by promoting integrin recycling. Cell *139*, 1327-1341.

Murphy, R.A., Walker, J.S., and Strauss, J.D. (1997). Myosin isoforms and functional diversity in vertebrate smooth muscle. Comparative biochemistry and physiology Part B, Biochemistry & molecular biology *117*, 51-60.

Nakano, T., Tani, M., Nishioka, M., Kohno, T., Otsuka, A., Ohwada, S., and Yokota, J. (2005). Genetic and epigenetic alterations of the candidate tumor-suppressor gene MYO18B, on chromosome arm 22q, in colorectal cancer. Genes, chromosomes & cancer *43*, 162-171.

Oh, W.K., Galsky, M.D., Stadler, W.M., Srinivas, S., Chu, F., Bubley, G., Goddard, J., Dunbar, J., and Ross, R.W. (2011). Multicenter phase II trial of the heat shock protein 90 inhibitor, retaspimycin hydrochloride (IPI-504), in patients with castration-resistant prostate cancer. Urology *78*, 626-630.

Ohmura, G., Tsujikawa, T., Yaguchi, T., Kawamura, N., Mikami, S., Sugiyama, J., Nakamura, K., Kobayashi, A., Iwata, T., Nakano, H.*, et al.* (2015). Aberrant Myosin 1b Expression Promotes Cell Migration and Lymph Node Metastasis of HNSCC. Molecular cancer research : MCR *13*, 721-731.

Omelchenko, T., and Hall, A. (2012). Myosin-IXA regulates collective epithelial cell migration by targeting RhoGAP activity to cell-cell junctions. Current biology : CB *22*, 278-288.

Oren, M., and Rotter, V. (2010). Mutant p53 gain-of-function in cancer. Cold Spring Harbor perspectives in biology *2*, a001107.

Orsted, D.D., and Bojesen, S.E. (2013). The link between benign prostatic hyperplasia and prostate cancer. Nature reviews Urology *10*, 49-54.

Ostrom, Q.T., Bauchet, L., Davis, F.G., Deltour, I., Fisher, J.L., Langer, C.E., Pekmezci, M., Schwartzbaum, J.A., Turner, M.C., Walsh, K.M.*, et al.* (2014). The epidemiology of glioma in adults: a "state of the science" review. Neuro-oncology *16*, 896-913.

Ouderkirk, J.L., and Krendel, M. (2014). Non-muscle myosins in tumor progression, cancer cell invasion, and metastasis. Cytoskeleton (Hoboken, NJ) *71*, 447-463.

Parker, C.C., Pascoe, S., Chodacki, A., O'Sullivan, J.M., Germa, J.R., O'Bryan-Tear, C.G., Haider, T., and Hoskin, P. (2013). A randomized, double-blind, dose-finding, multicenter, phase 2 study of radium chloride (Ra 223) in patients with bone metastases and castration-resistant prostate cancer. European urology *63*, 189-197.

Parr, C., Davies, G., Nakamura, T., Matsumoto, K., Mason, M.D., and Jiang, W.G. (2001). The HGF/SF-induced phosphorylation of paxillin, matrix adhesion, and invasion of prostate cancer cells were suppressed by NK4, an HGF/SF variant. Biochemical and biophysical research communications *285*, 1330-1337.

Peckham, M., and Knight, P.J. (2009). When a predicted coiled coil is really a single alpha-helix, in myosins and other proteins. Soft Matter *5*, 2493–2503.

Plantard, L., Arjonen, A., Lock, J.G., Nurani, G., Ivaska, J., and Stromblad, S. (2010). PtdIns(3,4,5)P(3) is a regulator of myosin-X localization and filopodia formation. Journal of cell science *123*, 3525-3534.

Polyak, K., and Weinberg, R.A. (2009). Transitions between epithelial and mesenchymal states: acquisition of malignant and stem cell traits. Nature reviews Cancer *9*, 265-273.

Price, M.G., Landsverk, M.L., Barral, J.M., and Epstein, H.F. (2002). Two mammalian UNC-45 isoforms are related to distinct cytoskeletal and muscle-specific functions. Journal of cell science *115*, 4013-4023.

Prosperi, M.T., Lepine, P., Dingli, F., Paul-Gilloteaux, P., Martin, R., Loew, D., Knolker, H.J., and Coudrier, E. (2015). Myosin 1b functions as an effector of EphB signaling to control cell repulsion. The Journal of cell biology *210*, 347-361.

Pulukuri, S.M., Gondi, C.S., Lakka, S.S., Jutla, A., Estes, N., Gujrati, M., and Rao, J.S. (2005). RNA interference-directed knockdown of urokinase plasminogen activator and urokinase plasminogen activator receptor inhibits prostate cancer cell invasion, survival, and tumorigenicity in vivo. The Journal of biological chemistry *280*, 36529-36540.

Puri, C., Chibalina, M.V., Arden, S.D., Kruppa, A.J., Kendrick-Jones, J., and Buss, F. (2010). Overexpression of myosin VI in prostate cancer cells enhances PSA and VEGF secretion, but has no effect on endocytosis. Oncogene *29*, 188-200.

Quintero, O.A., DiVito, M.M., Adikes, R.C., Kortan, M.B., Case, L.B., Lier, A.J., Panaretos, N.S., Slater, S.Q., Rengarajan, M., Feliu, M.*, et al.* (2009). Human Myo19 is a novel myosin that associates with mitochondria. Current biology : CB *19*, 2008-2013.

Raines, A.N., Nagdas, S., Kerber, M.L., and Cheney, R.E. (2012). Headless Myo10 is a negative regulator of full-length Myo10 and inhibits axon outgrowth in cortical neurons. The Journal of biological chemistry *287*, 24873-24883.

Raposo, G., Cordonnier, M.N., Tenza, D., Menichi, B., Durrbach, A., Louvard, D., and Coudrier, E. (1999). Association of myosin I alpha with endosomes and lysosomes in mammalian cells. Molecular biology of the cell *10*, 1477-1494.

Reinhard, J., Scheel, A.A., Diekmann, D., Hall, A., Ruppert, C., and Bahler, M. (1995). A novel type of myosin implicated in signalling by rho family GTPases. The EMBO journal *14*, 697-704.

Richardson, G.P., Forge, A., Kros, C.J., Fleming, J., Brown, S.D., and Steel, K.P. (1997). Myosin VIIA is required for aminoglycoside accumulation in cochlear hair cells. The Journal of neuroscience : the official journal of the Society for Neuroscience *17*, 9506-9519.

Ridley, A.J. (2011). Life at the leading edge. Cell *145*, 1012-1022.

Ridley, A.J., and Hall, A. (1992). The small GTP-binding protein rho regulates the assembly of focal adhesions and actin stress fibers in response to growth factors. Cell *70*, 389-399.

Ridley, A.J., Schwartz, M.A., Burridge, K., Firtel, R.A., Ginsberg, M.H., Borisy, G., Parsons, J.T., and Horwitz, A.R. (2003). Cell migration: integrating signals from front to back. Science (New York, NY) *302*, 1704-1709.

Ruppert, C., Kroschewski, R., and Bahler, M. (1993). Identification, characterization and cloning of myr 1, a mammalian myosin-I. The Journal of cell biology *120*, 1393-1403.

Sachdev, J.C., and Jahanzeb, M. (2012). Blockade of the HER family of receptors in the treatment of HER2-positive metastatic breast cancer. Clinical breast cancer *12*, 19-29.

Saha, S., Dey, S.K., Das, P., and Jana, S.S. (2011). Increased expression of nonmuscle myosin IIs is associated with 3MC-induced mouse tumor. The FEBS journal *278*, 4025-4034.

Salas-Cortes, L., Ye, F., Tenza, D., Wilhelm, C., Theos, A., Louvard, D., Raposo, G., and Coudrier, E. (2005). Myosin Ib modulates the morphology and the protein transport within multi-vesicular sorting endosomes. Journal of cell science *118*, 4823-4832.

Saporita, A.J., Ai, J., and Wang, Z. (2007). The Hsp90 inhibitor, 17-AAG, prevents the ligand-independent nuclear localization of androgen receptor in refractory prostate cancer cells. The Prostate *67*, 509-520.

Schaar, B.T., and McConnell, S.K. (2005). Cytoskeletal coordination during neuronal migration. Proceedings of the National Academy of Sciences of the United States of America *102*, 13652-13657.

Schoumacher, M., Goldman, R.D., Louvard, D., and Vignjevic, D.M. (2010). Actin, microtubules, and vimentin intermediate filaments cooperate for elongation of invadopodia. The Journal of cell biology *189*, 541-556.

Schramek, D., Sendoel, A., Segal, J.P., Beronja, S., Heller, E., Oristian, D., Reva, B., and Fuchs, E. (2014). Direct in vivo RNAi screen unveils myosin IIa as a tumor suppressor of squamous cell carcinomas. Science (New York, NY) *343*, 309-313.

Selivanova, G., and Ivaska, J. (2009). Integrins and mutant p53 on the road to metastasis. Cell *139*, 1220-1222.

Sharifi, N., Gulley, J.L., and Dahut, W.L. (2010). An update on androgen deprivation therapy for prostate cancer. Endocrine-related cancer *17*, R305-315.

Sousa, A.D., Berg, J.S., Robertson, B.W., Meeker, R.B., and Cheney, R.E. (2006). Myo10 in brain: developmental regulation, identification of a headless isoform and dynamics in neurons. Journal of cell science *119*, 184-194.

Stone, K.R., Mickey, D.D., Wunderli, H., Mickey, G.H., and Paulson, D.F. (1978). Isolation of a human prostate carcinoma cell line (DU 145). International journal of cancer Journal international du cancer *21*, 274-281.

Stupp, R., Hegi, M.E., Gilbert, M.R., and Chakravarti, A. (2007). Chemoradiotherapy in malignant glioma: standard of care and future directions. Journal of clinical oncology : official journal of the American Society of Clinical Oncology *25*, 4127-4136.

Su, A.I., Welsh, J.B., Sapinoso, L.M., Kern, S.G., Dimitrov, P., Lapp, H., Schultz, P.G., Powell, S.M., Moskaluk, C.A., Frierson, H.F., Jr.*, et al.* (2001). Molecular classification of human carcinomas by use of gene expression signatures. Cancer research *61*, 7388-7393.

Sun, Y., Ai, X., Shen, S., and Lu, S. (2015). NF-kappaB-mediated miR-124 suppresses metastasis of non-small-cell lung cancer by targeting MYO10. Oncotarget *6*, 8244-8254.

Swailes, N.T., Colegrave, M., Knight, P.J., and Peckham, M. (2006). Non-muscle myosins 2A and 2B drive changes in cell morphology that occur as myoblasts align and fuse. Journal of cell science *119*, 3561-3570.

Tacon, D., Knight, P.J., and Peckham, M. (2004). Imaging myosin 10 in cells. Biochemical Society transactions *32*, 689-693.

Tan, I., Yong, J., Dong, J.M., Lim, L., and Leung, T. (2008). A tripartite complex containing MRCK modulates lamellar actomyosin retrograde flow. Cell *135*, 123-136.

Tang, N., and Ostap, E.M. (2001). Motor domain-dependent localization of myo1b (myr-1). Current biology : CB *11*, 1131-1135.

Tani, M., Ito, J., Nishioka, M., Kohno, T., Tachibana, K., Shiraishi, M., Takenoshita, S., and Yokota, J. (2004). Correlation between histone acetylation and expression of the MYO18B gene in human lung cancer cells. Genes, chromosomes & cancer *40*, 146-151.

Thorne, R.G., and Nicholson, C. (2006). In vivo diffusion analysis with quantum dots and dextrans predicts the width of brain extracellular space. Proceedings of the National Academy of Sciences of the United States of America *103*, 5567-5572.

Torre, L.A., Bray, F., Siegel, R.L., Ferlay, J., Lortet-Tieulent, J., and Jemal, A. (2015). Global cancer statistics, 2012. CA: a cancer journal for clinicians *65*, 87-108.

Trepel, J., Mollapour, M., Giaccone, G., and Neckers, L. (2010). Targeting the dynamic HSP90 complex in cancer. Nature reviews Cancer *10*, 537-549.

Trybus, K.M. (1994). Role of myosin light chains. Journal of muscle research and cell motility *15*, 587-594.

Turner, C.E. (2000). Paxillin and focal adhesion signalling. Nature cell biology *2*, E231-236.

Umeki, N., Jung, H.S., Sakai, T., Sato, O., Ikebe, R., and Ikebe, M. (2011). Phospholipid-dependent regulation of the motor activity of myosin X. Nature structural & molecular biology *18*, 783-788.

Ussowicz, M., Jaskowiec, A., Meyer, C., Marschalek, R., Chybicka, A., Szczepanski, T., and Haus, O. (2012). A three-way translocation of MLL, MLLT11, and the novel reciprocal partner gene MYO18A in a child with acute myeloid leukemia. Cancer genetics *205*, 261-265.

Vasioukhin, V. (2006). Lethal giant puzzle of Lgl. Developmental neuroscience *28*, 13-24.

Vega, F.M., Colomba, A., Reymond, N., Thomas, M., and Ridley, A.J. (2012). RhoB regulates cell migration through altered focal adhesion dynamics. Open biology *2*, 120076.

Vicente-Manzanares, M., Ma, X., Adelstein, R.S., and Horwitz, A.R. (2009). Non-muscle myosin II takes centre stage in cell adhesion and migration. Nature reviews Molecular cell biology *10*, 778-790.

Wang, Z., Edwards, J.G., Riley, N., Provance, D.W., Jr., Karcher, R., Li, X.D., Davison, I.G., Ikebe, M., Mercer, J.A., Kauer, J.A.*, et al.* (2008). Myosin Vb mobilizes recycling endosomes and AMPA receptors for postsynaptic plasticity. Cell *135*, 535-548.

Ware, M.J., Tinger, S., Colbert, K.L., Corr, S.J., Rees, P., Koshkina, N., Curley, S., Summers, H.D., and Godin, B. (2015). Radiofrequency treatment alters cancer cell phenotype. Scientific reports *5*, 12083.

Watanabe, T.M., Tokuo, H., Gonda, K., Higuchi, H., and Ikebe, M. (2010). Myosin-X induces filopodia by multiple elongation mechanism. The Journal of biological chemistry *285*, 19605-19614.

Weber, K.L., Sokac, A.M., Berg, J.S., Cheney, R.E., and Bement, W.M. (2004). A microtubule-binding myosin required for nuclear anchoring and spindle assembly. Nature *431*, 325-329.

Wei, S., Dunn, T.A., Isaacs, W.B., De Marzo, A.M., and Luo, J. (2008). GOLPH2 and MYO6: putative prostate cancer markers localized to the Golgi apparatus. The Prostate *68*, 1387-1395.

Weil, D., Blanchard, S., Kaplan, J., Guilford, P., Gibson, F., Walsh, J., Mburu, P., Varela, A., Levilliers, J., Weston, M.D.*, et al.* (1995). Defective myosin VIIA gene responsible for Usher syndrome type 1B. Nature *374*, 60-61.

Wellbrock, C., and Hurlstone, A. (2010). BRAF as therapeutic target in melanoma. Biochemical pharmacology *80*, 561-567.

Wells, C.M., Ahmed, T., Masters, J.R., and Jones, G.E. (2005). Rho family GTPases are activated during HGF-stimulated prostate cancer-cell scattering. Cell motility and the cytoskeleton *62*, 180-194.

Wenzel, J., Ouderkirk, J.L., Krendel, M., and Lang, R. (2015). Class I myosin Myo1e regulates TLR4-triggered macrophage spreading, chemokine release, and antigen presentation via MHC class II. European journal of immunology *45*, 225-237.

Wilkinson, S., Paterson, H.F., and Marshall, C.J. (2005). Cdc42-MRCK and Rho-ROCK signalling cooperate in myosin phosphorylation and cell invasion. Nature cell biology *7*, 255-261.

Wirth, J.A., Jensen, K.A., Post, P.L., Bement, W.M., and Mooseker, M.S. (1996). Human myosin-IXb, an unconventional myosin with a chimerin-like rho/rac GTPase-activating protein domain in its tail. Journal of cell science *109 (Pt 3)*, 653-661.

Wolff, J.M., and Mason, M. (2012). Drivers for change in the management of prostate cancer - guidelines and new treatment techniques. BJU international *109 Suppl 6*, 33-41.

Wong, S.Y., Ulrich, T.A., Deleyrolle, L.P., MacKay, J.L., Lin, J.M., Martuscello, R.T., Jundi, M.A., Reynolds, B.A., and Kumar, S. (2015). Constitutive activation of myosin-dependent contractility sensitizes glioma tumor-initiating cells to mechanical inputs and reduces tissue invasion. Cancer research *75*, 1113-1122.

Wu, H.C., Hsieh, J.T., Gleave, M.E., Brown, N.M., Pathak, S., and Chung, L.W. (1994). Derivation of androgen-independent human LNCaP prostatic cancer cell sublines: role of bone stromal cells. International journal of cancer Journal international du cancer *57*, 406-412.

Yamada, A., Mamane, A., Lee-Tin-Wah, J., Di Cicco, A., Prevost, C., Levy, D., Joanny, J.F., Coudrier, E., and Bassereau, P. (2014). Catch-bond behaviour facilitates membrane tubulation by non-processive myosin 1b. Nature communications *5*, 3624.

Yanaihara, N., Nishioka, M., Kohno, T., Otsuka, A., Okamoto, A., Ochiai, K., Tanaka, T., and Yokota, J. (2004). Reduced expression of MYO18B, a candidate tumor-suppressor gene on chromosome arm 22q, in ovarian cancer. International journal of cancer Journal international du cancer *112*, 150-154.

Yano, A., Tsutsumi, S., Soga, S., Lee, M.J., Trepel, J., Osada, H., and Neckers, L. (2008). Inhibition of Hsp90 activates osteoclast c-Src signaling and promotes growth of prostate carcinoma cells in bone. Proceedings of the National Academy of Sciences of the United States of America *105*, 15541-15546.

Yoshida, H., Cheng, W., Hung, J., Montell, D., Geisbrecht, E., Rosen, D., Liu, J., and Naora, H. (2004). Lessons from border cell migration in the Drosophila ovary: A role for myosin VI in dissemination of human ovarian cancer. Proceedings of the National Academy of Sciences of the United States of America *101*, 8144-8149.

Yu, X., Zech, T., McDonald, L., Gonzalez, E.G., Li, A., Macpherson, I., Schwarz, J.P., Spence, H., Futo, K., Timpson, P.*, et al.* (2012). N-WASP coordinates the delivery and F-actin-mediated capture of MT1-MMP at invasive pseudopods. The Journal of cell biology *199*, 527-544.

Yu, Y.P., Landsittel, D., Jing, L., Nelson, J., Ren, B., Liu, L., McDonald, C., Thomas, R., Dhir, R., Finkelstein, S.*, et al.* (2004). Gene expression alterations in prostate cancer predicting tumor aggression and preceding development of malignancy. Journal of clinical oncology : official journal of the American Society of Clinical Oncology *22*, 2790-2799.

Zeigler-Johnson, C.M., Spangler, E., Jalloh, M., Gueye, S.M., Rennert, H., and Rebbeck, T.R. (2008). Genetic susceptibility to prostate cancer in men of African descent: implications for global disparities in incidence and outcomes. The Canadian journal of urology *15*, 3872-3882.

Zhang, H., Berg, J.S., Li, Z., Wang, Y., Lang, P., Sousa, A.D., Bhaskar, A., Cheney, R.E., and Stromblad, S. (2004). Myosin-X provides a motor-based link between integrins and the cytoskeleton. Nature cell biology *6*, 523-531.

Zhao, R., Davey, M., Hsu, Y.C., Kaplanek, P., Tong, A., Parsons, A.B., Krogan, N., Cagney, G., Mai, D., Greenblatt, J.*, et al.* (2005). Navigating the chaperone network: an integrative map of physical and genetic interactions mediated by the hsp90 chaperone. Cell *120*, 715-727.

Zhu, J., Sammons, M.A., Donahue, G., Dou, Z., Vedadi, M., Getlik, M., Barsyte-Lovejoy, D., Al-awar, R., Katona, B.W., Shilatifard, A.*, et al.* (2015). Gain-of-function p53 mutants co-opt chromatin pathways to drive cancer growth. Nature *525*, 206-211.

Zhu, X.J., Wang, C.Z., Dai, P.G., Xie, Y., Song, N.N., Liu, Y., Du, Q.S., Mei, L., Ding, Y.Q., and Xiong, W.C. (2007). Myosin X regulates netrin receptors and functions in axonal path-finding. Nature cell biology *9*, 184-192.

Zlotta, A.R., and Schulman, C.C. (1999). Clinical evolution of prostatic intraepithelial neoplasia. European urology *35*, 498-503.

Cancer Research UK, http://www.cancerresearchuk.org/health-professional/cancer-statistics/statistics-by-cancer-type/prostate-cancer, Accessed September 2015